

Chapter 6

Underwater granular flows

6.1 Introduction

Avalanches, landslides, and debris flows are geophysical hazards, which involve rapid mass movement of granular solids, water, and air as a single phase system. Globally, landslides cause billions of pounds in damage, and thousands of deaths and injuries each year. Hence, it is important to understand the triggering mechanism and the flow evolution. The momentum transfer between the discrete and the continuous phases significantly affects the dynamics of the flow as a whole (Topin et al., 2012). Although certain macroscopic models are able to capture the simple mechanical behaviours (Peker and Helvacı, 2007), the complex physical mechanisms occurring at the grain scale, such as hydrodynamic instabilities, formation of clusters, collapse, and transport (Topin et al., 2011), have largely been ignored. In particular, when the solid phase reaches a high volume fraction, the strong heterogeneity arising from the contact forces between the grains, and the hydrodynamic forces, are difficult to integrate into the homogenization process involving global averages.

In order to describe the mechanism of immersed granular flows, it is important to consider both the dynamics of the solid phase and the role of the ambient fluid (Denlinger and Iverson, 2001). The dynamics of the solid phase alone are insufficient to describe the mechanism of granular flows in fluid. It is important to consider the effect of hydrodynamic forces that reduce the weight of the solids inducing a transition from dense-compacted to dense-suspended flows, and the drag interactions which counteract the movement of the solids (Meruane et al., 2010). Transient regimes characterized by a change in the solid fraction, dilation at the onset of flow and the development of excess pore-pressure, result in altering the balance between the stress carried by the fluid and that carried by the grains, thereby changing the overall behaviour of the flow.

The presence of a fluid phase in a granular medium has profound effects on its mechanical behaviour. In dry granular media, the rheology is governed by grain inertia and static stresses sustained by the contact network depending on the shear-rate and the confining pressure, respectively (Midi, 2004). As the fluid inertia and viscosity come into play, complications arise as a result of contradictory effects. On one hand, the fluid may delay the onset of granular flow or prevent the dispersion of the grains by developing negative pore-pressure (Pailha et al., 2008; Topin et al., 2011). On the other hand, the fluid lubricates the contacts between grains, enhancing the rate of granular flow, but it has a retarding effect at the same time by inducing drag forces on the grains. The objective of the present study is to understand the differences in the mechanism of flow initiation and kinematics between dry and submerged granular flows. In the present study, a coupled 2D Lattice-Boltzmann and Discrete Element Method is used to model the fluid-soil interactions in underwater granular flows. The 2D geometry does not take into account the movement of grains perpendicular to the plane. Also, due to the 2D nature of the geometry fluid flows and fluid-solid interactions in the direction perpendicular to the plane are not considered. However, the movement of fluid in the plane normal to the direction of flow is minimal and the choice of 2D geometry is justified. LBM - DEM approach is computationally expensive as it models the fluid - solid interaction at a scale that is orders of magnitude smaller than the grain size. It is important to consider a representative volume element that is large enough to capture the granular flow dynamics in the fluid. The 2D geometry has the advantage of cheaper computational effort than a 3D case, making it feasible to simulate very large systems. The configuration and parameters studied in this chapter are presented in table 6.1.

6.2 LBM-DEM permeability

In a 3D granular assembly, the pore spaces between the grains are interconnected, whereas in a 2-D assembly, a non-interconnected pore-fluid space is formed as the grains are in contact with each other. This means that the fluid enclosed between the grains cannot flow to the neighbouring pore-spaces. This results in an unnatural no flow condition in a 2-D case (figure 6.1). In order to overcome this effect, a reduction in radius is assumed only during the LBM computation (fluid and fluid – solid interaction) steps. The reduced radius of the soil grain, i.e., the *hydrodynamic radius* r , allows for interconnected pore space through which the pore-fluid can flow similar to the 3D behaviour. The reduction in the radius is assumed only during LBM computations, hence this technique has no effect on the grain – grain interactions computed using DEM.

Table 6.1 Configurations for LBM-DEM simulations of granular collapse in fluid

Simulations	Aspect ratio	Hydrodynamic radius	Packing density (%)	Slope angle (°)
Collapse on a horizontal surface				
Effect of initial aspect ratio	0.2 - 6	$r = 0.7 R$	83	0
Effect of permeability	0.2 - 6	$r = 0.7, 0.75, 0.8, 0.85, 0.9 \& 0.95 R$	83	0
Effect of initial density	0.8	$r = 0.7, 0.75, 0.8, 0.85, 0.9 \& 0.95 R$	79 & 83	0
Collapse on an inclined plane				
Effect of initial density	0.8	$r = 0.9 R$	79 & 83	0, 2.5, 5 & 7.5
Effect of permeability	0.8	$r = 0.7, 0.75, 0.8, 0.85 \& 0.9 R$	79 & 83	0 & 5
Tall columns	6	$r = 0.85 R$	79 & 83	0, 2.5, 5 & 7.5

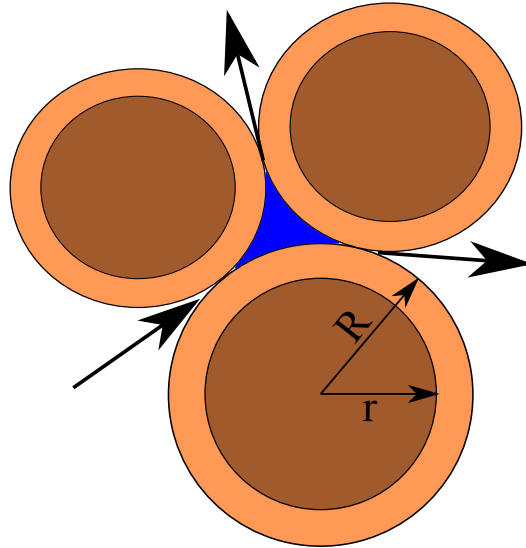


Figure 6.1 Schematic representation of the hydrodynamic radius in LBM-DEM computation.

Realistically, the hydrodynamic radius can be varied from $r = 0.7R$ to $0.95R$, where R is the grain radius. Different permeabilities can be obtained for any given initial packing by varying the hydrodynamic radius of the grains, without having to change the actual granular packing. This introduces a new parameter into the system. In a physical sense, a hydrodynamic radius represents the three-dimensional permeability of a granular assembly simulated as a two-dimensional geometry.

In order to understand the relation between the hydrodynamic radius and the permeability of the granular assembly, horizontal permeability tests are performed by varying the hydrodynamic radius as $0.7 R$, $0.75 R$, $0.8 R$, $0.85 R$, $0.9 R$ and $0.95 R$. A square sample of $50 \text{ mm} \times 50 \text{ mm}$ filled with poly-disperse ($d_{\max}/d_{\min} = 1.8$) grains having a mean diameter of 1.7 mm is used to determine the relation between the hydrodynamic radius and the permeability. Dirichlet boundary conditions (discussed in ??), i.e., density constraint, are applied along the left and the right boundaries of the sample. The fluid density on the left boundary is increased in small steps ($10^{-4}\Delta P$), while a constant density is maintained on the right boundary. This results in a pressure gradient (figure 6.2a) causing the fluid to flow through the pore-space. Figure 6.2b show the horizontal velocity of flow through the interconnected pore-space.

For a given hydrodynamic radius, the pressure gradient ΔP is varied to obtain different flow rates. Probing the fluid space showed a Poiseuille flow behaviour between the grains. The flow is still within the Darcy's laminar flow regime. Figure 6.3 shows the linear relationship between the applied mean pressure to the mean horizontal flow velocity for different hydrodynamic radii, this proves that the flow is laminar. From the mean flow velocity (v), the

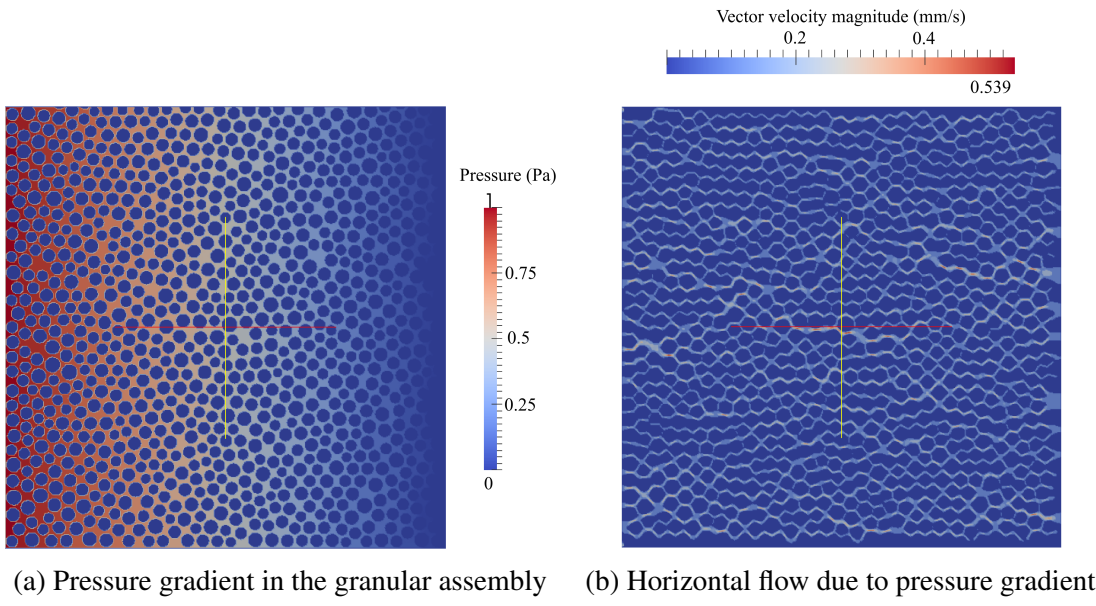


Figure 6.2 Evaluation of the horizontal permeability for a hydrodynamic radius of $0.7 R$.

transverse permeability (k) of the sample is computed as

$$k = v \cdot \mu \cdot \frac{\Delta x}{\Delta P}, \quad (6.1)$$

where μ is the dynamic viscosity of the fluid (Pas), Δx is the thickness of the bed of porous medium m, and ΔP is the applied pressure difference Pa. It can be observed that with increase in the hydrodynamic radius the permeability decreases, i.e., the slope of the mean flow velocity to the pressure gradient decreases. At very low pressure gradients ($\Delta P \leq 0.1$), both $0.9 R$ and $0.95 R$ have no flow. Even at higher pressure gradients, a hydrodynamic radius of $r = 0.95R$ shows almost no flow behaviour. A high value of hydrodynamic radius $r > 0.95R$ results in unnatural flow/no-flow behaviour. Hence in the present study, a hydrodynamic radius in the range of 0.7 to $0.95 R$ is adopted.

Increasing the hydrodynamic radius from 0.7 to 0.95 reduces the quasi-porosity from 0.60 to 0.27 . The permeability computed from LB – DEM method is verified by comparing it with the analytical solution. One of the widely used analytical solution for permeability is the Carman – Kozeny equation (CK Model), which is based on the Poiseuille's flow through a pipe and is mainly used for 3D, homogeneous, isotropic, granular porous media at moderate porosities. In the present study, a modified Carman – Kozeny equation that takes into account of the micro-structure of the fibres and that is valid in a wide range of porosities

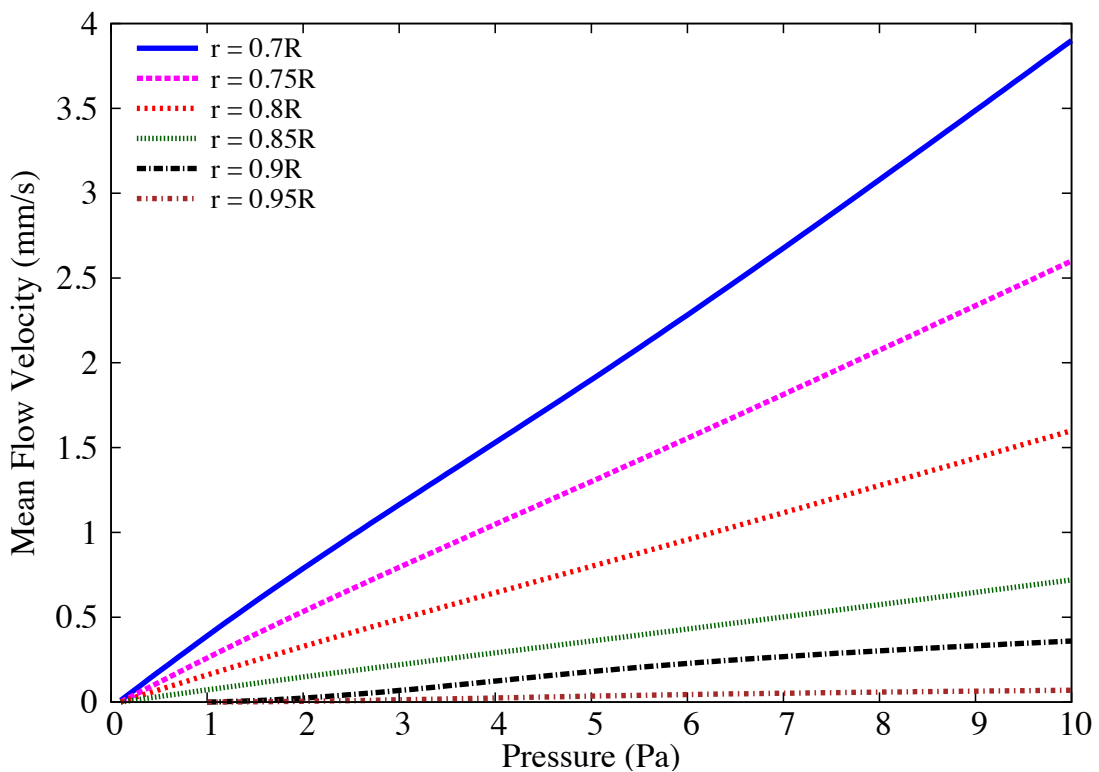


Figure 6.3 Variation of the mean flow velocity with pressure gradient for different hydrodynamic radius.

is adopted (Yazdchi et al., 2011). The normalized permeability is defined as

$$\frac{k}{d^2} = \frac{\varepsilon}{\psi_{CK}(1-\varepsilon)^2}. \quad (6.2)$$

In the CK model, the hydraulic diameter D_h , is expressed as a function of measurable quantities: porosity and specific surface area

$$D_h = \frac{4\varepsilon V}{S_v} = \frac{\varepsilon d}{(1-\varepsilon)}, \quad (6.3)$$

$$a_v = \frac{\text{grain surface}}{\text{grain volume}} = \frac{S_v}{(1-\varepsilon)V} = \frac{4}{d}, \quad (6.4)$$

where S_v is the total wetted surface, and a_v is the specific surface area. The above value of a_v is for circles (cylinders) - for spheres $a_v = 6/d$. ψ_{CK} is the empirically measured CK factor, which represents both the shape factor and the deviation of flow direction from that in a duct. It is approximated for randomly packed beds of spherical grains. The variation of normalized permeability with porosity, obtained by varying the radius from $0.7 R$ to $0.95 R$, is presented in figure 6.4. The permeability values obtained from LBM - DEM simulations are found to match the qualitative trend of the Carman-Kozeny equation. The LB - DEM permeability curve lies between the permeability curves for spherical and cylindrical grain arrangements implying a better simulation of three-dimensional permeability using a 2D granular assembly. Thus using a hydrodynamic radius, realistic 3D fluid - grain interactions can be simulated in a 2D geometry.

6.3 Granular collapse in fluid

The collapse of a granular column, which mimics the collapse of a cliff, has been extensively studied in the case of dry granular material, when the interstitial fluid plays no role (??). The problem of the granular collapse in a liquid, which is of importance for submarine landslides, has attracted less attention (Rondon et al., 2011). Thompson and Hupper (2007) observed that the presence of liquid dramatically changes the way a granular column collapses compared to the dry case. The destabilization of a granular pile strongly depends on the initial volume fraction. For dense packings the granular flow is localized at the free surface of the pile, whereas for loose packings the destabilization occurs in the bulk of the material and has a parabolic profile (Bonnet et al., 2010; Iverson, 2000; Topin et al., 2011).

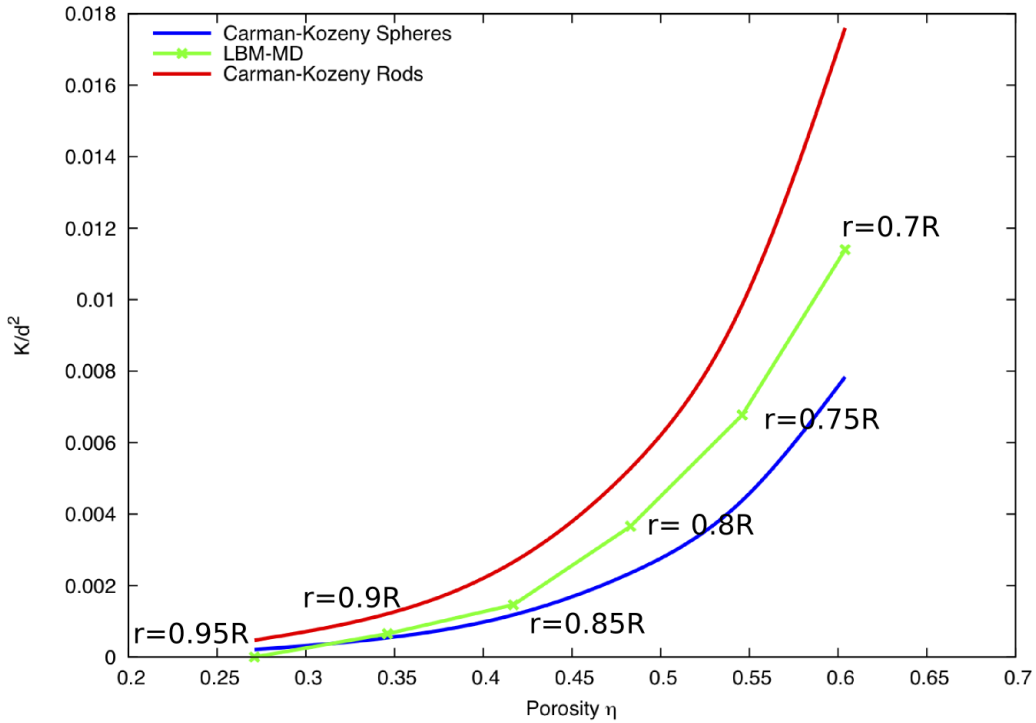
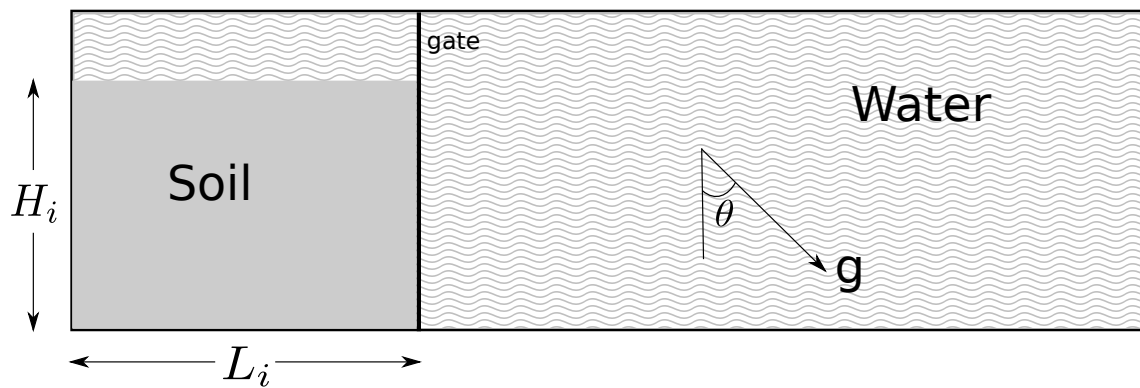


Figure 6.4 Relation between permeability and porosity for different hydrodynamic radius and comparison with the analytical solution.

6.3.1 LBM-DEM set-up

In the present study, the collapse of a granular column in fluid is studied using 2D LBM - DEM. The effect of initial aspect ratio on the run-out behaviour is investigated. The flow kinematics are compared with the dry and buoyant granular collapse to understand the influence of hydrodynamic forces and lubrication on the run-out. Unlike dry column, the permeability and the initial volume fraction are expected to have a significant influence on the flow dynamics. Hence the effect of these parameters on the run-out behaviour is investigated.

The granular column collapse set-up in fluid is very similar to the dry granular column collapse. A rectangular channel of length L_0 and height H_0 is filled with poly-dispersed discs, $d_{max}/d_{min} = 1.8$ (figure 6.5a). Once the DEM soil grains reach equilibrium in the dry condition, the granular sample is then placed in the fluid domain simulated using LBM. The LBM-DEM set-up of a granular column with an aspect ratio a of 6 in fluid is shown in figure 6.5b. The fluid has a density of 1000 kg/m^3 and a kinematic viscosity of $1 \times 10^{-6} \text{ m}^2/\text{s}$. The gate supporting the right-hand side boundary of the granular column is opened allowing the column to collapse and flow in a fluid. The final run-out distance is measured as L_f and final collapse height as H_f . The collapse takes place on a horizontal surface. The initial aspect ratio of the column is varied as 0.2, 0.4, 0.6, 0.8, 1, 2, 4 and 6.



(a) Schematic view of underwater granular collapse set-up.

(b) LBM-DEM simulation of underwater granular collapse set-up ($a = 6$).

Figure 6.5 Underwater granular collapse set-up.

The cumulative β distribution is adopted to generate a distribution of grain sizes ($d_{max} = 2.2$ mm, $d_{min} = 1.25$ mm). The soil column is modelled using ~ 2000 discs of density 2650 kg/m^3 and a contact friction angle of 26° . A linear-elastic contact model is used in the DEM simulations. The granular assembly has a packing fraction of 83%. The critical time step for DEM is computed based on the local contact natural frequency and damping ratio. A sub-cycling time integration is adopted in DEM (??). A fluid flow (LBM) time step of $\Delta t = 2.0 \times 10^{-5}\text{ s}$ is determined based on the viscosity and the relaxation parameter $\tau = 0.506$. An integer ratio n_s , between the fluid flow time step Δt and the DEM time step Δt_D is determined as 15, i.e., every LBM iteration involves a sub-cycle of 15 DEM iterations.

In order to capture the realistic physical behaviour of the fluid – grain systems, it is essential to model the boundary condition between the fluid and the grain as a non-slip boundary condition, i.e. the fluid near the grain should have similar velocity as the grain boundary. The solid grains inside the fluid are represented by lattice nodes. The discrete nature of the lattice results in a stepwise representation of the surfaces (figure 6.6), which are otherwise circular, hence sufficiently small lattice spacing h is required. The smallest DEM grain in the system controls the size of the lattice. In the present study, a very fine discretisation of $d_{min}/h = 10$ is adopted, i.e., the smallest grain with a diameter d_{min} in the system is discretised into 100 lattice nodes ($10h \times 10h$). This provides a very accurate representation of the interaction between the solid and the fluid nodes. A hydrodynamic radius of $0.7 R$ is adopted during the LBM computations. The fluid pressure on the top and right boundaries are maintained constant. Hence, any pressure wave that is generated during the collapse is absorbed in the boundary. Frictional boundary constraint is applied along the bottom boundary.

6.3.2 Collapse in fluid: Flow evolution

Two-dimensional plane-strain LBM-DEM simulations of granular column collapse are performed by varying the initial aspect ratio of the column from 0.2 to 6. The normalized final run-out distance is measured as $\Delta L = (L_f - L_0)/L_0$. Similar to the dry granular collapse, the duration of collapse is normalised with a critical time $\tau_c = \sqrt{H/g}$, where H is the initial height of the granular column and g is the acceleration due to gravity. Dry and buoyant analyses of granular column collapse are also performed to understand the effect of hydrodynamic forces on the run-out distance.

Snapshots of the flow evolution of a granular column collapse with an initial aspect ratio of 0.4 are shown in figure 6.7. The failure begins at the toe end of the column, and the shear-failure surface propagates into the column at an angle of about 50° , similar to the dry column collapse. For the short column, the failure is due to collapse of the flank. Once the

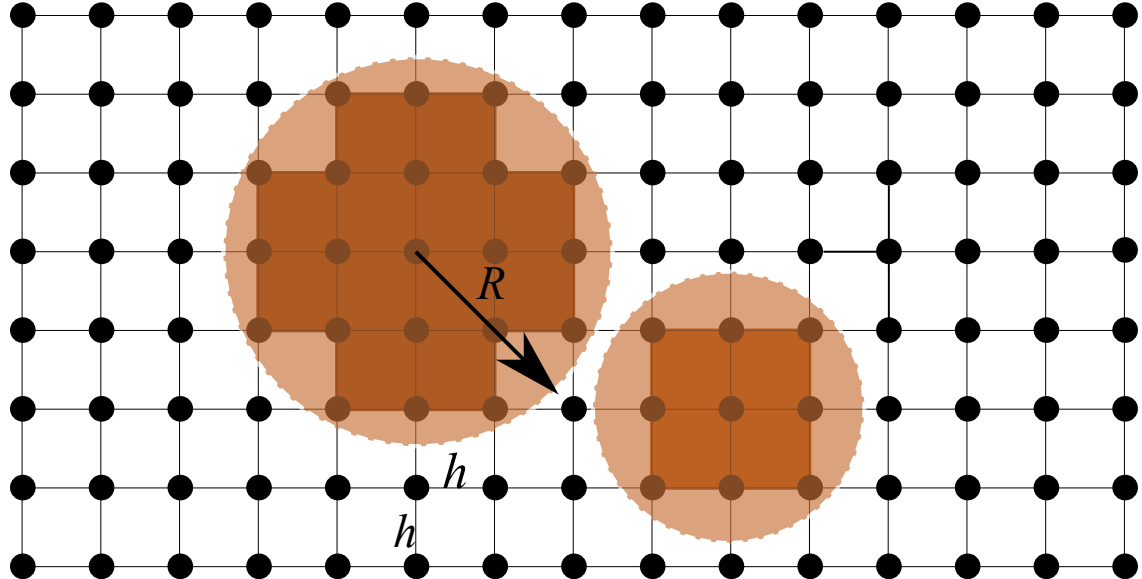


Figure 6.6 Discretisation of solid grains in LBM grid. Shows the step-wise representation of circular disks in the lattice.

material is destabilised, the granular mass interacts with the surrounding fluid resulting in formation of turbulent vortices. These vortices interact with the grains at the surface resulting in an irregular free surface. Force chains can be observed in the static region of collapse, which indicates the granular flow in fluid can still be described using continuum theories. As the granular material ceases to flow, force chains develop at the flow front, revealing consolidation of the granular mass resulting in an increase in the shear strength.

The evolution of normalised run-out $(L_f - L_0)/L_0$ with normalised time t/τ_c for a short column ($a = 0.4$) in dry and submerged conditions is presented in figure 6.8a. The dry column exhibits longer run-out distance in comparison to the submerged column. The collapse of a dry column using DEM represents a collapse in a vacuum, without any influence of drag forces or viscosity of air. A LBM-DEM simulation of a granular column collapse using the kinematic viscosity of air is performed to compare the dry column with the collapse in air. Although the effect of viscous drag can be observed in the collapse in the air, both the “dry” condition and the collapse in air show almost the same run-out behaviour. However, the collapse in fluid (water) results in a much shorter run-out distance. The granular mass in fluid has the buoyant mass, in contrast to the dry density. A dry granular collapse with the buoyant unit weight also exhibits longer run-out behaviour than the collapse in fluid. However, due to decrease in the initial potential energy, the run-out observed in the buoyant condition is shorter than the dry condition. The column collapse in fluid takes longer to evolve, which might be due to the development of large negative pore water pressure that is generated

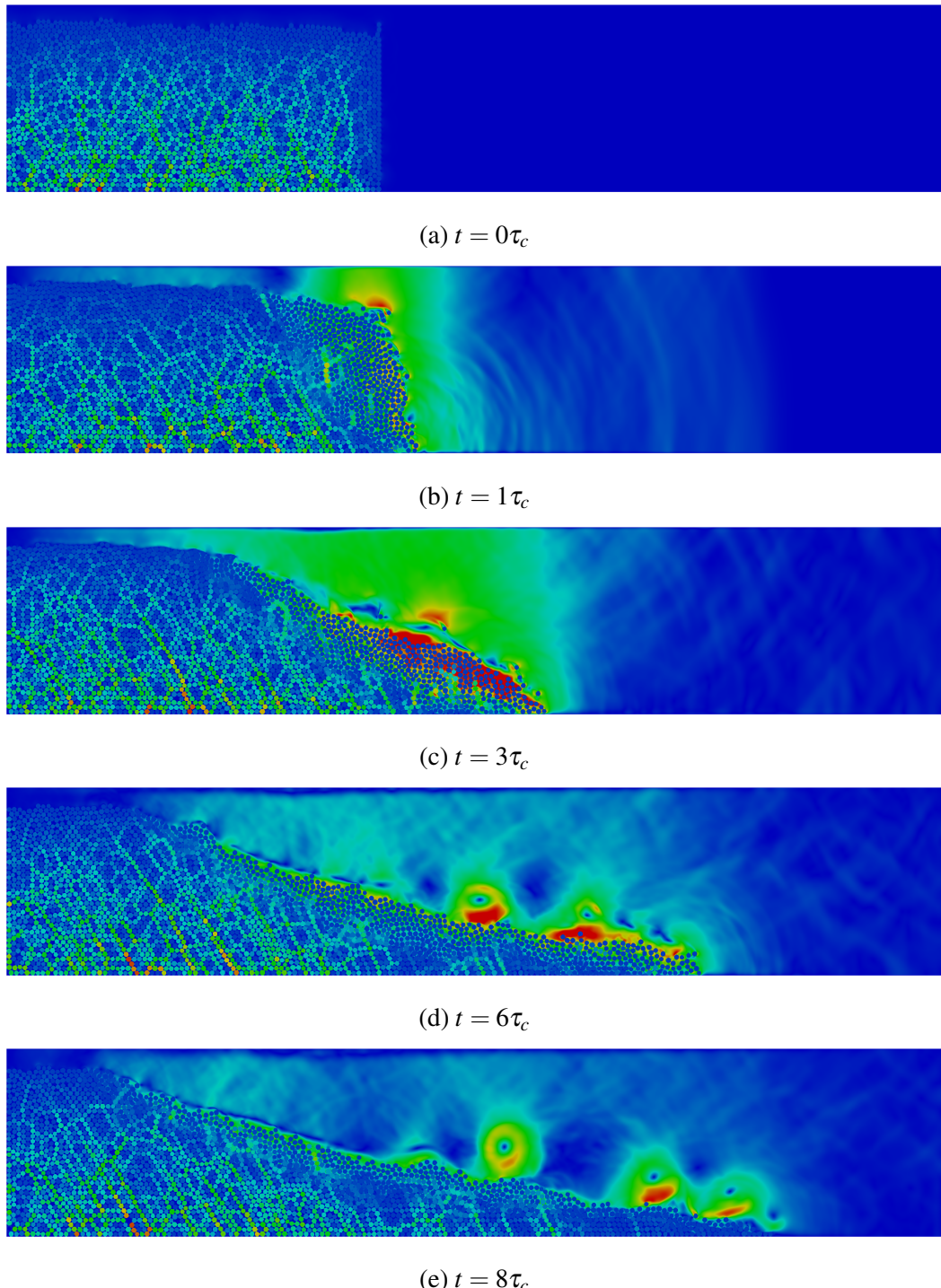
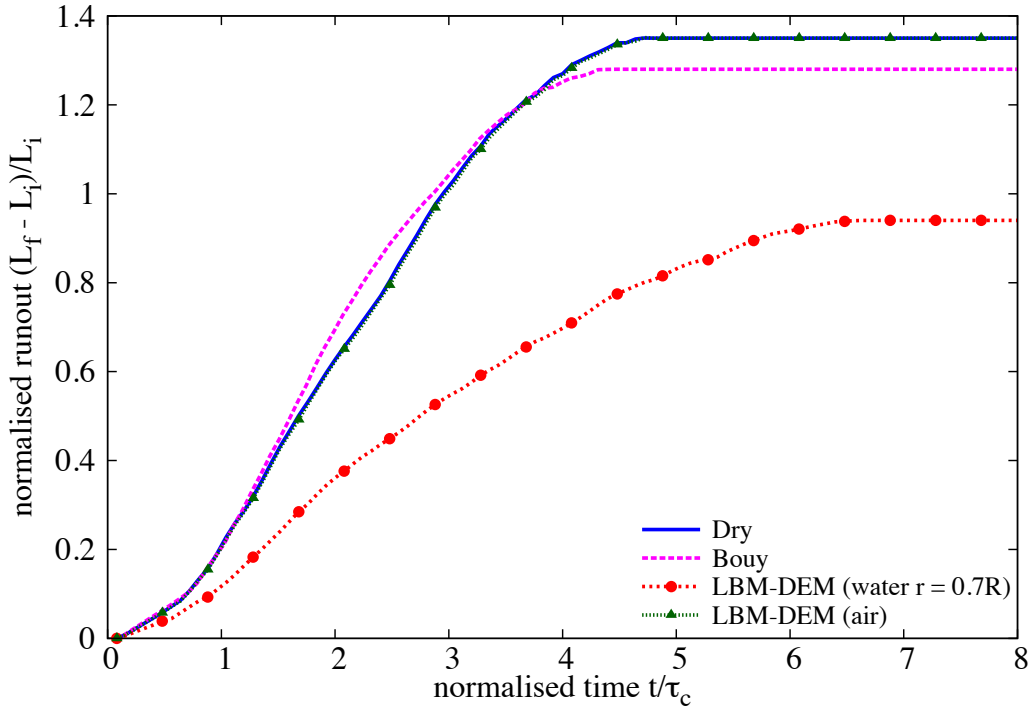


Figure 6.7 Flow evolution of a granular column collapse in fluid ($a = 0.4$). Shows the velocity profile of fluid due to interaction with the grains (red - higher velocity).

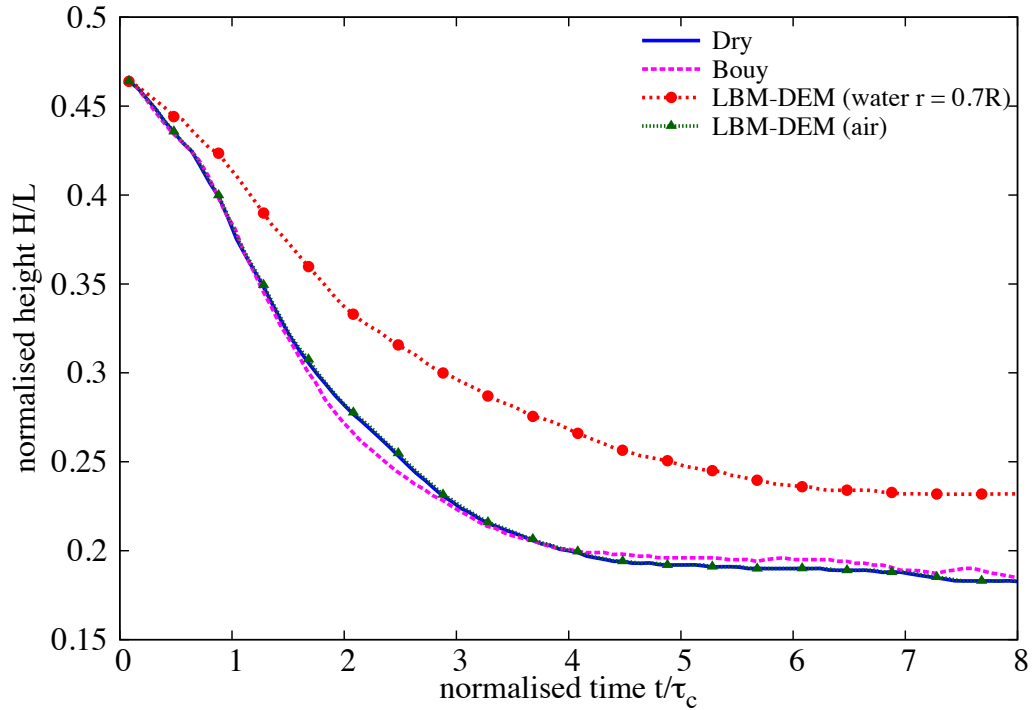
during the shear failure along the shear-failure surface. This large negative pore-pressure has to be dissipated before the granular mass, above the shear-failure surface, can collapse and flow. The shorter run-out distance in the fluid case, in comparison with the dry and buoyant conditions, shows that the collapse in fluid is significantly affected by the hydrodynamic drag forces acting on the soil grains. The evolution of normalised height H/L with time under dry and submerged conditions is presented in figure 6.8b. Since the failure of the column is only at the flank, the central static region remains unaffected. Hence, the final height of the column is the same in both dry and submerged conditions.

The evolution of the normalised kinetic energy E_k/E_{p0} with time under dry and submerged conditions for a column with an initial aspect ratio of 0.4 is shown in figure 6.9. It can be observed that the peak kinetic energy is attained later in the submerged condition than the dry collapse. This can be attributed to the time required to overcome the negative pore-pressure generated during the shear along the shear-failure surface. For short columns the critical time τ_c is controlled by the vertical kinetic energy. The amount of kinetic energy in submerged case is significantly lower than the dry condition. Also, the evolution of the normalised potential energy E_p/E_{p0} with time under dry and submerged conditions is presented in figure 6.10. The potential energy drops faster in dry and buoyant conditions in comparison to submerged condition. This shows a significant influence of the hydrodynamic forces on the amount of material destabilised during the collapse. The drag forces on the soil grains reduce and slow down the amount of material that undergo collapse resulting in a shorter run-out distance for the collapse of short columns in fluid.

Snapshots of the flow evolution of a granular column collapse with an initial aspect ratio of 4 is shown in figure 6.11. For a tall column, the collapse mechanism changes. The entire column is involved in the collapse. The height of the static region, which is below the shear-failure surface, is shorter than the total height of the column. This results in a free-fall of grains above the shear-failure surface. As the grains experience free-fall they interact with the surrounding fluid. However, no vortices are observed during the initial stage of collapse. In the second phase, when the grains reach the base, the vertical velocity gained during the free-fall is converted into horizontal velocity. As the grains are ejected horizontally, the free surface of the granular mass interacts with the fluid resulting in the formation of turbulent vortices. Unlike short columns, these vortices have a significant influence on the mass distribution along the run-out. Heaps of granular material can be observed in front of each vortex. The number of vortices formed during a collapse is found to be proportional to the amount of material destabilised, i.e., the length of free-surface interacting with the fluid influences the number of vortices generated during the collapse. The reappearance of force

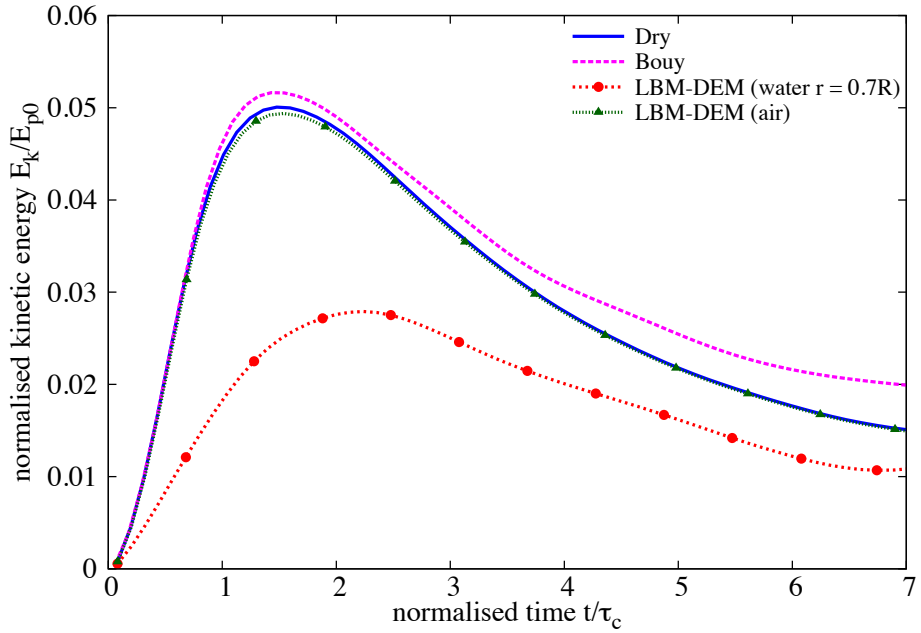


(a) Evolution of run-out with time

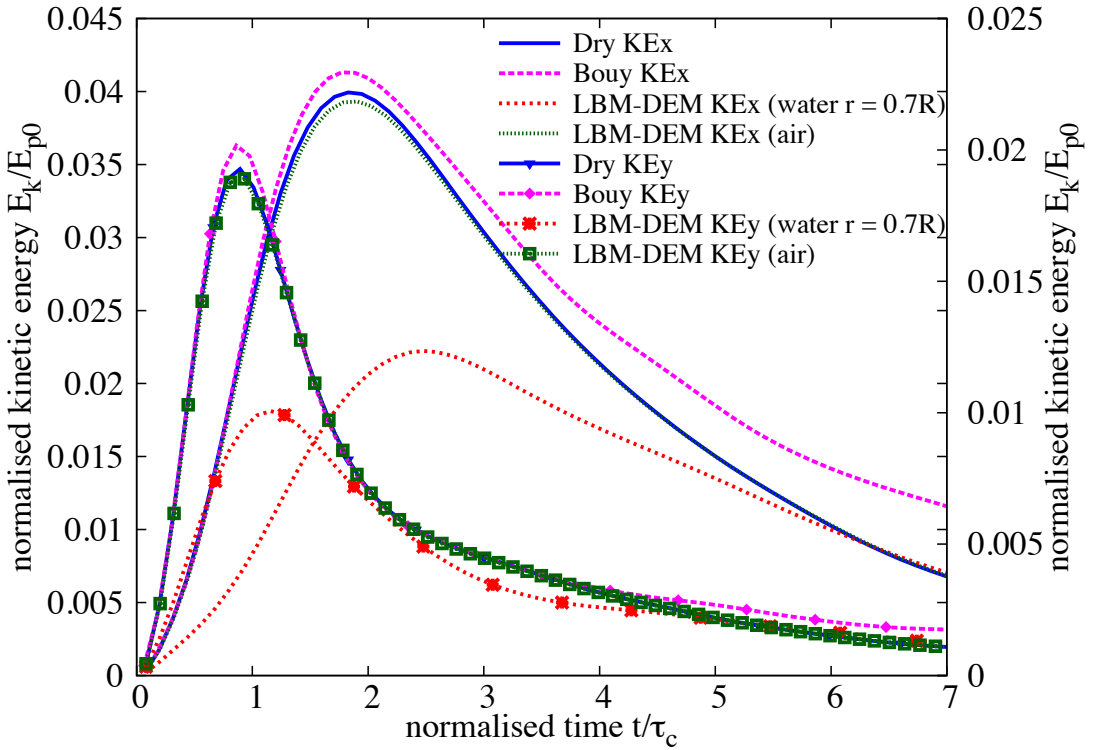


(b) Evolution of height with time

Figure 6.8 Evolution of height and run-out with time for a column collapse in fluid ($a = 0.4$).



(a) Evolution of the total kinetic energy.



(b) Evolution of horizontal and vertical kinetic energies.

Figure 6.9 Evolution of kinetic energies with time for a granular column collapse in fluid ($a = 0.4$)

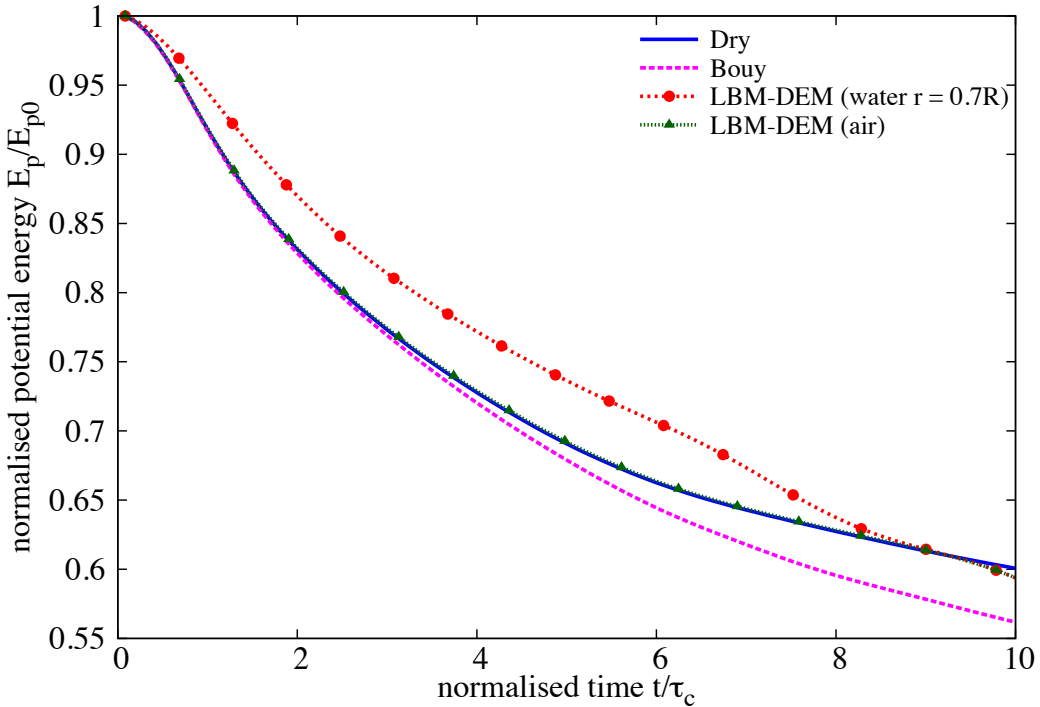
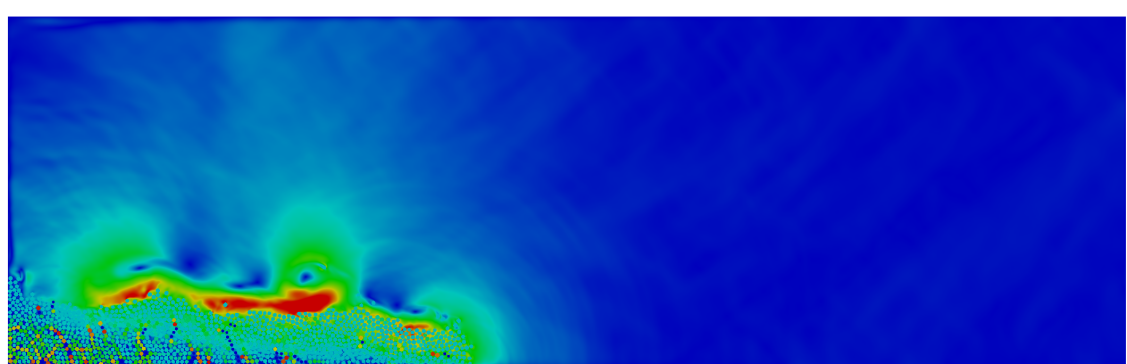


Figure 6.10 Evolution of the potential energy with time for a granular column collapse in fluid ($a = 0.4$)

chains at $t = 6\tau_c$ and $8\tau_c$ indicates the granular mass is consolidating resulting in an increase in the shear strength.

The time evolution of the run-out and the height of a tall column ($a = 4$) is presented in figure 6.12a and figure 6.12b, respectively. Similar to the short column, the run-out observed in the dry condition is much longer than that observed in the submerged condition. Also, the evolution of run-out is slower in the case of submerged condition, which indicates the influence of drag force on the run-out evolution. Figures 6.12b and 6.13 shows the evolution of normalised height and potential energy with time. The submerged column collapse at a slower rate than its dry counterpart. The hydrodynamic forces in fluid causes an increase in the drag force thus reducing the amount of material destabilised during the collapse.

The evolution of kinetic energies with time for an initial aspect ratio 4 is presented in figure 6.14. Even during the free-fall stage, the peak vertical kinetic energy is delayed in the case of fluid, which shows the influence of viscosity on the flow evolution. Almost half of the kinetic energy that is available in the case of dry granular collapse is dissipated through the drag forces experienced by the grains. This shows that the influence of viscous drag on the run-out evolution is significantly higher than the effect of lubrication.

 $t = 0\tau_c$  $t = 1\tau_c$  $t = 3\tau_c$

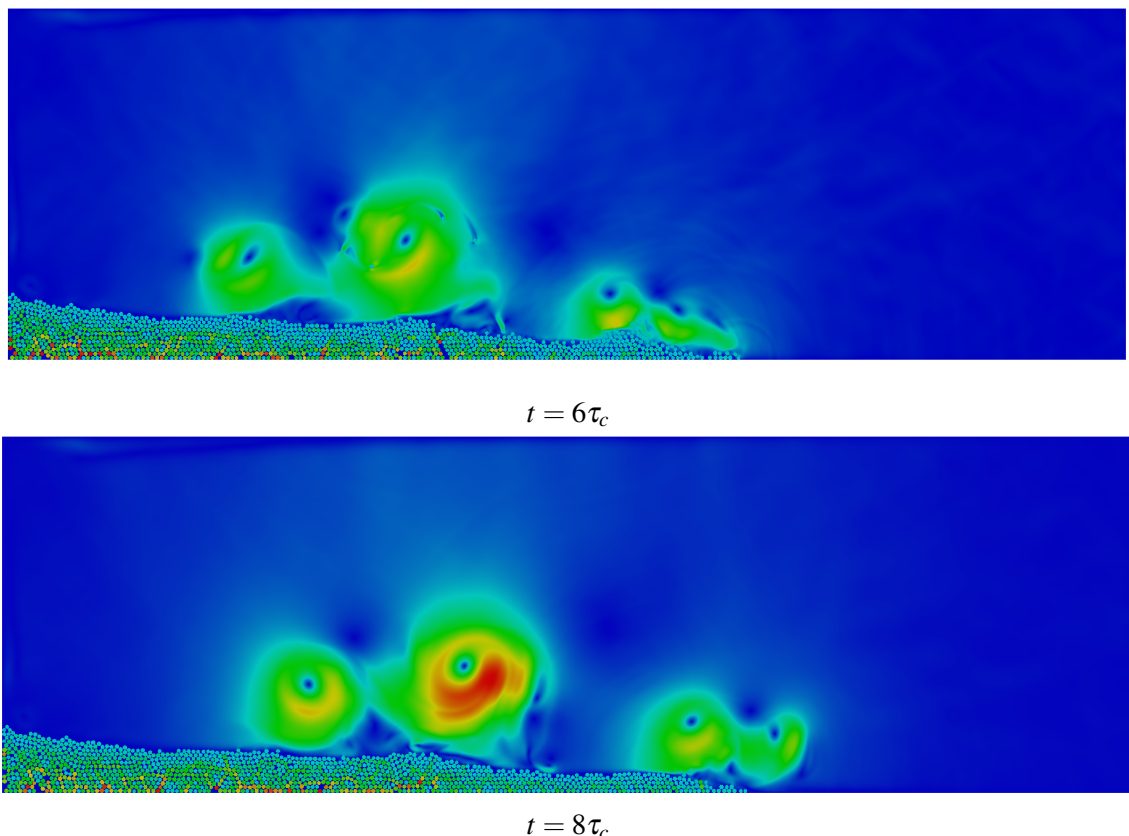


Figure 6.11 Flow evolution of a granular column collapse in fluid ($a = 4$). Shows the velocity profile of fluid due to interaction with the grains (red - higher velocity).

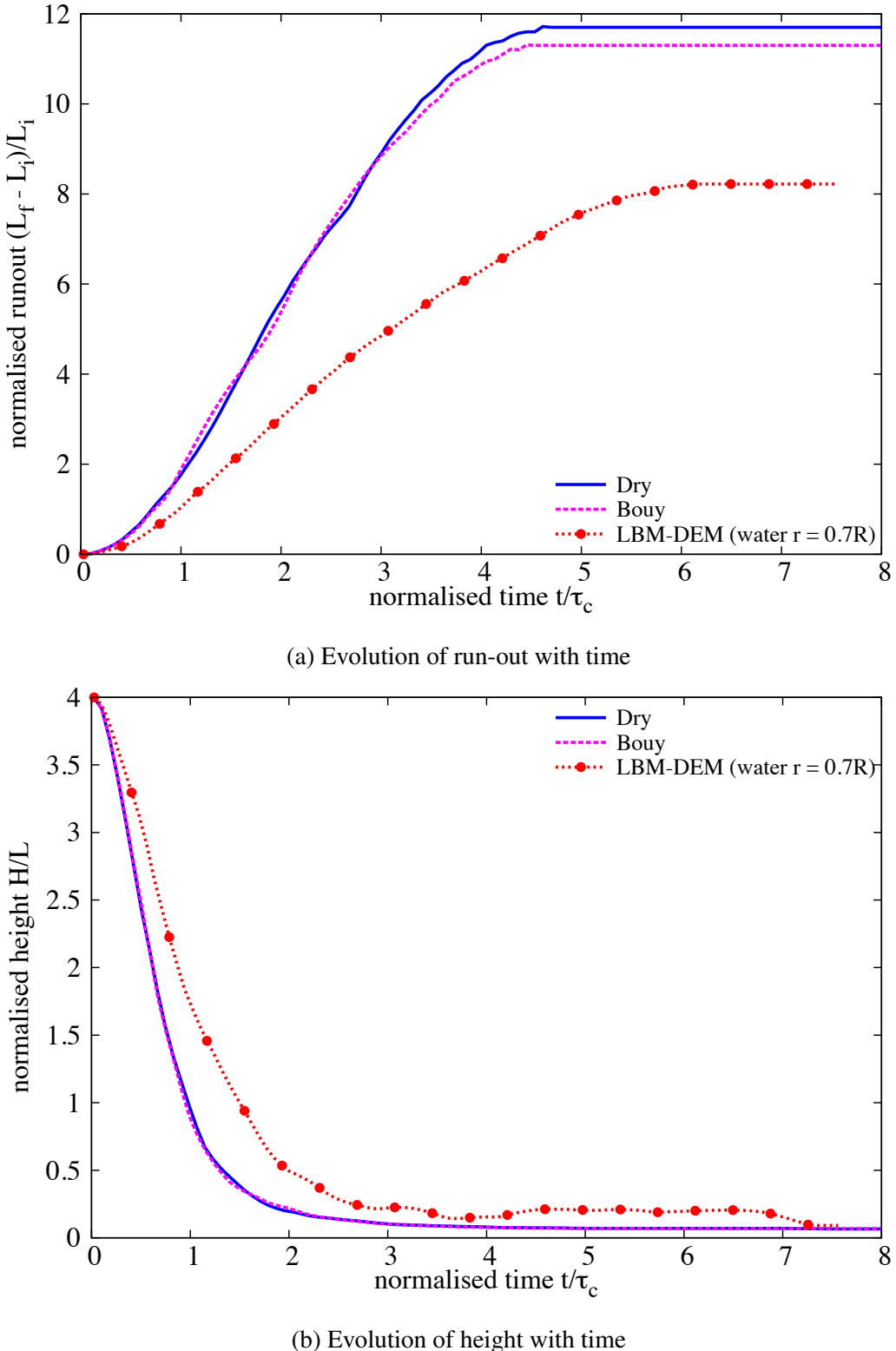


Figure 6.12 Evolution of run-out and height with time for a column collapse in fluid ($a = 4$)

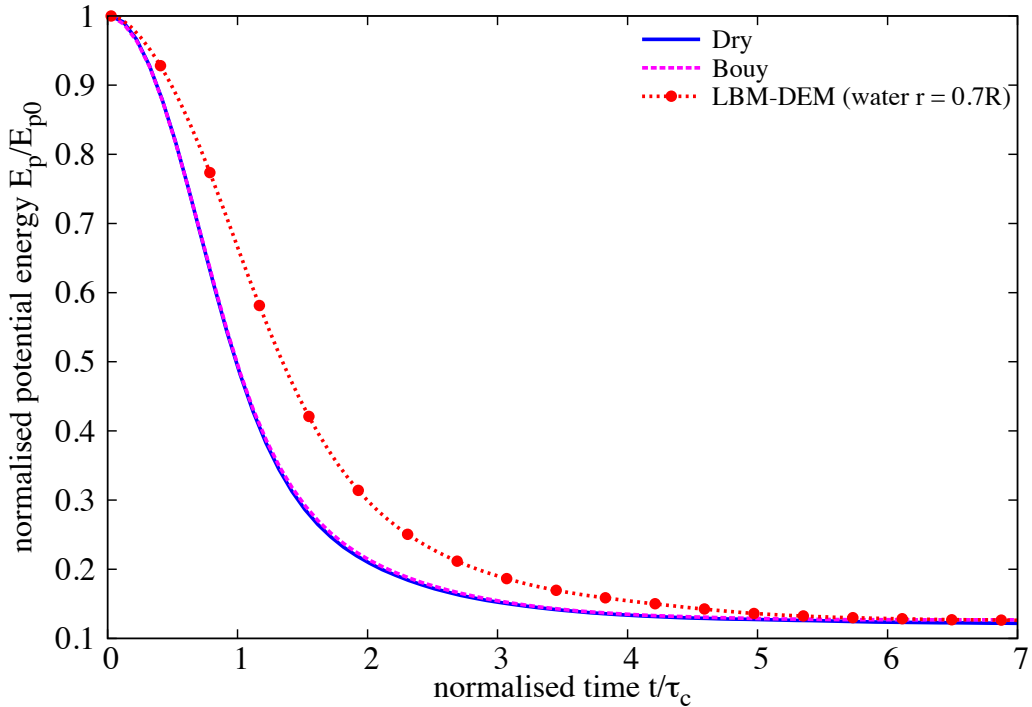


Figure 6.13 Evolution of the potential energy with time for a granular column collapse in fluid ($a = 4$)

The normalised final run-out distance as a function of the initial aspect ratio of the column under dry and submerged conditions is presented in figure 6.15a. For all aspect ratios, the run-out observed in the dry case is significantly higher than the submerged condition. For short columns, the run-out distance is found to have a linear relationship with the initial aspect ratio of the column. A power law relation is observed between the run-out and the initial aspect ratio of the column.

$$\frac{L_f - L_0}{L_0} \propto \begin{cases} a, & a \lesssim 2.7 \\ a^{2/3}, & a \gtrsim 2.7 \end{cases} \quad (6.5)$$

The normalised final height as a function of the initial aspect ratio of the column under dry and submerged conditions is presented in figure 6.15b. It can be observed that the final collapse height is much higher in the submerged condition than the dry collapse. The drag force on the granular column reduces the amount of granular mass participating in the collapse, resulting in a shorter run-out distance. The drag force seems to have a predominant influence on the run-out behaviour than the lubrication effect in fluid.

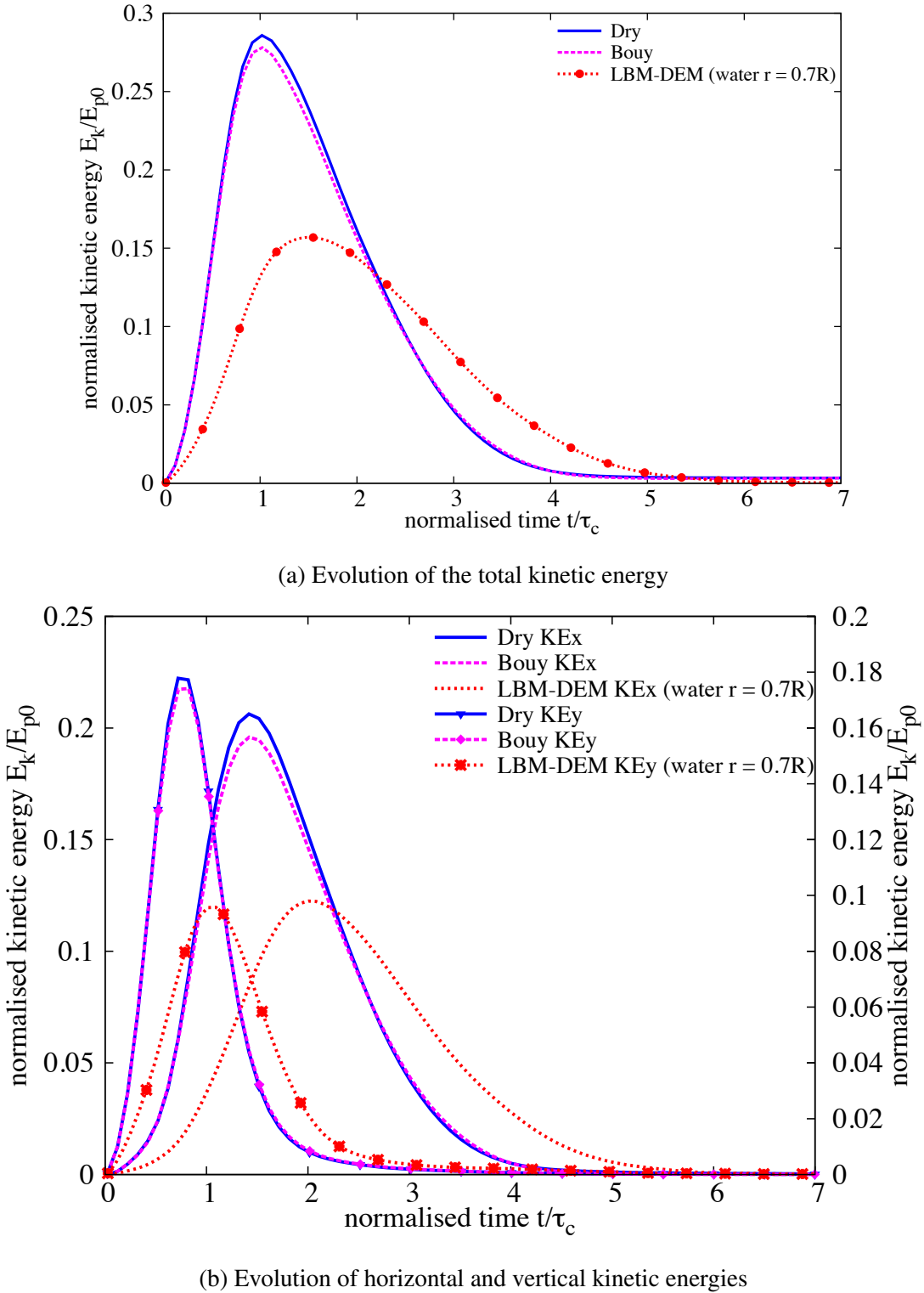
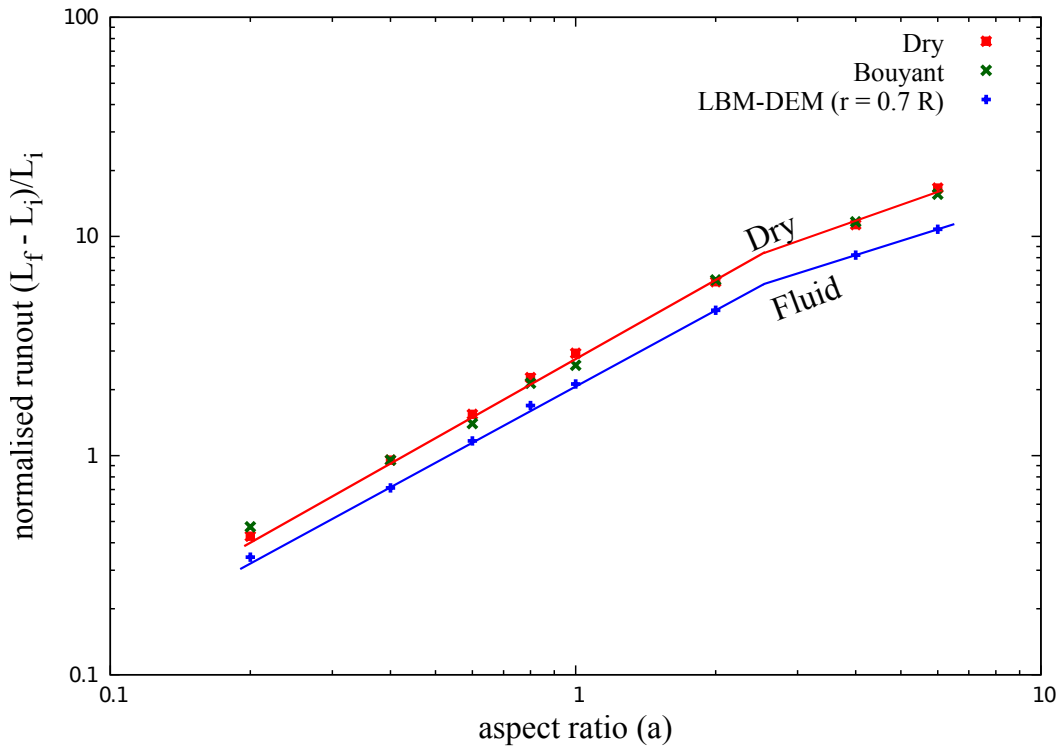
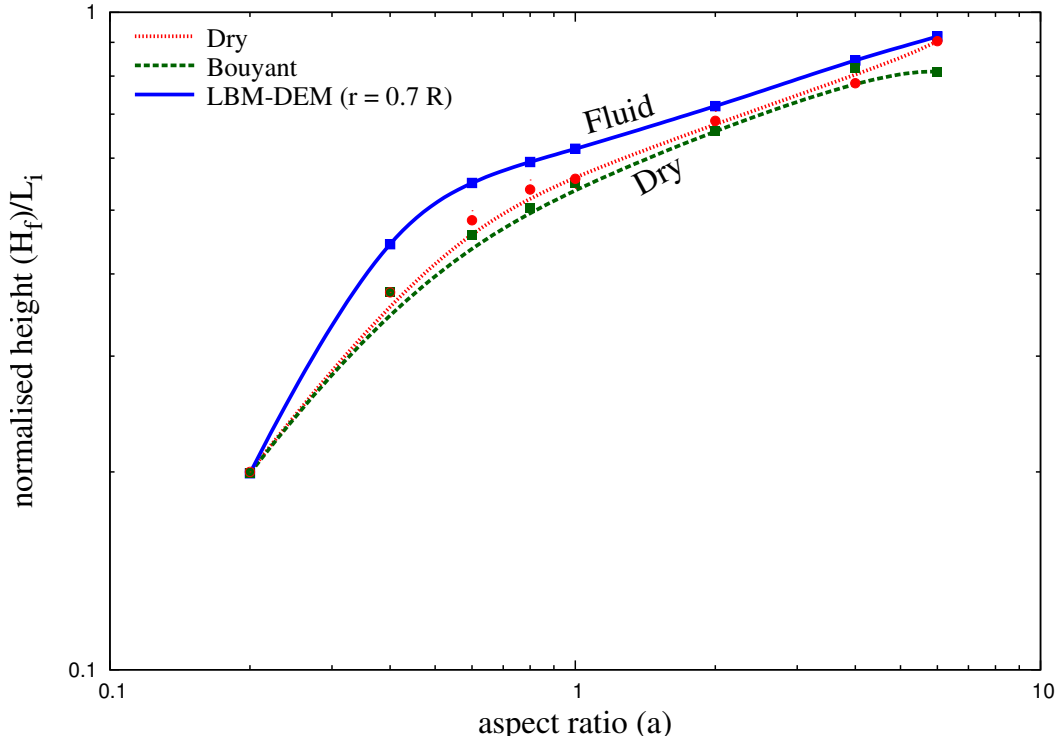


Figure 6.14 Evolution of kinetic energies with time for a granular column collapse in fluid ($a = 4$)



(a) Normalised final run-out distance for columns with different initial aspect ratios. Comparison of dry and submerged granular column collapse.



(b) Normalised final collapse height for columns with different initial aspect ratios. Comparison of dry and submerged granular column collapse.

Figure 6.15 Normalised final collapse run-out and height for columns with different initial aspect ratios.

6.3.3 Effect of permeability

Topin et al. (2011) using Direct Numerical Simulation of underwater granular collapse observed development of large negative pore-pressure during dispersion of grains. The rate of dissipation of the negative pore-pressure is directly proportional to the permeability of the granular assembly. In the previous section, the evolution of run-out with the initial aspect ratio is studied using a constant hydrodynamic radius $r = 0.7 R$. In order to understand the effect of permeability on the run-out behaviour, the hydrodynamic radius r is varied from $0.7 R$ to $0.95 R$ for all aspect ratios. Increase in the hydrodynamic radius decreases the permeability of the granular assembly resulting in a longer duration for the dissipation of negative pore-pressure.

The normalised run-out for different hydrodynamic radii for a granular column with an initial aspect ratio of 0.8 are presented in figure 6.16. The run-out increases with decrease in the permeability, which is equivalent to an increase in the hydrodynamic radius. An increase in the hydrodynamic radius from 0.7 to $0.95 R$ increases the normalised run-out by 25%. However, even under a very low permeability condition ($r = 0.95 R$), the run-out observed in fluid is shorter than the dry and the buoyant conditions.

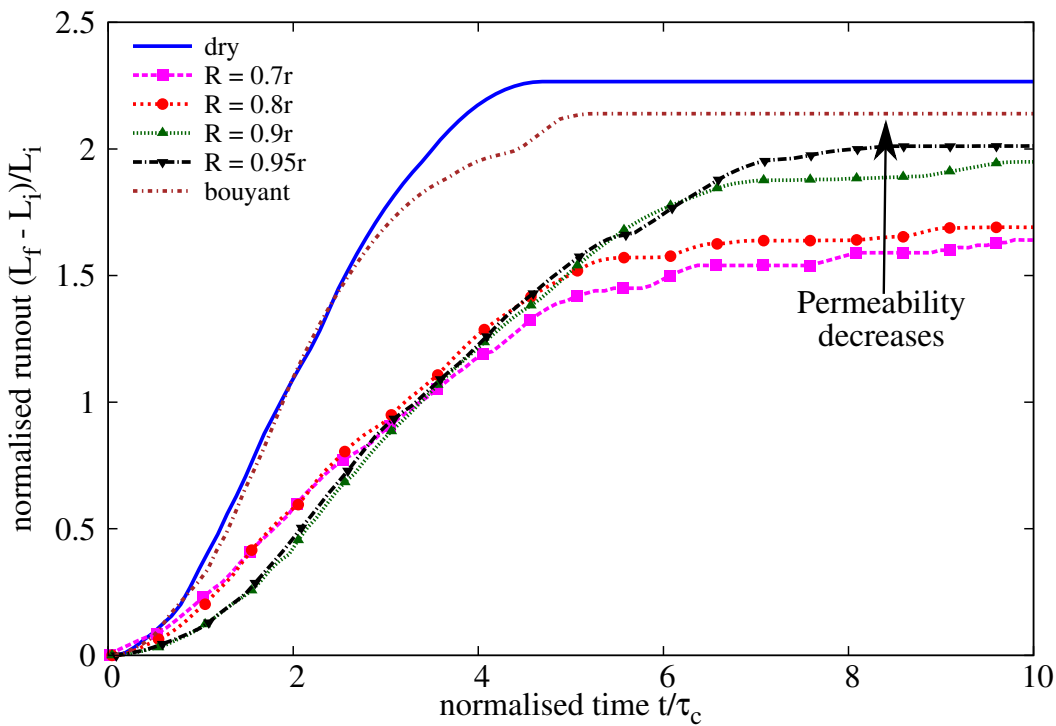


Figure 6.16 Effect of permeability on the evolution of run-out for a column collapse in fluid ($a = 0.8$)

At a high permeability ($r = 0.7 R$), the evolution of run-out at the initial stage is quicker, which means that the negative pore-pressure that is developed during the shearing along the

shear-failure surface is dissipated faster. Even though the negative pore-pressure is dissipated, due to the development of negative pore-pressure the evolution of run-out in fluid is slower than its dry counterpart. The rate of pore-pressure dissipation decreases with decrease in the permeability. This can be observed by a flatter slope in the run-out evolution with decrease in the permeability. Figure 6.17 shows the distribution of pore-pressure in high and low permeability granular media along the horizontal direction at a height of $10 \times d$ from the base. In LBM, the pore-pressure in fluid is a function of fluid density distribution functions. At time $t = \tau_c$, the highly permeable ($r = 0.7 R$) granular column shows smaller negative pore-pressure in comparison to large negative pore-pressures observed in the shearing zone of a low permeable column ($r = 0.9 R$). This shows that not only does it take longer for the pore-pressure to dissipate with a decrease in permeability, but also results in almost twice the negative pore-pressure than what is observed in the high permeable case (figure 6.17b).

Although the low permeability granular columns require a longer duration for the run-out to evolve, the final run-out distance is found to be much longer than in the high permeable condition. Figure 6.18 shows that the potential energy mobilised during the flow of a low permeability column is 20% smaller than the collapse of a high permeability granular column. Normalised kinetic energy evolution with time (figure 6.19) shows that the low permeability column has a wider peak kinetic energy distribution in comparison to a sharp peak observed in the high permeability condition. This indicates the influence of lubrication, i.e., hydroplaning of the granular flow in low permeability conditions. The evolution of the horizontal kinetic energy with time reveals that the peak kinetic energy is sustained longer as the permeability of the granular material decreases (figure 6.19b). Although the peak kinetic energy is smaller in the low permeability case, the hydroplaning of the flowing granular mass results in a longer run-out distance. Figure 6.20b shows the distribution of pore-pressure for a dense granular column collapse in fluid along the bottom plane. A high positive pore-pressure is observed at the base of the granular flow at the flow front in low permeability condition indicating the occurrence of hydroplaning. The positive pore-pressure at the flow front decreases the effective stress thus the creating lubrication effect. The evolution of local packing density with time shows that the packing density decreases with decrease in permeability (figure 6.21). This drop in the value of packing density between $t = 2\tau_c$ and $t = 3\tau_c$ corroborates with the duration of hydroplaning during which a large amount of water is entrained at the flow front.

The high permeability granular column shows lower water entrainment (figure 6.21), which indicates that for highly permeable flows the drag force acting on the soil grains predominates over the lubrication effect on the run-out behaviour. In both the low and high permeable granular flows, the granular material consolidates at the final stage of the flow (figure 6.21). This can be observed by the increase in the packing density at the final stage

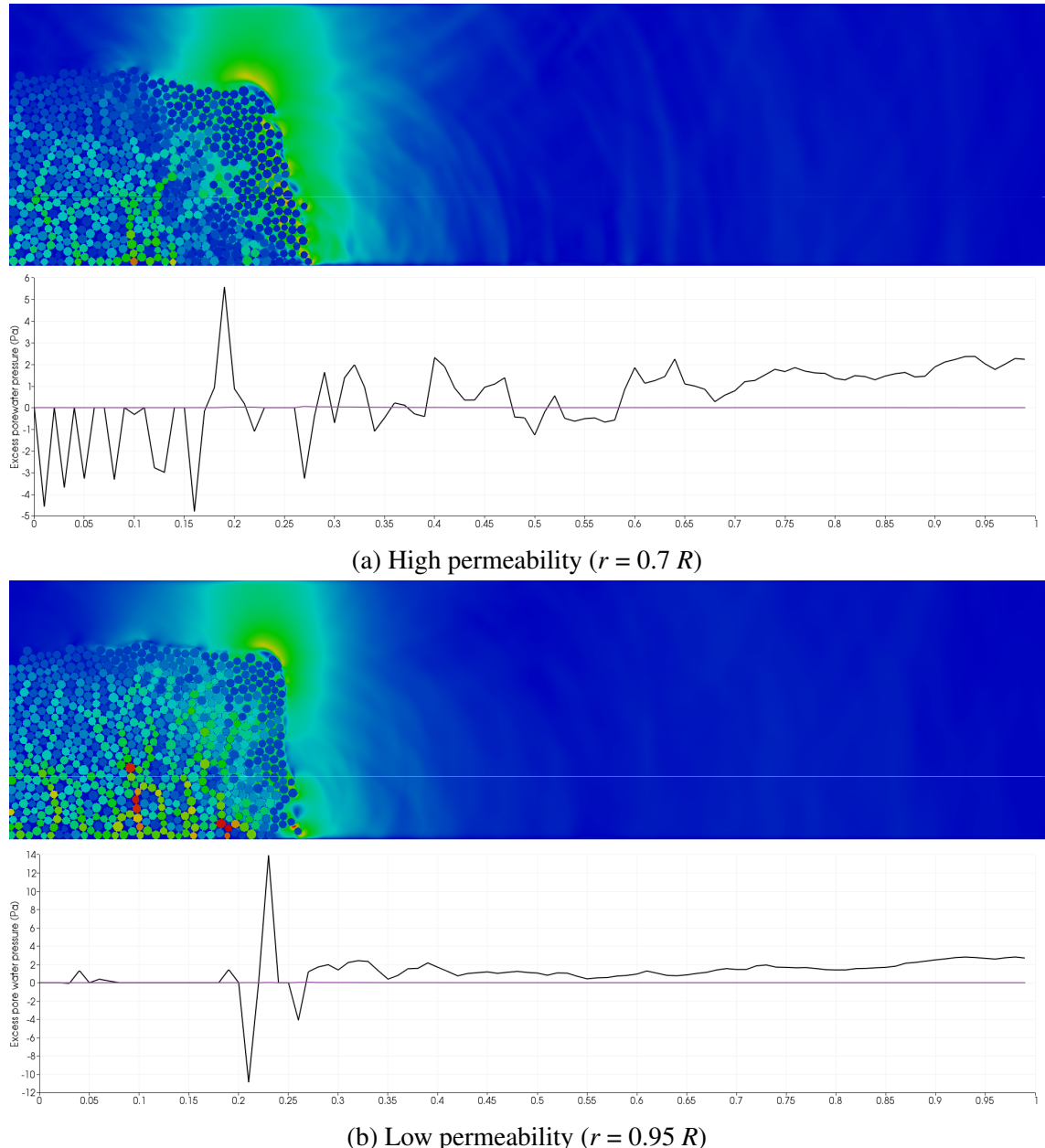


Figure 6.17 Effect of permeability on the excess pore water pressure distribution for a granular column collapse in fluid ($a = 0.8$ & dense packing) at $t = \tau_c$ along the horizontal direction at a height of 10d from the base.

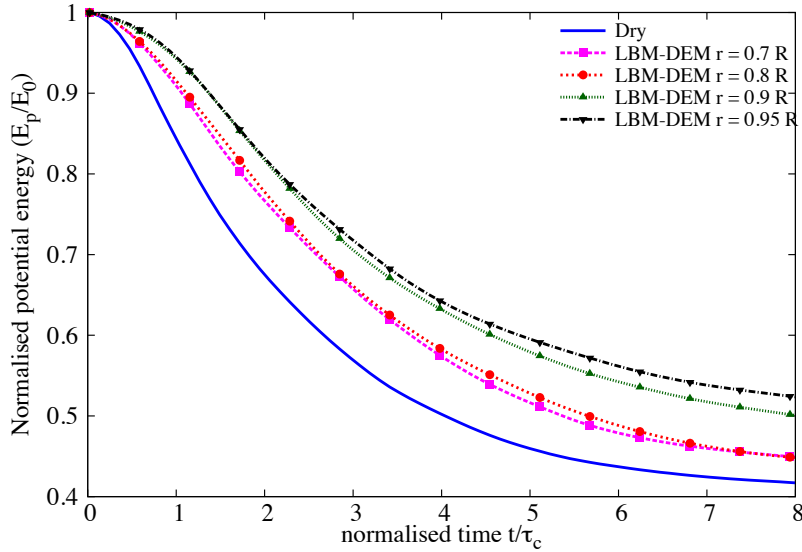


Figure 6.18 Effect of permeability on the evolution of the potential energy with time for a granular column collapse in fluid ($a = 0.8$)

due to settlement of grains and expulsion of entrained water. The final deposit profile for both low and high permeability conditions are shown in figure 6.22. The high permeability collapse shows a more parabolic (convex) deposit profile in contrast to the more concave profile observed in the low permeability condition. In high permeable condition, once the granular mass is mobilised, the drag forces slows down the rate of flow, which allows the grains to densify resulting in a more parabolic profile. This is in contrast to the hydroplaning observed in the low permeability condition, where the granular mass thickness is smaller than the dense condition. The observation of hydroplaning in the low permeable condition may be due to the difference in the distribution of granular mass at the flow front. Instigation of hydroplaning is controlled by the balance of gravity and inertia forces at the debris front and is suitably characterized by the densimetric Froude's number:

$$Fr_d = \frac{U}{\sqrt{(\frac{\rho_d}{\rho_w} - 1)gH \cos \theta}}, \quad (6.6)$$

where U is the average velocity of sliding mass, ρ_d and ρ_w are the densities of soil and water, respectively, H is the thickness of the sliding mass, g is acceleration due to gravity and θ represents the slope angle. Harbitz (2003) observed hydroplaning above a critical value of densimetric Froude's number of 0.4. A Froude's Fr_d value of 0.427 is observed for the low permeable flow ($r = 0.95 R$), which indicates the occurrence of hydroplaning. Whereas, a $Fr_d = 0.273$ is observed for the high permeable granular flow indicating absence

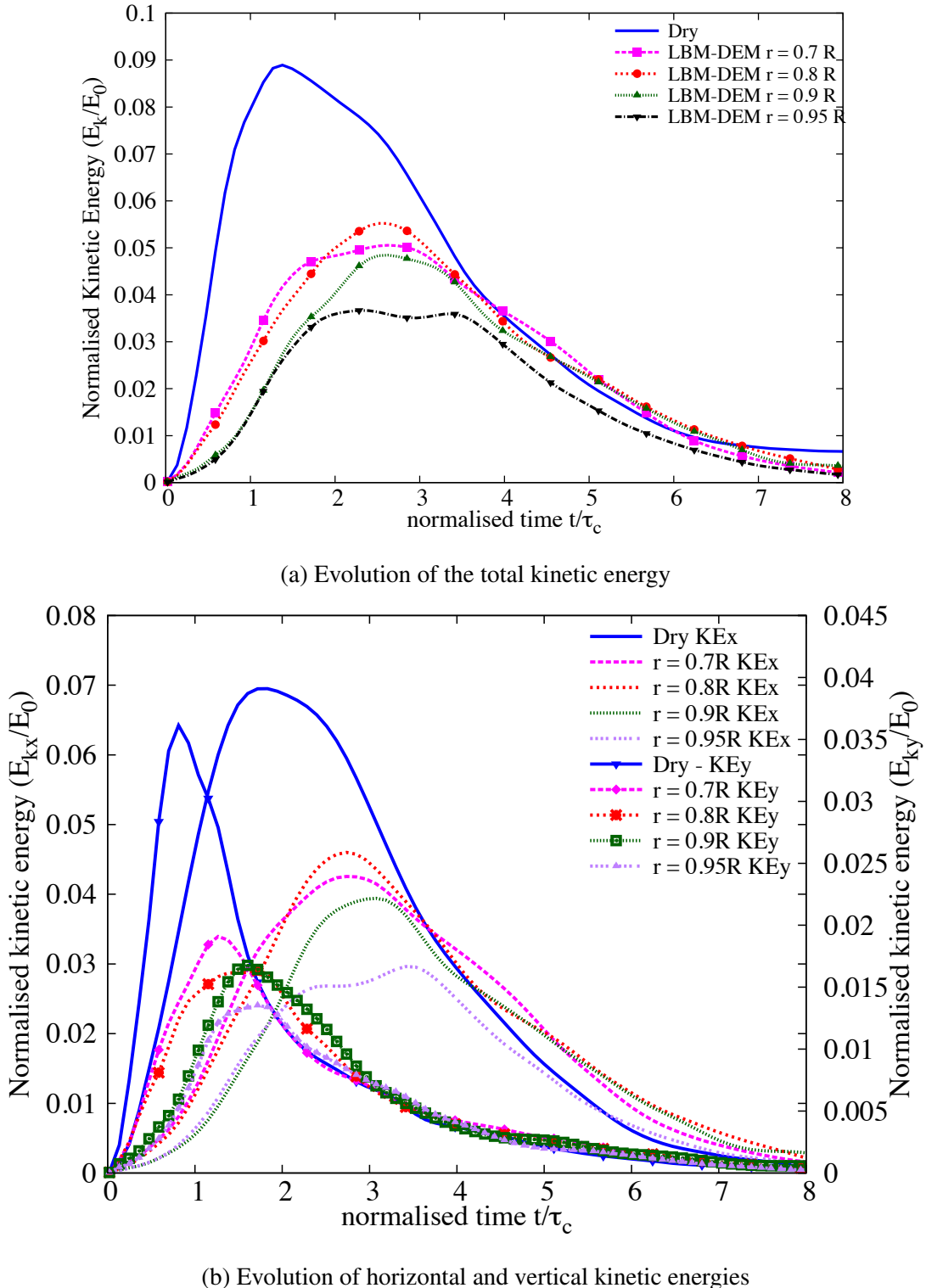


Figure 6.19 Effect of permeability on the evolution of kinetic energies with time for a granular column collapse in fluid ($a = 0.8$)

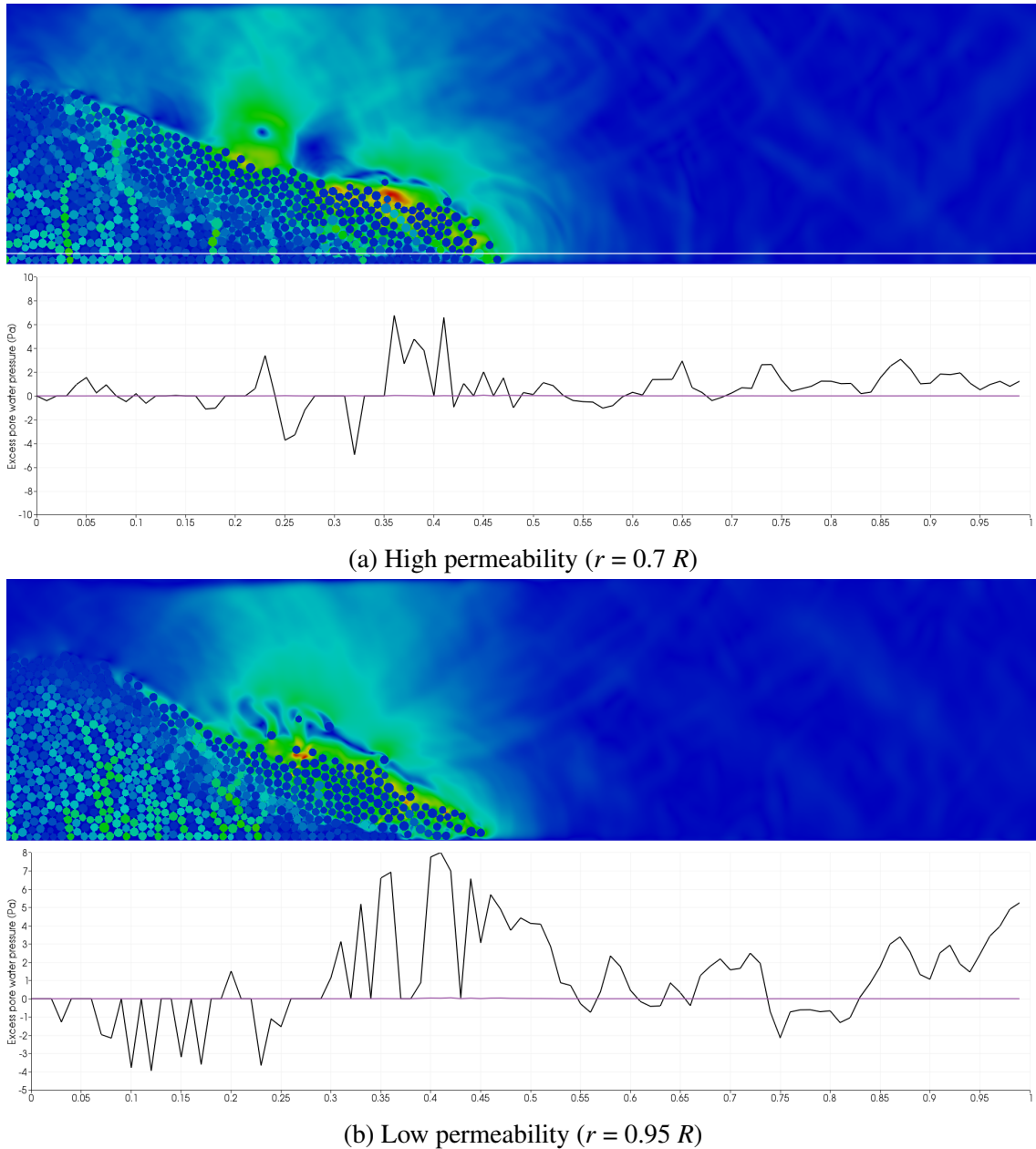


Figure 6.20 Effect of permeability on the excess pore water pressure distribution along the bottom plane for a granular column collapse in fluid ($a = 0.8$ & dense packing) at $t = 2\tau_c$.

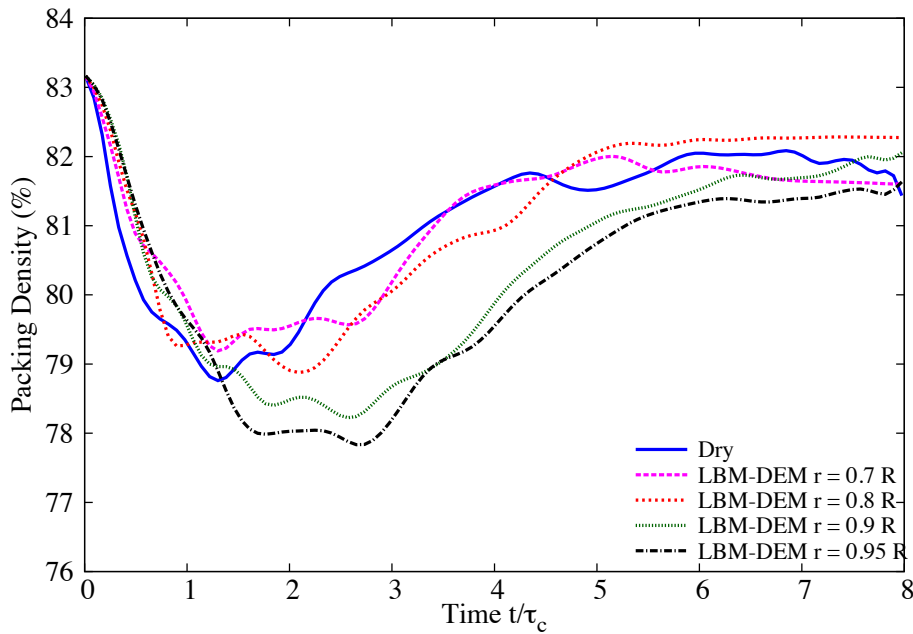
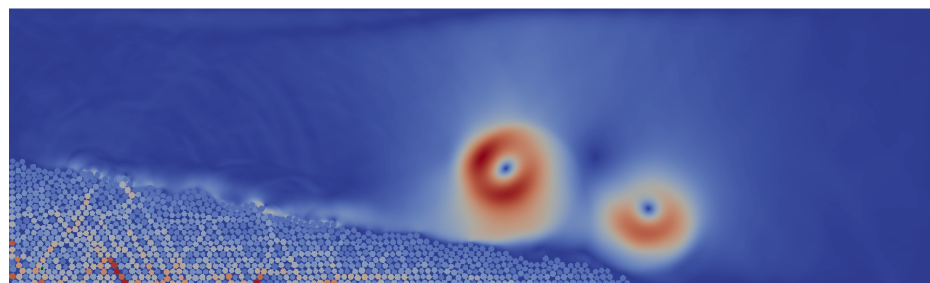


Figure 6.21 Effect of permeability on the evolution of packing density for a granular column collapse in fluid ($a = 0.8$ & dense initial packing)

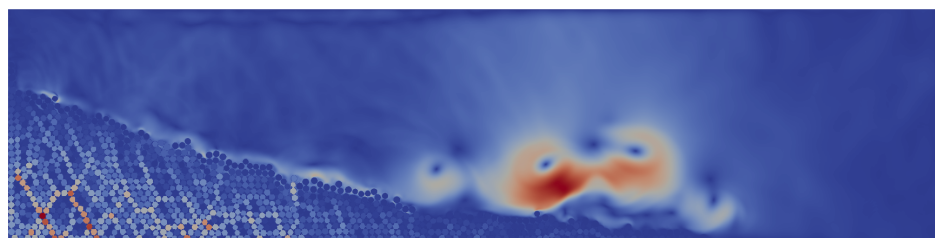
of hydroplaning, the low permeable collapse is predominated by the viscous drag force resulting in a parabolic profile and shorter run-out distance.

The normalised final run-out distance as a function of the initial aspect ratio of the column for different values of permeability and in dry case is presented in figure 6.23. For all aspect ratios, the dry condition yields the farthest run-out distance. For a given aspect ratio, the dry collapse acquires the highest peak kinetic energy due to the lack of viscous dissipation during vertical collapse. This extra kinetic energy is high enough to propel the heap, in spite of a high frictional dissipation, over a distance that is longer than the run-out distance in the fluid regime. In the submerged condition, for the same aspect ratio, the kinetic energy available for spreading is lower and the dissipation due to viscous drag is higher, thus leading to a much shorter run-out distance.

For short columns, with a decrease in permeability the run-out distance increases, however, the run-out distance is not higher than the dry condition. At higher aspect ratios, a decrease in permeability from $r = 0.8 R$ to $r = 0.9 R$ does not have a significant influence on the run-out behaviour. This can be attributed to the turbulent nature of the granular flows for tall columns. The run-out behaviour is a result of transformation of (part of) the initial potential energy to the peak kinetic energy, which in turn controls the subsequent run-out along the plane. For dry and submerged conditions with different values of permeability, the run-out distance is plotted as a function of the normalised peak kinetic energy in figure 6.24. It can be observed



(a) High permeability ($r = 0.7 R$)



(b) Low permeability ($r = 0.95 R$)

Figure 6.22 Effect of permeability on the deposit morphology of a granular column collapse in fluid ($a = 0.8$)

that for the same aspect ratio, the peak kinetic energy is higher in the case of dry column. This represents grain inertial regime in dry granular collapse, which indicates that a part of the potential energy, in the presence of the fluid, is dissipated during the vertical collapse due to viscous friction. In all regimes, the run-out distance increases as a power law $L_f \propto KE_{max}^\gamma$. For the same value of peak kinetic energy, the run-out distance in fluid is longer than the dry column collapse. Also, with a decrease in permeability the run-out distance increases for the same peak kinetic energy.

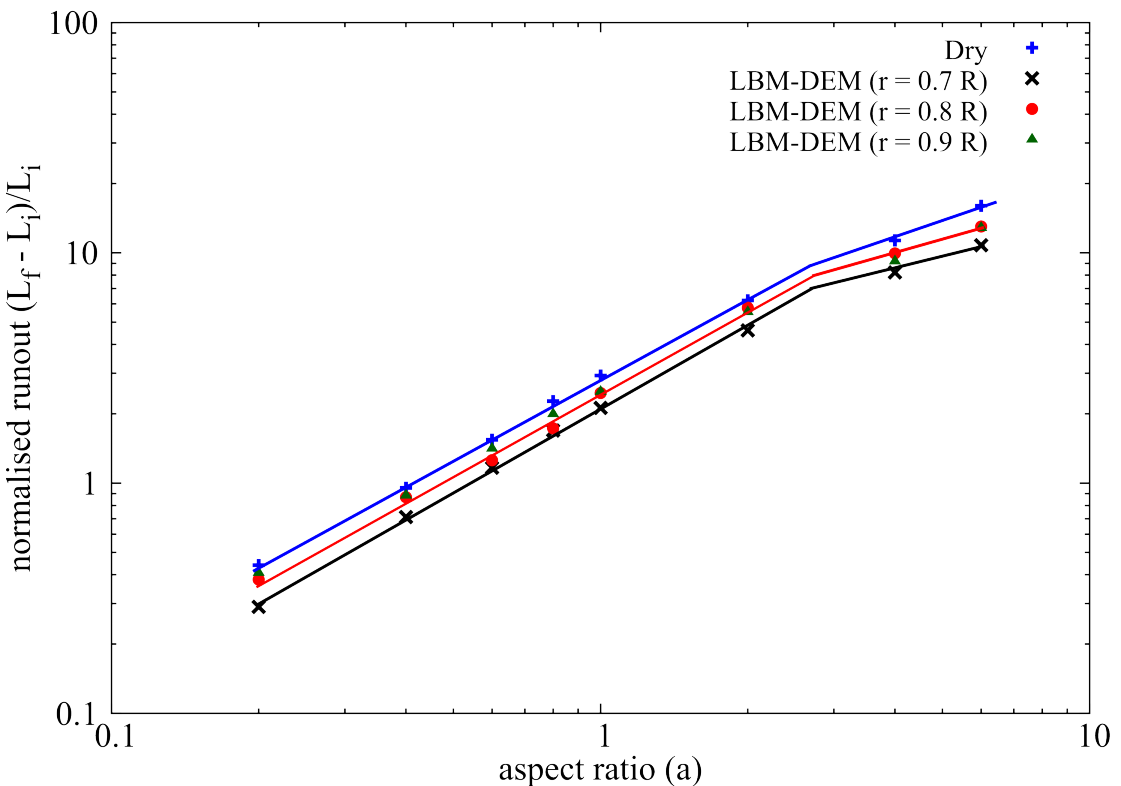


Figure 6.23 Normalised final run-out distance for columns with different initial aspect ratios. Comparison of dry and submerged granular column collapse for different hydrodynamic radius ($0.7 R$, $0.8 R$ and $0.9 R$).

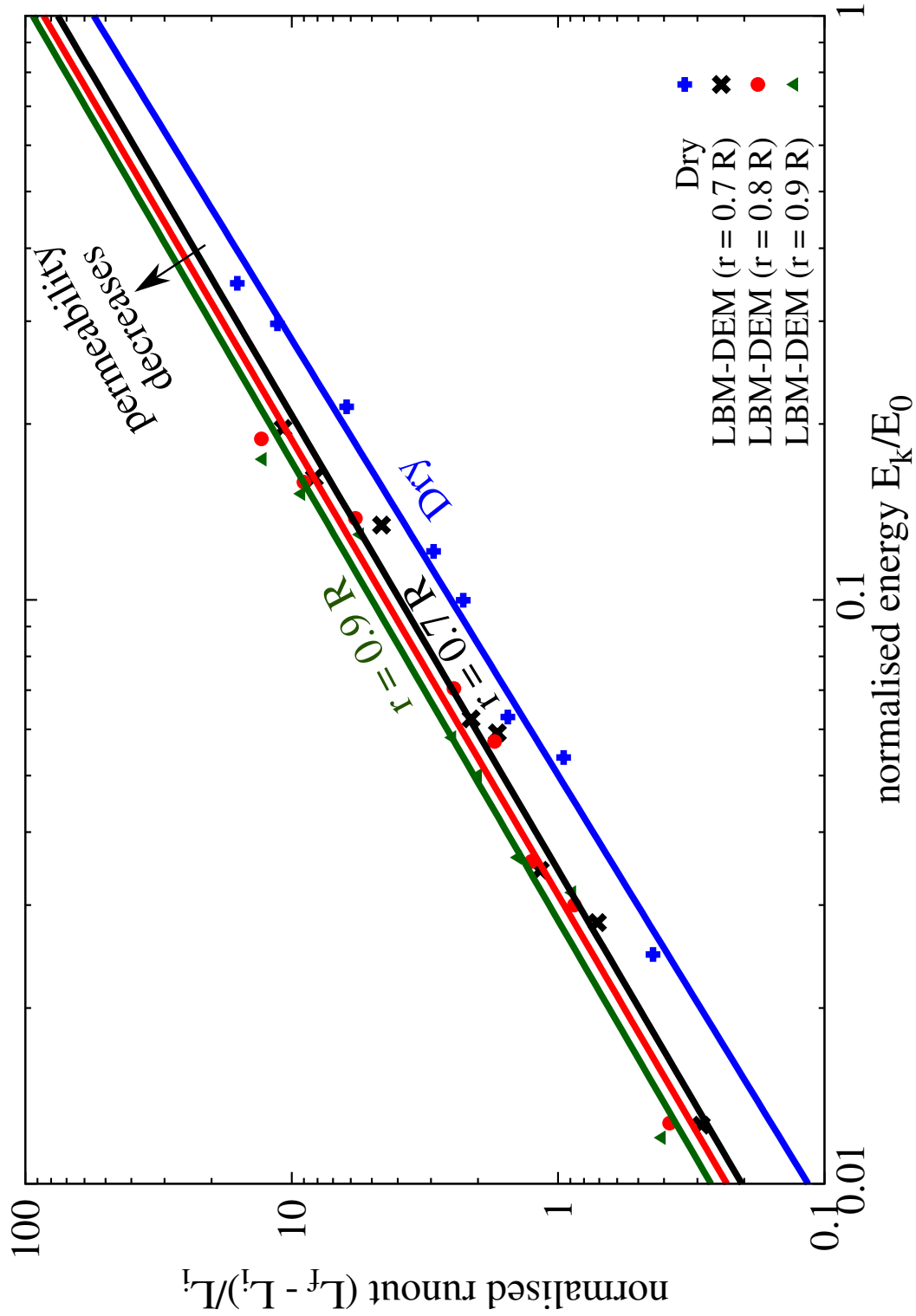


Figure 6.24 Normalised final run-out distance for columns as a function of peak kinetic energy. Comparison of dry and submerged granular column collapse for different hydrodynamic radius ($0.7 R$, $0.8 R$ and $0.9 R$).

6.3.4 Effect of initial packing density

Rondon et al. (2011) observed that the loose packings flow rapidly on a time scale proportional to the initial height and results in longer run-out distance in comparison to the dense packing. Hydroplaning occurs above a critical Froude's number of 0.4. The Froude's number is inversely related to the thickness of the flow and its density. Hence, for the same thickness of flow, a loose granular column will experience more hydroplaning than a dense granular flow. This effect might result in longer run-out behaviour in fluid than the dry condition for the same initial aspect ratio. The initial packing density and the permeability of a 2D granular column, with an aspect ratio of 0.8, are varied to understand their influence on the run-out behaviour. The run-out behaviour of the dense case (83% packing density), discussed in the previous section, is compared with a loose granular column (79% packing fraction). The permeability is varied by changing the hydrodynamic radius from $0.7 R$ to $0.95 R$.

The normalised run-out evolution with time for a loose initial packing (79% packing fraction) with different hydrodynamic radii $0.7 R$, $0.8 R$, 0.9 and $0.95 R$ are presented in figure 6.25. The run-out evolution a column of grains in suspension is compared with the dry and submerged granular columns to understand the influence of hydrodynamic forces on the flow kinematics. Similar to the dense granular column, the run-out distance increases with increase in the hydrodynamic radius (i.e., decrease in permeability). At low permeabilities ($r = 0.9$ and $0.95 R$), the run-out distance is longer than the dry condition. This shows that the lubrication effect in low permeability conditions overcomes the influence of the drag force and the development of large negative pore-pressure resulting in a longer run-out distance. Although the suspended granular masses experience higher drag forces and turbulent effects, the run-out evolves almost at the same rate in comparison with granular columns with high permeability. This shows the effect of permeability on the dissipation rate of negative pore-pressure developed during the initial stage of collapse.

Figure 6.26 shows the development of negative pore-pressure in low permeability ($r = 0.95 R$) and dissipation of negative pore-pressure in high permeability ($r = 0.7 R$) at the same time $t = \tau_c$. This difference in the quantity and the rate of dissipation of negative pore-pressure results in a difference in the rate of flow evolution. A low permeability column requires a longer duration to evolve. Figure 6.27 shows the distribution of the excess pore-pressure along the bottom for low and high permeability conditions. As the flow progresses, the low permeability of the granular column causes hydroplaning to occur at the base of the column, which can be observed by high positive pore-pressure at the base of the flow front, resulting in a longer run-out distance.

The evolution of the potential energy with time (figure 6.28) reveals that at a very low permeability ($r = 0.95 R$), the initial potential energy mobilised is smaller than at $r = 0.9 R$.

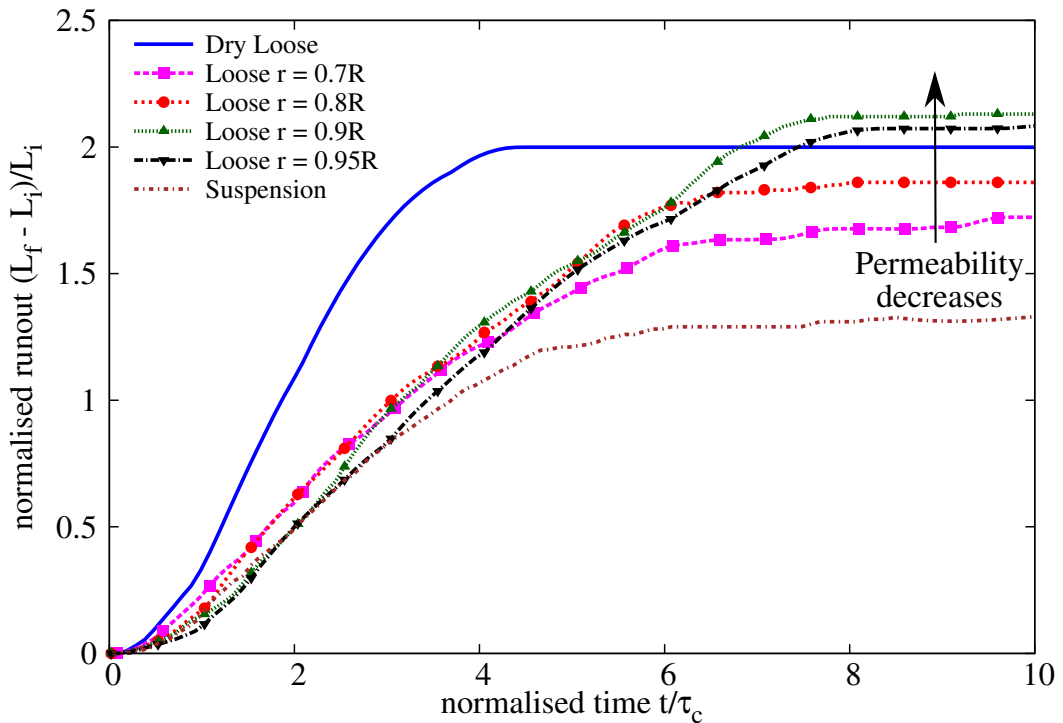


Figure 6.25 Effect of permeability on the evolution of run-out for a column collapse in fluid ($a = 0.8$ & loose packing)

Also with decreasing permeability, the time required to dissipate the negative pore-pressure increases. This results in a shorter run-out distance in the case of $r = 0.95 R$ to that of $r = 0.9 R$. As the quantity of material destabilised is small, the flow is thinner and thus has a high Froude's number (0.59). Figure 6.29b shows that the peak horizontal kinetic velocity observed in the case of $r = 0.9 R$ is higher than $r = 0.95 R$. A Froude's number of 0.59 for $r = 0.9 R$ is observed in contrast to 0.46 for $r = 0.95 R$. Both values of hydrodynamic radii result in a Froude's number that indicate the occurrence of hydroplaning. However, the difference in the amount of material destabilised for $r = 0.95 R$ and the decreased effect of hydroplaning results in a shorter run-out distance for $r = 0.95 R$ in comparison to $r = 0.9 R$.

Figure 6.30 shows the evolution of packing fraction with time for different values of permeability. As the column collapses, water is entrained at the flow front. This can be observed by the decrease in the packing fraction during $t = \tau_c$ and $t = 3\tau_c$. As the flow progresses, the entrained water is expelled and the soil grains consolidate to reach a critical packing density at the end of the flow. The permeability (i.e., hydrodynamic radius) plays a crucial role in the rate of dissipation of the entrained water. As the permeability decreases, the water entrained at the flow front takes longer time to be dissipated resulting in lubrication of the flow at

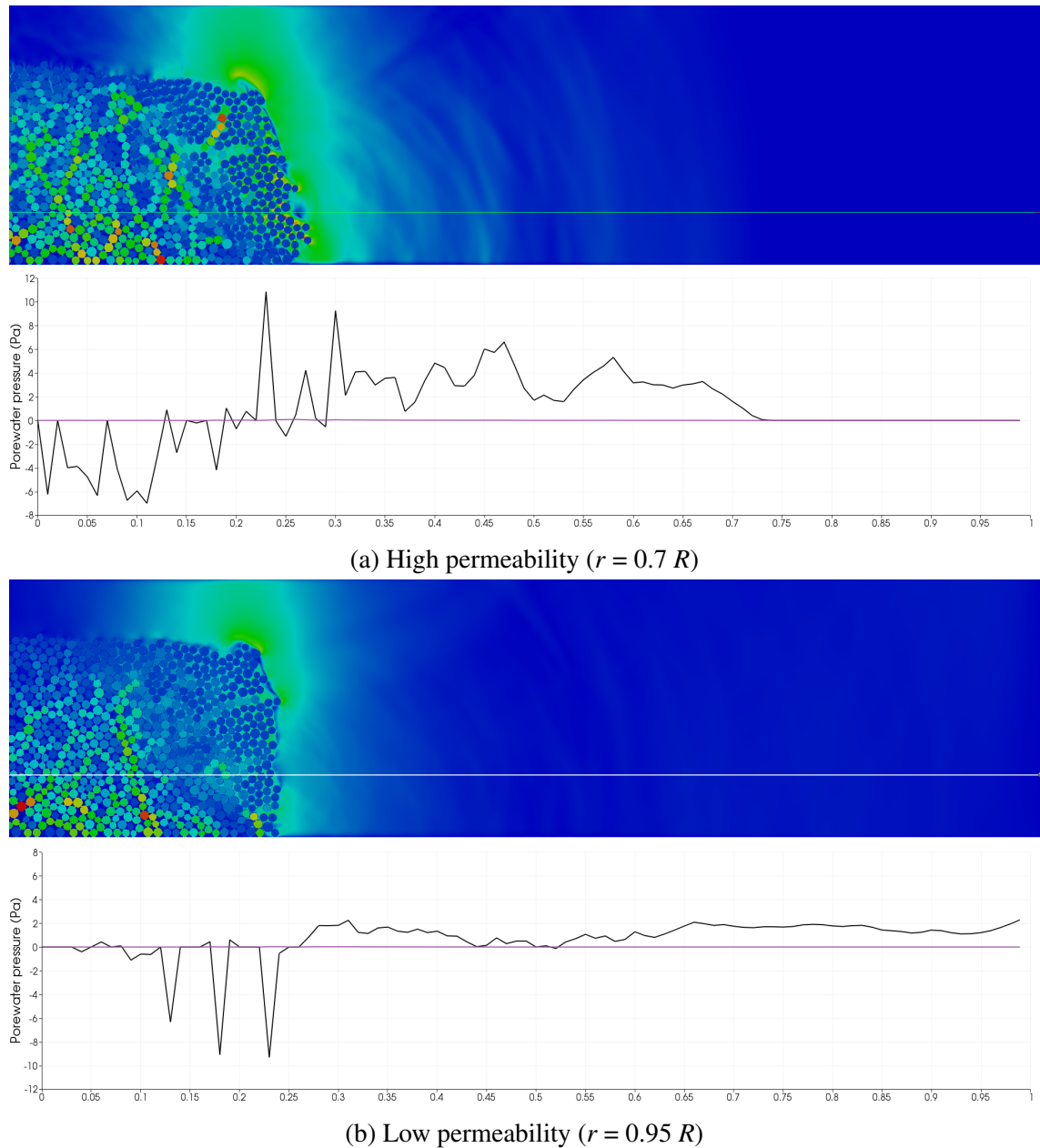


Figure 6.26 Effect of permeability on the excess pore water pressure distribution along the base of a granular column collapse in fluid ($a = 0.8$ & loose packing) at $t = \tau_c$

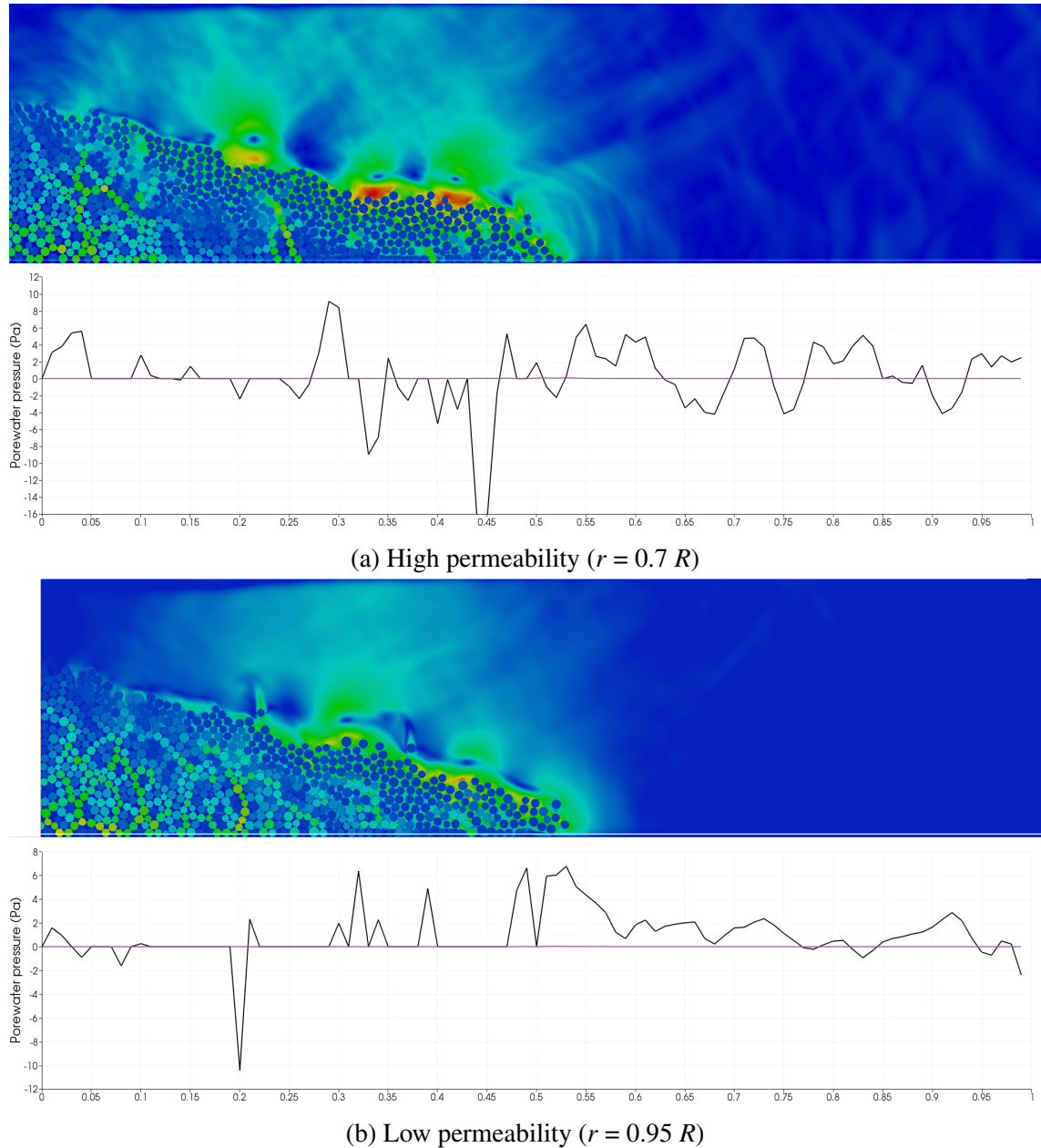


Figure 6.27 Effect of permeability on the excess pore water pressure distribution for a granular column collapse in fluid ($a = 0.8$ & loose packing) at $t = 2\tau_c$

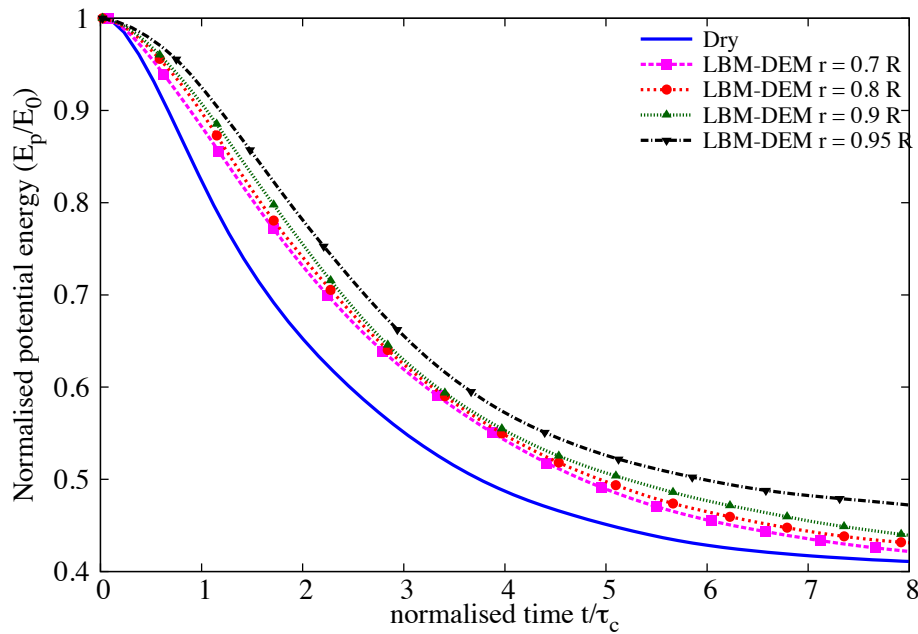
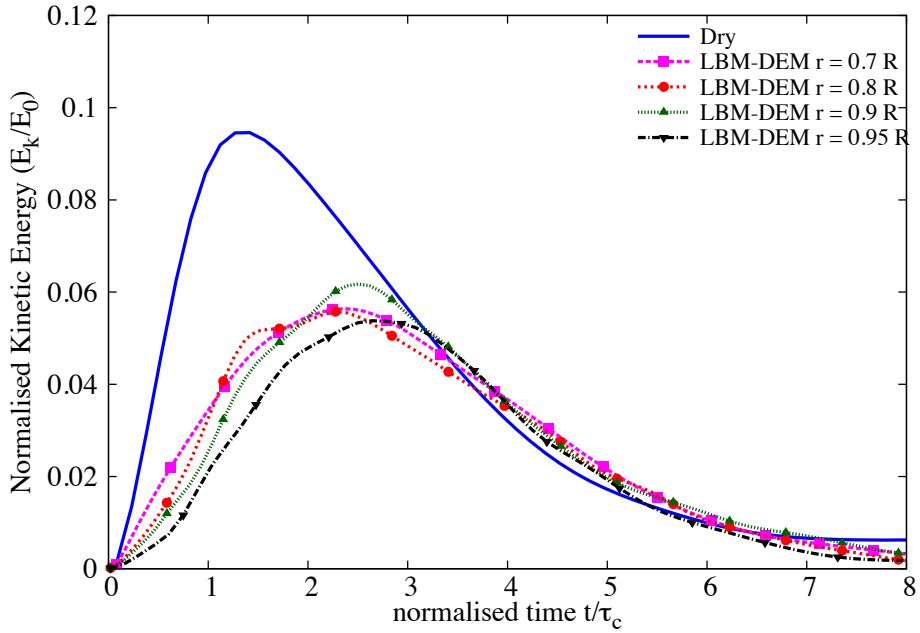


Figure 6.28 Effect of permeability on the evolution of the potential energy with time for a granular column collapse in fluid ($a = 0.8$ & loose packing)

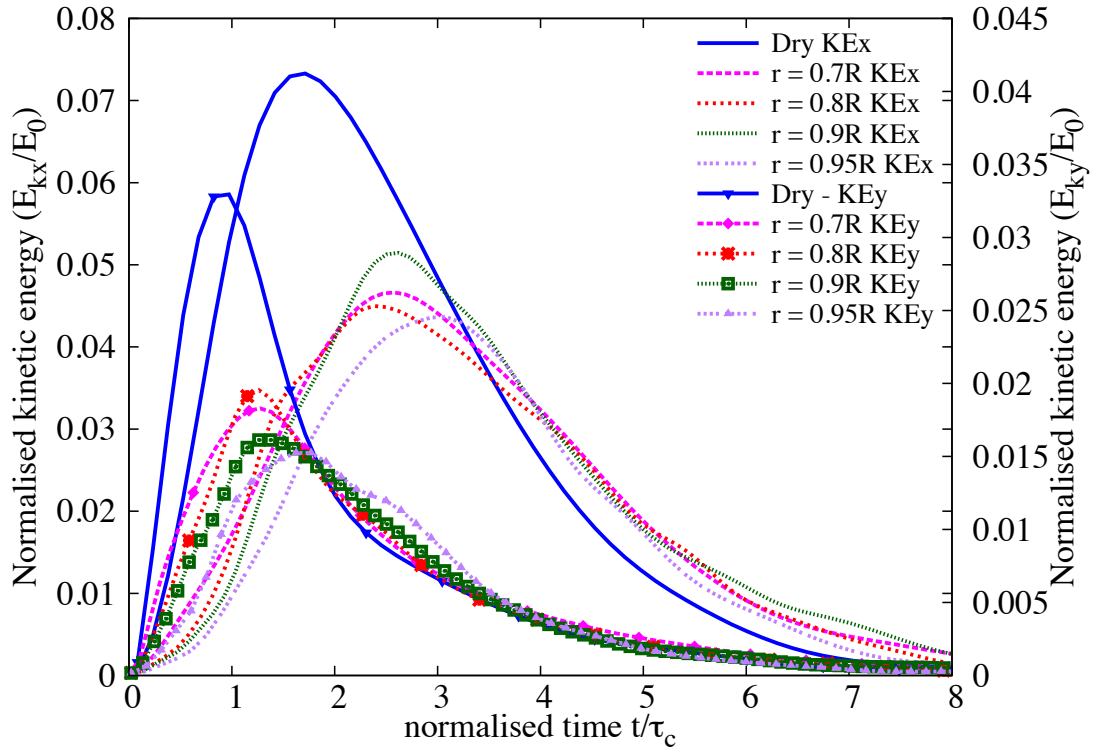
low permeabilities. This lubrication effect results in an increase in the run-out distance for columns with low permeabilities.

The evolution of grain trajectories with time are presented in figure 6.31 for low ($r = 0.95 R$) and high ($r = 0.9 R$) permeability conditions. It can be observed that a high permeability column shows a parabolic (convex) final profile in contrast to the more concave profile observed in low permeability condition, due to the effect of drag forces on the flow front. This difference in the flow thickness results in a higher value of Froude's number (0.59) and the occurrence of hydroplaning in the low permeability condition. Due to the high permeability, the water entrained at the flow front is dissipated quicker and thus no lubrication effect is observed. A Froude's number of 0.272 (no hydroplaning) is observed for the high permeability condition ($r = 0.7 R$). The thick flow front in dense condition results in higher effective stress, in contrast to the low effective stress in loose condition due to positive pore-pressure at the flow front. The higher effective stress results in more frictional dissipation in dense condition, while the loose column experiences lubrication effect. This shows that the drag force predominates at high permeability, while the low permeability condition is characterised by hydroplaning and lubrication.

Figure 6.32 shows the normalised pressure at the base for the low and high permeability flows at $t = 2\tau_c$. The normalised effective stress plotted is obtained as the average over 5 time steps at $2\tau_c$. The effective stress at the base is normalised to the effective stress of a



(a) Evolution of the total kinetic energy



(b) Evolution of horizontal and vertical kinetic energies

Figure 6.29 Effect of permeability on the evolution of kinetic energies with time for a granular column collapse in fluid ($\alpha = 0.8$ & loose packing)

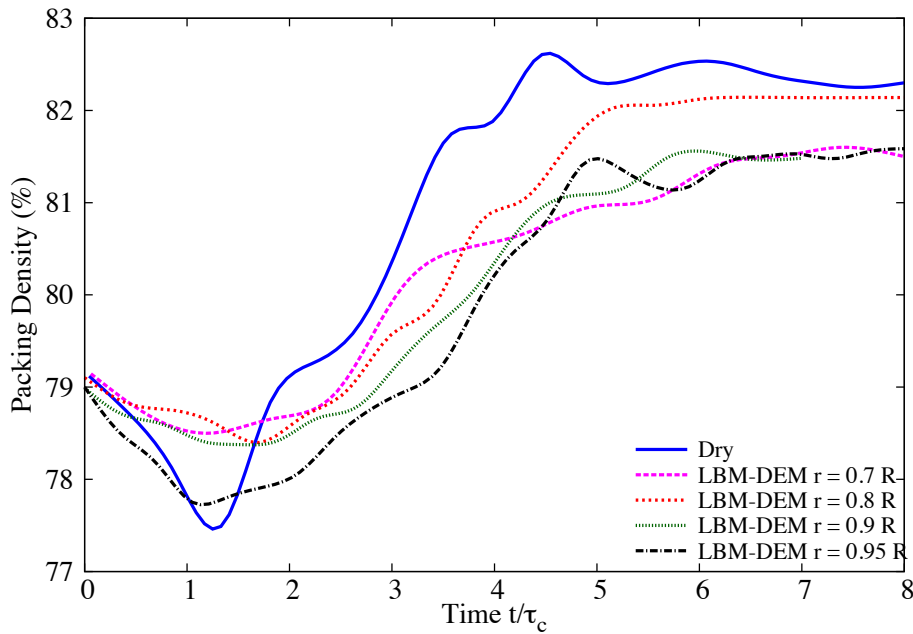
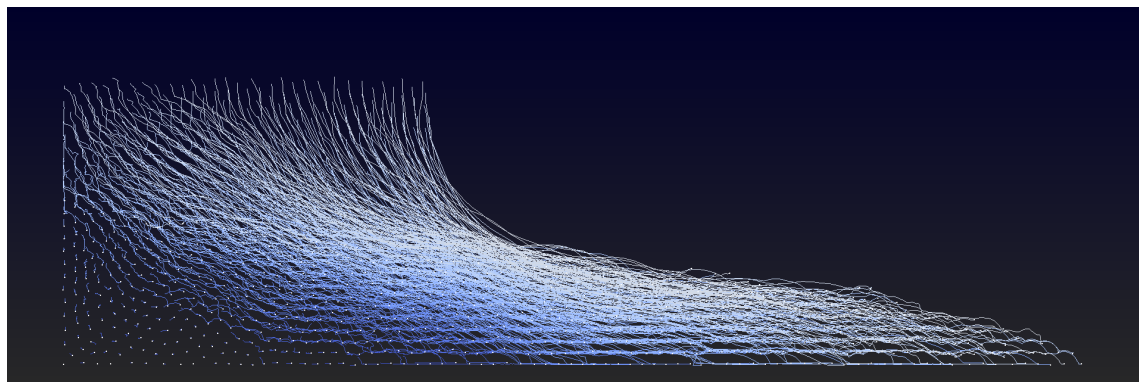


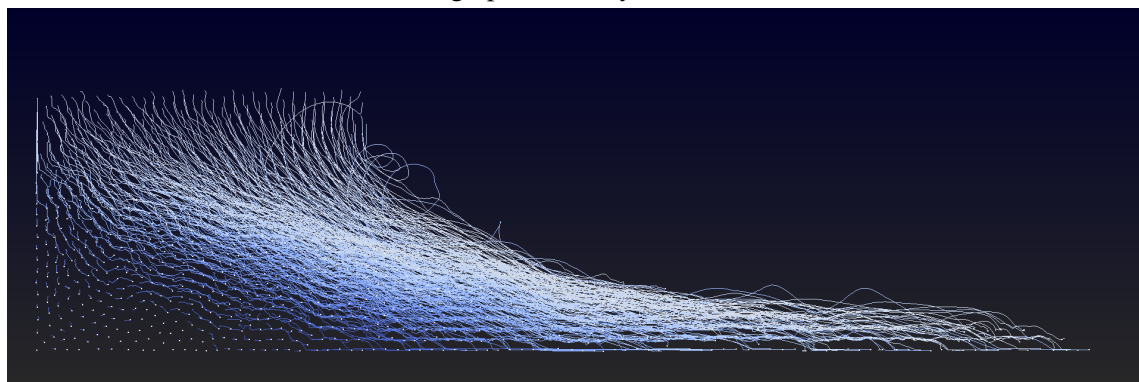
Figure 6.30 Effect of permeability on the evolution of packing density for a granular column collapse in fluid ($a = 0.8$ & loose initial packing)

static granular column before the collapse. A value of 1 indicates that the effective stress hasn't changed, which can be observed in the static region of the granular column. It can be observed that the normalised effective stress is significantly higher for the high permeability condition at the flow front in comparison to the almost non-existence of effective stress in the low permeability condition. The observation of trivial effective stress at the flow front corroborates the lubrication effect observed at low permeability conditions.

Figure 6.33 shows the grain trajectories of a dense and a loose initial packing for a hydrodynamic radius ($r = 0.95 R$). It can be observed that the dense initial packing results in a lot of turbulent behaviour at the flow surface in contrast to the more uniform flow behaviour in the loose condition. The thickness of the deposit in both dense and loose condition is almost the same, however the density of the flow results in a Froude's number of 0.59 and 0.429 for loose and dense conditions, respectively. The low initial density results in more hydroplaning in the loose condition. The effect of water entrainment at the flow front in dense and loose conditions can be seen in figure 6.34. Water entrainment at the flow front can be observed in the loose condition, this is shown by white-coloured (empty voronoi cells) at the flow front. This empty region in the granular packing between the granular mass and the base at the flow front represents the entrained water, which results in hydroplaning. Comparing the evolution packing densities in dense and loose conditions (figures 6.21 and 6.30) reveal almost the same packing density when the flow is fully mobilised. Hence, it is the density of the flowing



(a) High permeability ($r = 0.7 R$)



(b) Low permeability ($r = 0.95 R$)

Figure 6.31 Particle tracking of the deposit morphology for a granular column collapse in fluid ($a = 0.8$ & loose packing), influence of permeability

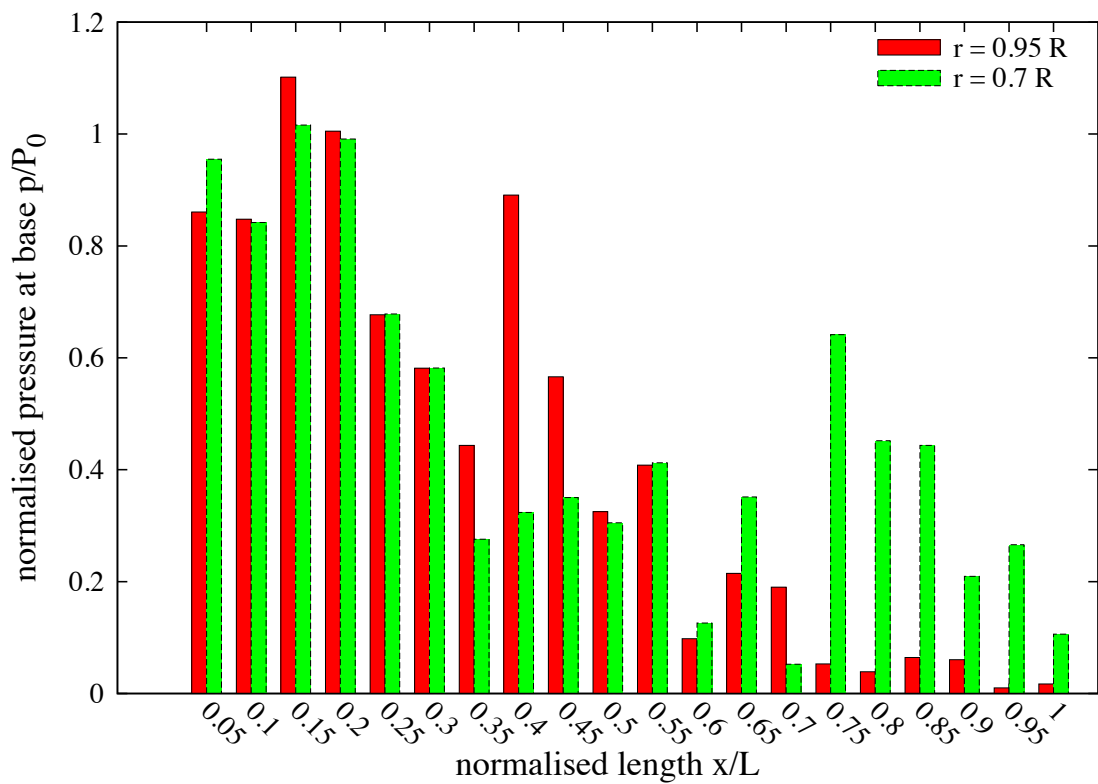
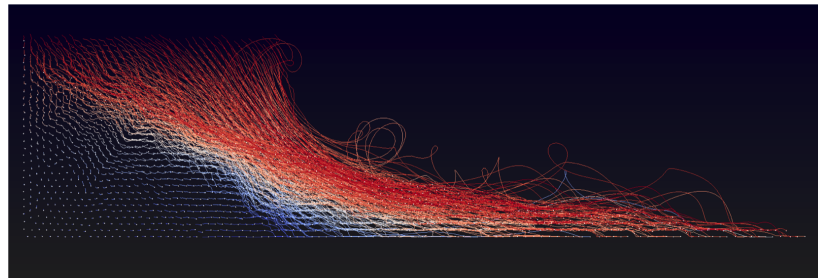


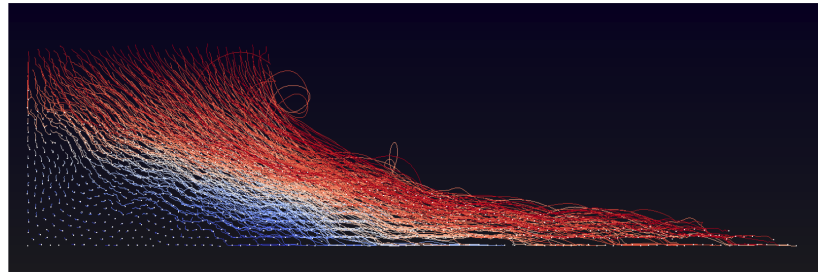
Figure 6.32 Effect of permeability on the normalised effective stress for loose initial packing at $t = 2\tau_c$

granular mass that controls the influence of hydroplaning for a given hydrodynamic radius and initial aspect ratio. A loosely packed granular column with low permeability entrains more water at the flow front, resulting in a hydroplaning effect that overcomes the influence of viscous drag forces and thereby yields a higher run-out distance than the dry condition.

Rondon et al. (2011) also observed that the collapse of a granular column in a viscous fluid is mainly controlled by the initial volume fraction and not by the aspect ratio of the column. The role of the initial volume fraction observed explains the pore pressure feedback mechanism proposed by (Iverson, 2000; Schaeffer and Iverson, 2008) in the context of landslides. The compaction or dilation of grains can cause additional stress in the grains which can stabilise or destabilise the soil. The flow is thus controlled by the coupling between the dilatancy of the granular layer and the development of pore pressure in the fluid phase (Pailha et al., 2008). The dense column needs to dilate in order to flow. When it starts to fall, liquid is then sucked into the column, which is then stabilized by the additional viscous drag (Rondon et al., 2011; Topin et al., 2012). By opposition the loose column when it starts flowing expands and ejects liquid, leading to a partial fluidisation of the material.



(a) Dense initial packing (83%)



(b) Loose initial packing (79%)

Figure 6.33 Effect of initial density on the deposit morphology for a granular column collapse in fluid ($a = 0.8$). Dense vs loose initial packing fraction ($r = 0.95 R$). Darker means dense packing, white indicates loose packing density.



(a) Dense initial packing (83%)



(b) Loose initial packing (79%)

Figure 6.34 Evolution of packing fraction at $t = \tau_c$ for dense and loose initial packing fraction. Black means dense packing, while white colour denotes loose packing in the Voronoi cell.

6.4 Submarine granular flows down inclined planes

Slope failure is a problem of high practical importance for both civil engineering structures and natural hazards management. Catastrophic events such as landslides, debris flows, rock avalanches or reservoir embankment failures exemplify the potential consequences of a soil gravitational instability. One of the most critical situation concerns a submerged sandy slope as pore pressure changes; seepage or earthquakes can cause significant damages to off-shore structures and may generate a tsunami.

The influence of slope angle on the effect of permeability and the initial packing density on the run-out behaviour are studied. In this study, a 2D poly-disperse system ($d_{max}/d_{min} = 2$) of circular discs forming a granular column in fluid is used to understand the behaviour of granular flows down inclined planes (figure 6.5). The soil column is modelled using ~ 1000 to 2000 discs of density 2650 kg/m^3 and a contact friction angle of 26° . The collapse of the granular column is simulated inside a fluid with a density of 1000 kg/m^3 and a kinematic viscosity of $1 \times 10^{-6} \text{ m}^2/\text{s}$. A granular column with an initial aspect ratio a of 0.8 is used. A hydrodynamic radius $r = 0.9 R$ is adopted during the LBM computations. Dry analyses are also performed to study the effect of hydrodynamic forces on the run-out distance. The numerical configuration used in this study is shown in figure 6.5a. The slope angle θ is varied as 0° , 2.5° , 5° , and 7.5° . The influence of permeability (with hydrodynamic radius varied as 0.7 , 0.75 , 0.8 , 0.85 and $0.9 R$) on the run-out behaviour of collapse of granular columns on to an inclined plane with a slope angle of 5° is also analysed.

6.4.1 Effect of initial density

In order to understand the influence of the initial packing density on the run-out behaviour, a dense sand column (initial packing density, $\Phi = 83\%$) and a loose sand column ($\Phi = 79\%$) are considered. The granular columns collapse and flow down slopes of varying inclinations. The run-out behaviour is compared with the collapse of a granular column in fluid on a horizontal surface. For all slope angles, the flow kinematics in the submerged condition is compared with its dry counterpart to understand the influence of lubrication and viscous drag. A hydrodynamic radius of $r = 0.9 R$ is adopted in all cases, because low permeability conditions result in longer run-out distance as observed in the previous section.

The evolution of the normalised run-out with time for the collapse of a dense sand column in dry and submerged conditions for varying slope inclinations is presented in figure 6.35a. For all slope angles, the run-out distances in the dry condition are longer than those observed in the submerged condition. Similar to the case of collapse on a horizontal plane, the dense granular columns experience drag forces that have a significant influence than the lubrication

effect. The difference in the run-out between the dry and the submerged condition decreases with increase in the slope angle. At a slope angle of 5° the difference in the run-out between the dry and the submerged condition is the smallest. This is due to hydroplaning of a thin flowing layer, the occurrence of hydroplaning can be observed by a sustained peak kinetic energy (figure 6.35b). At higher slope angles ($> 5^\circ$), the drag force predominates over the lubrication effect and results in significantly shorter run-out distance than the dry condition. This can be observed by the difference in the kinetic energy evolution between the dry and the submerged conditions.

Similar to the case of collapse on a horizontal surface, the dense granular columns in fluid require a longer time to collapse and flow, due to the development of large negative pore-pressure. Large negative pore-pressure are developed as the dense granular material dilates due to shearing along the shear-failure surface in the initial phase of the flow. The snapshots of the dense granular column collapse down slopes of varying inclinations at the time ($t = \tau_c = 3\sqrt{H/g}$), are shown in figure 6.36. It can be observed that the amount of water entrainment increases with increase in slope angle. At a slope of 7.5° , a layer of entrained water (thickness $\sim 2d$) along the bottom of the flow front can be observed. However, with increase in slope angle, the surface area of granular mass experiencing the hydrodynamic drag increases, which results in a shorter run-out distance than the dry condition.

Figure 6.35b shows the evolution of normalised kinetic energy with time for dry and submerged collapse on different slope angles. It can be seen that the viscous drag on the dense column tends to be more dominant than influence of hydroplaning on the run-out behaviour. This influence can be observed in the smaller peak kinetic energy for the submerged granular material in comparison to the dry condition. With increasing slope angle, the volume of material that dilates increases. This results in large negative pore-pressure and more viscous drag on the granular material. Hence, the difference in the run-out between the dry and the submerged conditions, for a dense granular assembly, increases with increase in the slope angle above an inclination of 5° .

In contrast to the dense granular columns, the loose granular columns (packing fraction of 79%) show longer run-out distance in immersed conditions (figure 6.37a). The snapshots at $t = 3\tau_c$ of a loose granular column ($a = 0.8$) collapse down slopes inclined at an angle of 2.5° , 5° and 7.5° are presented in figure 6.38. The run-out distance in fluid increases with increase in the slope angle in comparison to the dry cases. The loose granular flow tends to entrain more water at the base of the flow front, creating a lubricating surface, which results in a longer run-out distance. For the same thickness of the flow, the loose granular flow has a smaller density and hence a higher Froude's number than the dense flow resulting in a higher

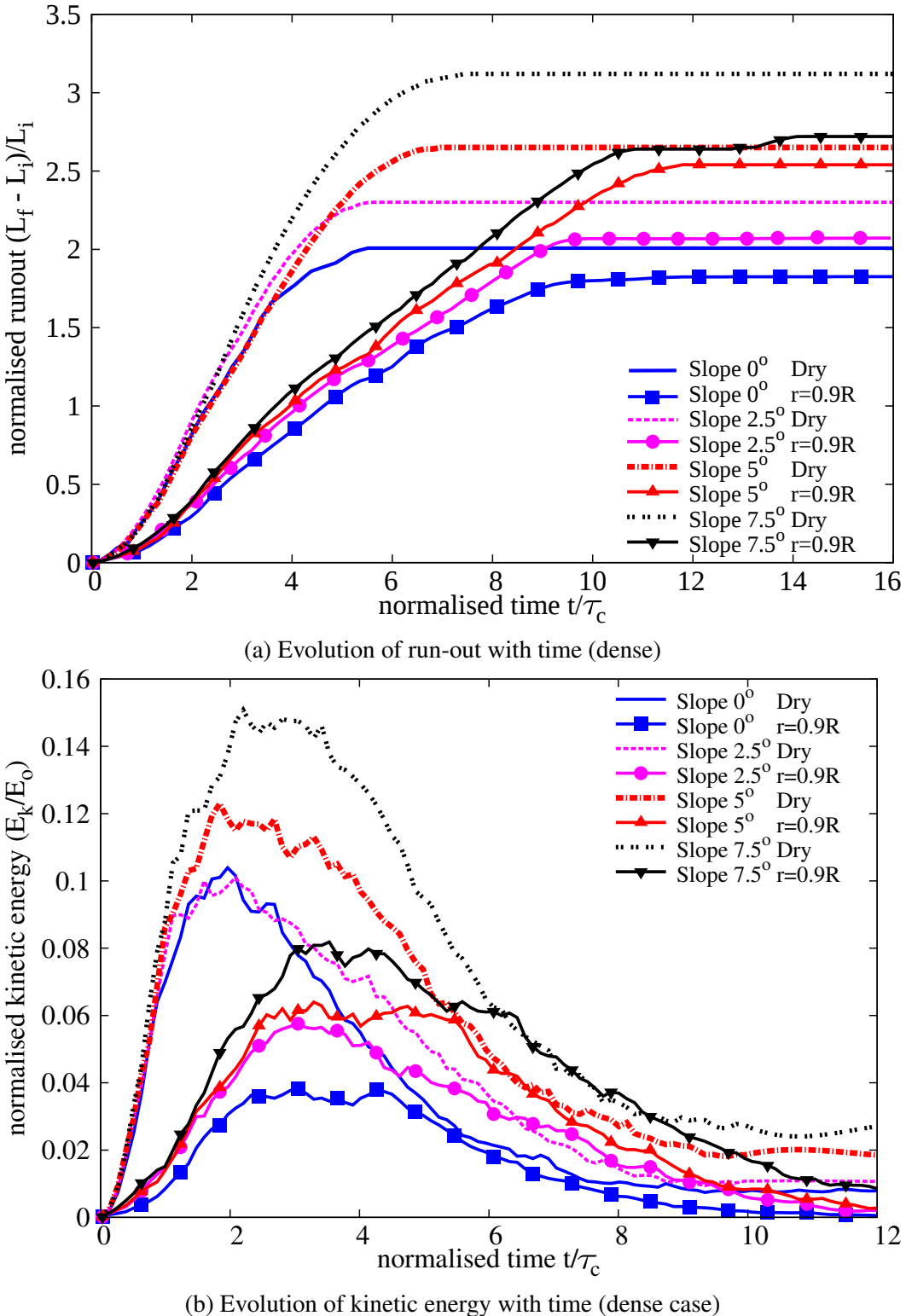


Figure 6.35 Evolution of run-out and kinetic energy with time (dense)

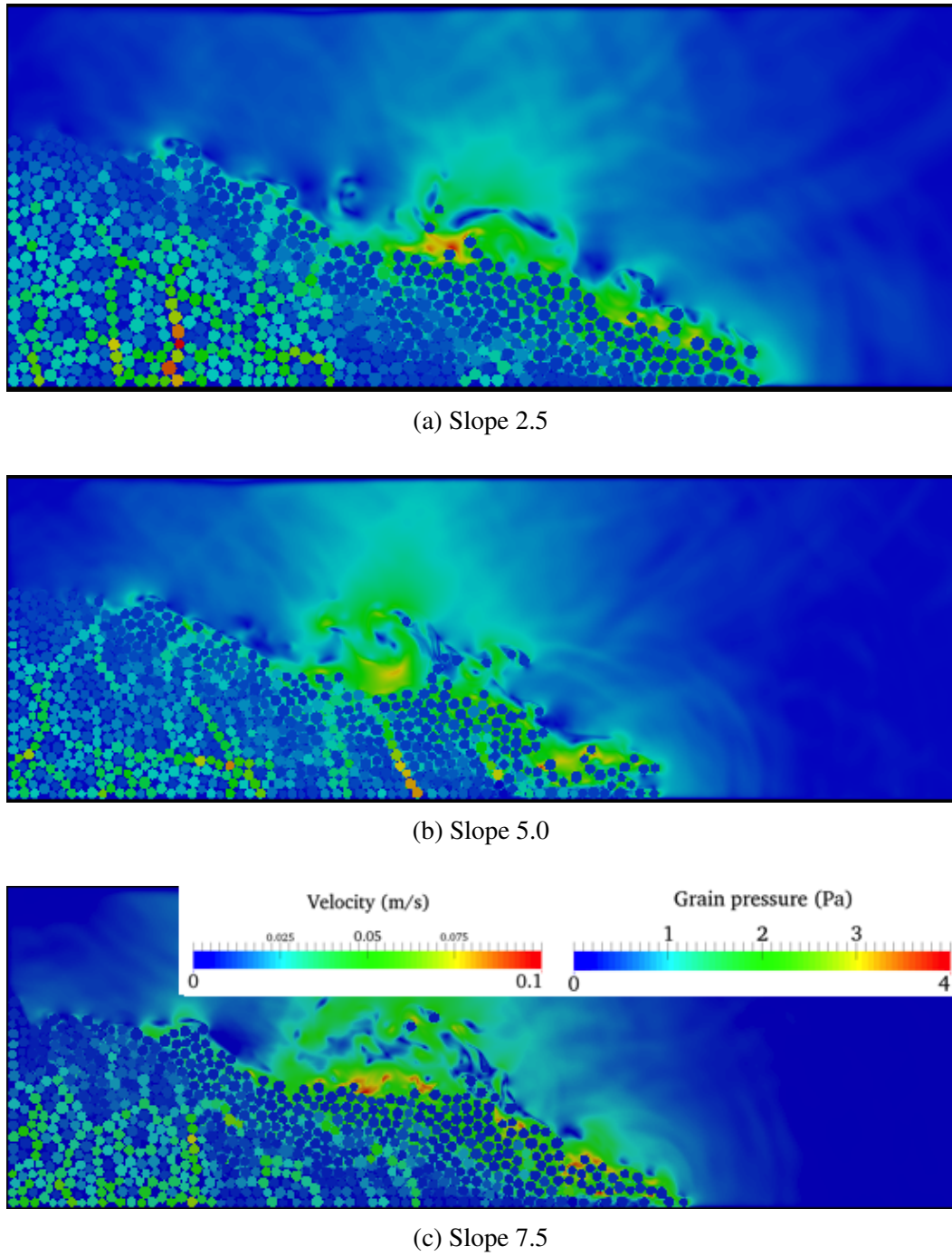


Figure 6.36 Flow morphology at $t = 3\tau_c$ for different slope angles (dense)

probability of hydroplaning. The hydroplaning effect causes an increase in the flow velocity for the loose granular material in comparison with the dense condition (figure 6.37b).

In contrast to dense granular flows, loose granular flows exhibit a plug-like flow (figure 6.37a). Due to the low permeability, the water entrapped in the flow front results in a drop in the density of the flowing mass, which causes lower effective stress thus enabling lubrication. The turbulence effect observed on the surface of the dense granular flow is absent in the loose granular collapse. This, along with the lubrication effect, results in a longer run-out distance in the submerged condition for a loose granular column than the dry collapse.

The evolution of packing density for dry and loose collapse in fluid for different slope angles (figure 6.39) shows that, at the end of the flow, both the dense and the loose conditions reach a similar packing density. The dense granular column dilates more, which results in large negative pore-pressure that is to be dissipated so as the granular mass is able to flow. Whereas in the loose condition, a positive pore-pressure is observed at the base of the flow, indicating entrainment of water at the base, i.e. lubrication and drop in the effective stress resulting in a longer run-out distance. The amount of water entrained in the loose granular column is higher than the dense condition, this can be observed by the low packing fraction observed between $2\tau_c$ and $5\tau_c$.

Figure 6.40a shows the evolution of run-out with slope angle for an initially dense granular column. As the slope angle increases, the run-out increases in both dry and submerged conditions. For all slope angles, the run-out in the dry condition is higher than the submerged conditions. As the slope angle increases, the drag force experienced by the dense granular column is more dominant than lubrication effect on the run-out behaviour, this results in an increase in the difference between the dry and the submerged conditions with increase in the slope angle. Whereas with an increase in the slope angle, the loose granular column flows longer than the dry conditions. The longer run-out in the loose granular column collapse is due to hydroplaning experienced at the flow front as a result of entrainment of water. Figure 6.41 shows that for a given initial aspect ratio and slope angle, the run-out distance in the loose granular collapse in fluid is higher than the dense condition. This observation in fluid is in contrast to the dry condition, where the dense granular column flows longer due to higher initial potential energy. A loose granular flow with low permeability ensures that water entrained at the base of the flow front is retained resulting in sustained lubrication effect. Also, the low permeability ensures that the density of the flowing mass remains in a slurry state resulting in a longer duration of hydroplaning. These effects in the loose granular column with low permeability condition result in a longer run-out distance.

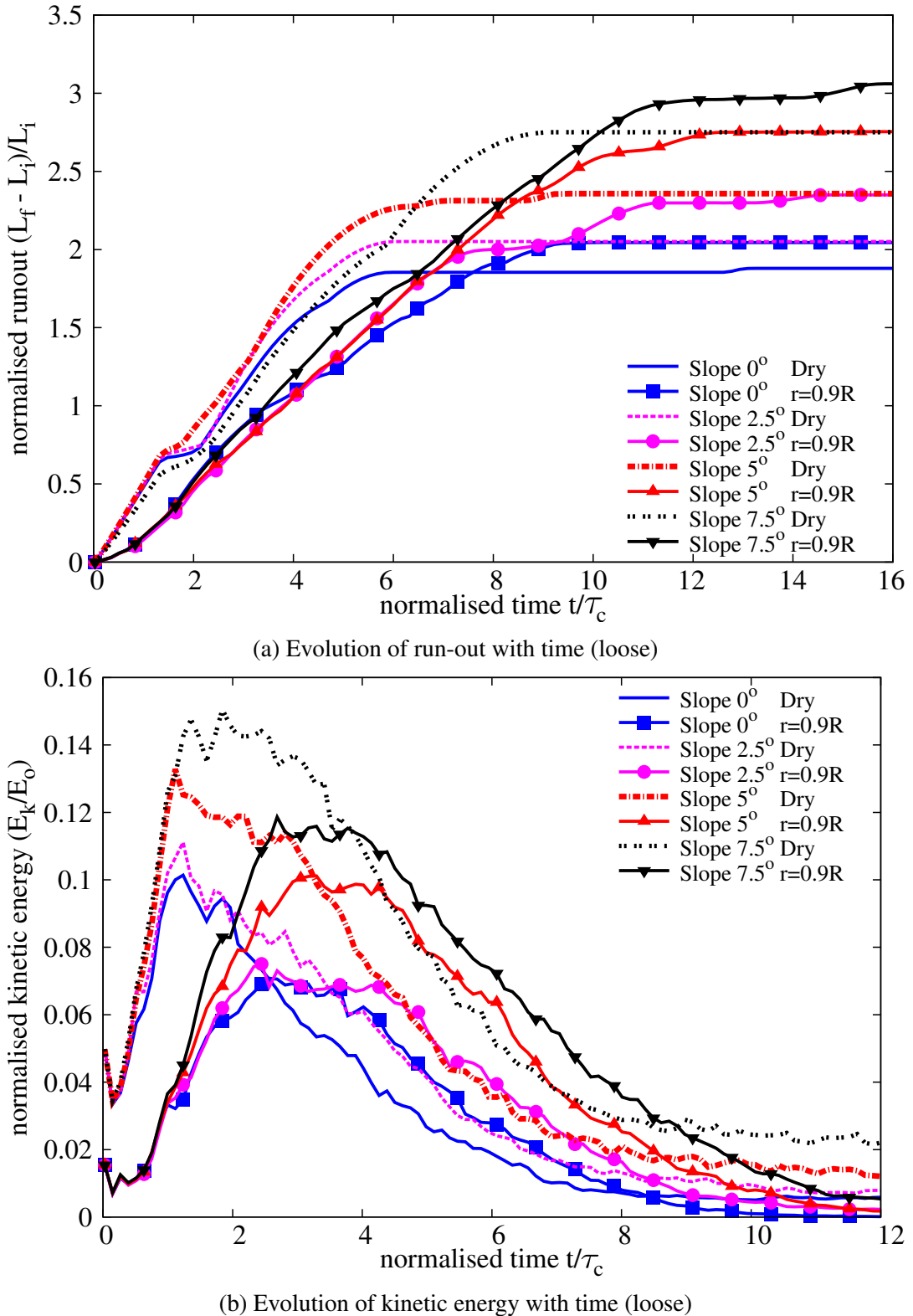
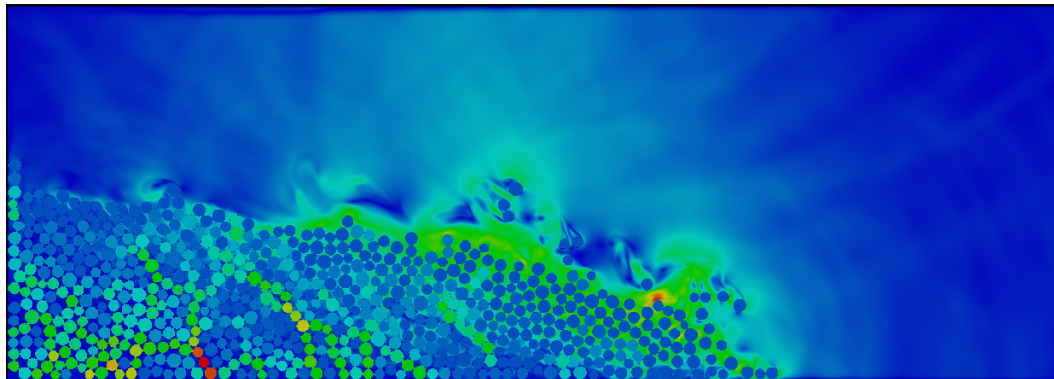
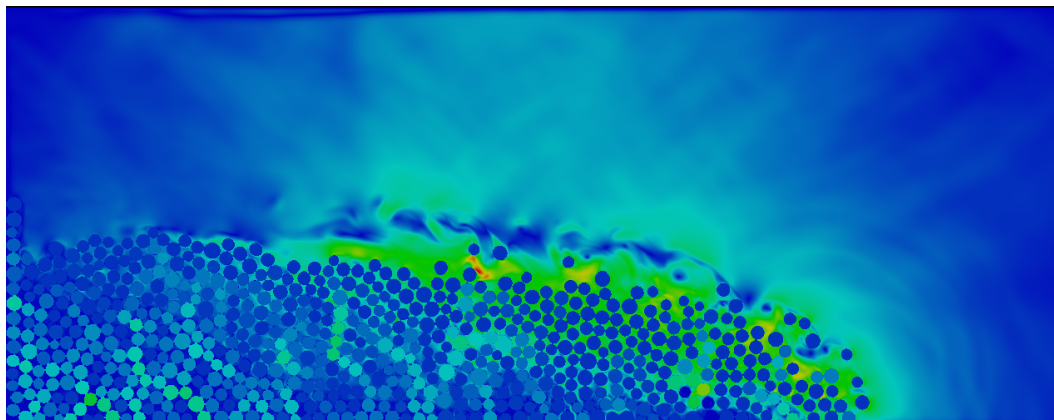


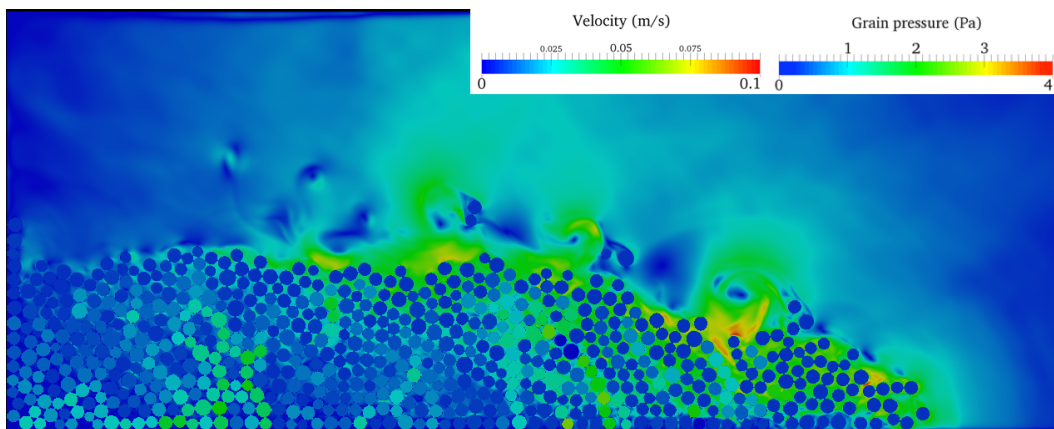
Figure 6.37 Evolution of run-out and kinetic energy with time (loose)



(a) Slope 2.5



(b) Slope 5.0



(c) Slope 7.5

Figure 6.38 Flow morphology at time $t = 3\tau_c$ for different slope angles (loose)

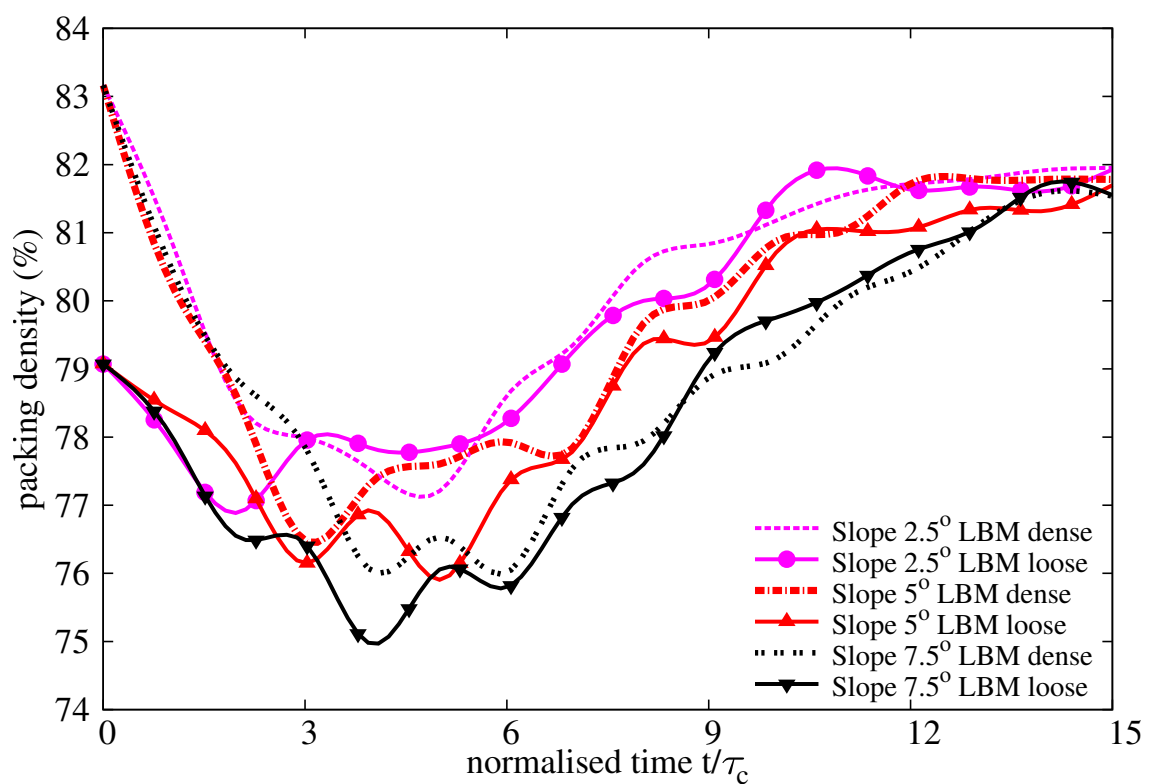
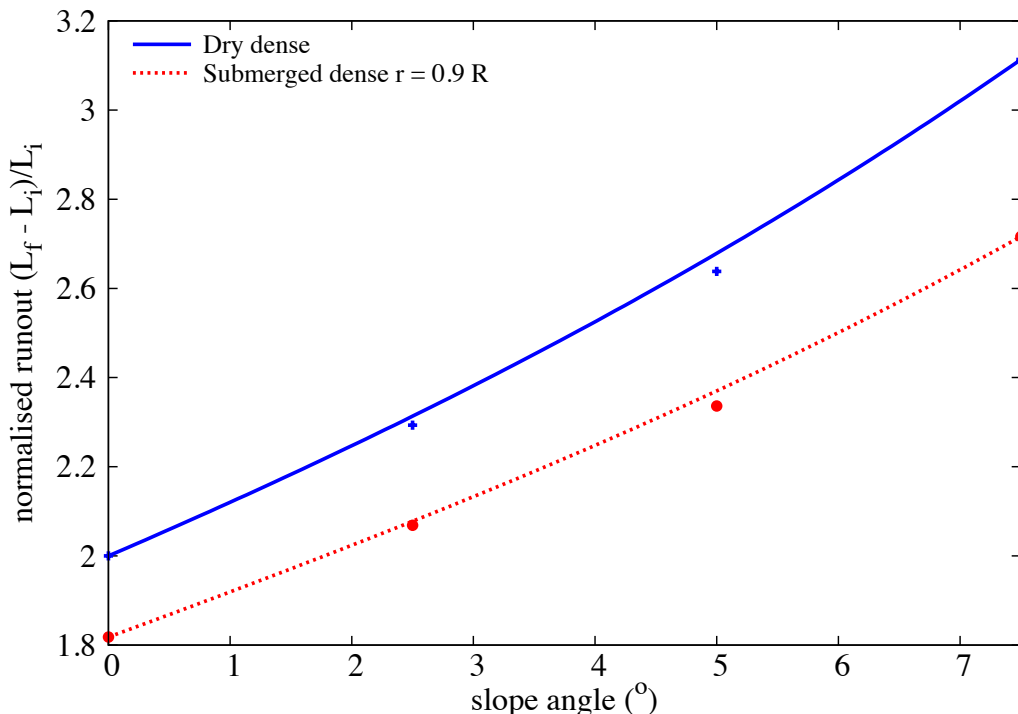
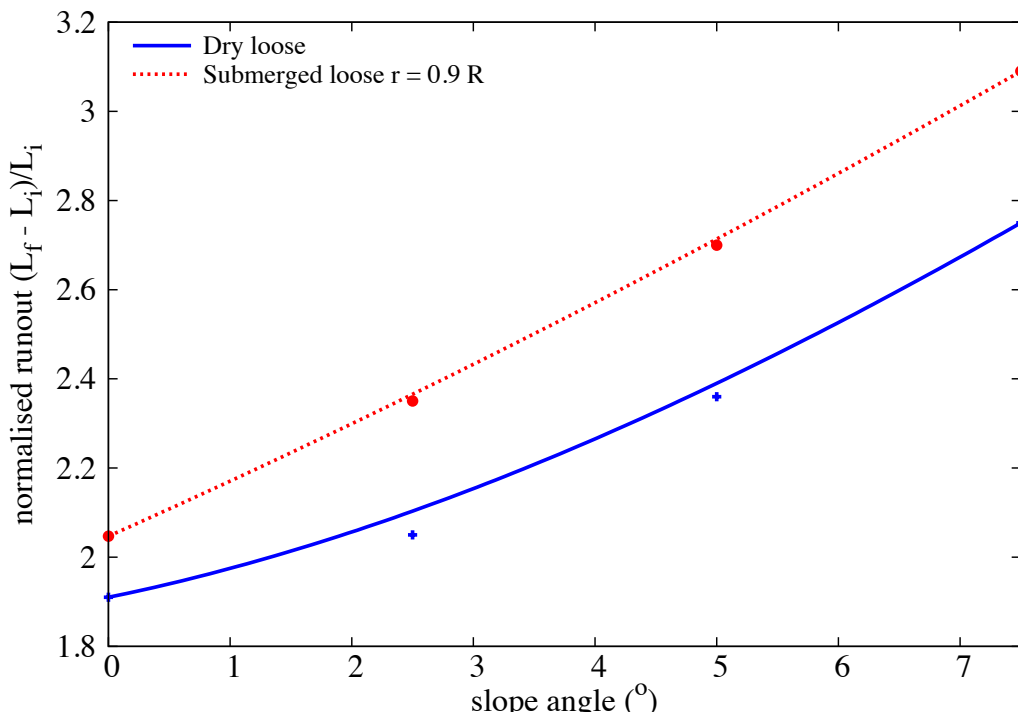


Figure 6.39 Evolution of packing density with time for different slope angles



(a) Dense



(b) Loose

Figure 6.40 Comparison between dry and submerged granular column on the effect of slope angle on the run-out distance (Dense and Loose).

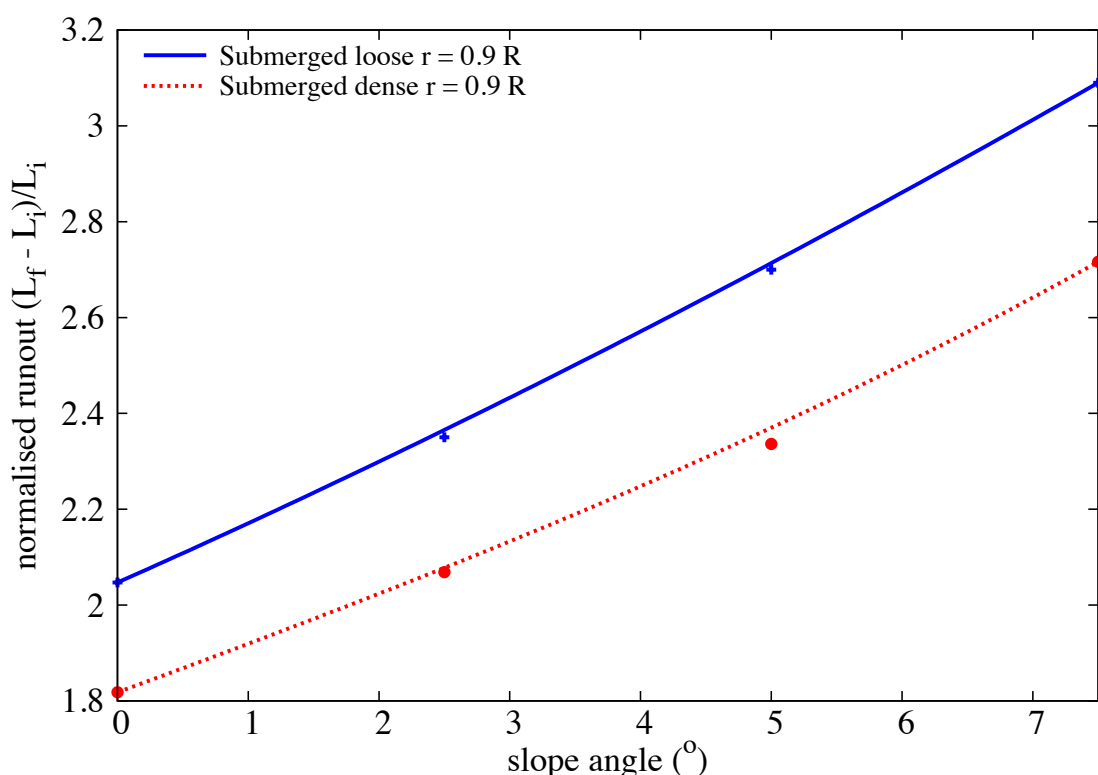


Figure 6.41 Effect of slope angle on the run-out behaviour for different initial packing density.

6.4.2 Effect of permeability

In order to understand the effect of permeability on granular flow down a slope angle of 5° , the collapse of a granular column with an initial aspect ratio of 0.8 is simulated with different permeabilities. The hydrodynamic radius of a loosely packed granular column is varied from $r = 0.7 R$ (high permeability), $0.75 R$, $0.8 R$, $0.85 R$ to $0.9 R$ (low permeability). The run-out distance is found to increase with decreasing permeability of the granular assembly (figure 6.42a). The run-out distance for high permeability conditions ($r = 0.7 R - 0.8 R$) are lower than their dry counterparts. Although, a decrease in permeability resulted in an increase in the run-out distance, no significant change in the run-out behaviour is observed for a hydrodynamic radii of up to $0.8 R$.

With a further decrease in permeability ($r = 0.85 R$ and $0.9 R$), the run-out distance in the fluid is longer than that observed in the dry condition. At a very low permeability ($r = 0.9 R$), the flowing granular mass entrains more water at the base, which causes a reduction in the effective stress accompanied by a lubrication effect. This can be seen by a significant increase in the peak kinetic energy and the sustained duration of the peak energy, in comparison to the dry and the highly permeable conditions (figure 6.43a). However, the permeability of the granular column did not have an influence on the evolution of height during the flow. But, the dry granular column tends to collapse more than the immersed granular column due to the lack of viscous dissipation (figure 6.42b).

Positive pore-pressure generation at the base of the flow is observed for low permeability conditions. Inspection of the local packing density showed entrainment of water at the base of the flow, which can also be observed by the steep decrease in the packing density (figure 6.43b) for the very low permeability condition ($r = 0.9 R$). At the end of the flow ($t \geq 10 \times \tau_c$), the excess pore-pressure dissipates and the granular flows, irrespective of their permeability, reach almost the same packing density.

Figure 6.45 shows the effect of permeability on the run-out behaviour for a dense and a loose granular column collapse on a slope of 5° and 0° . In both cases, the run-out distance increases with increase in the hydrodynamic radius (decrease in permeability). However in the dense case, the run-out distance observed in the fluid is shorter than the dry condition. Whereas in the loose condition, the run-out distance increases significantly at low permeabilities and results in a longer run-out distance in the submerged condition in comparison to the dry granular collapse. The comparison of loose and dense collapse on slopes of 0° and 5° shows that the initial packing density plays a significant role in the case of collapse on a horizontal plane, however at a slope of 5° , the run-out distance is unaffected by the initial packing density at high permeability conditions. This shows that at high permeabilities, the viscous drag forces predominate resulting in almost the same run-out

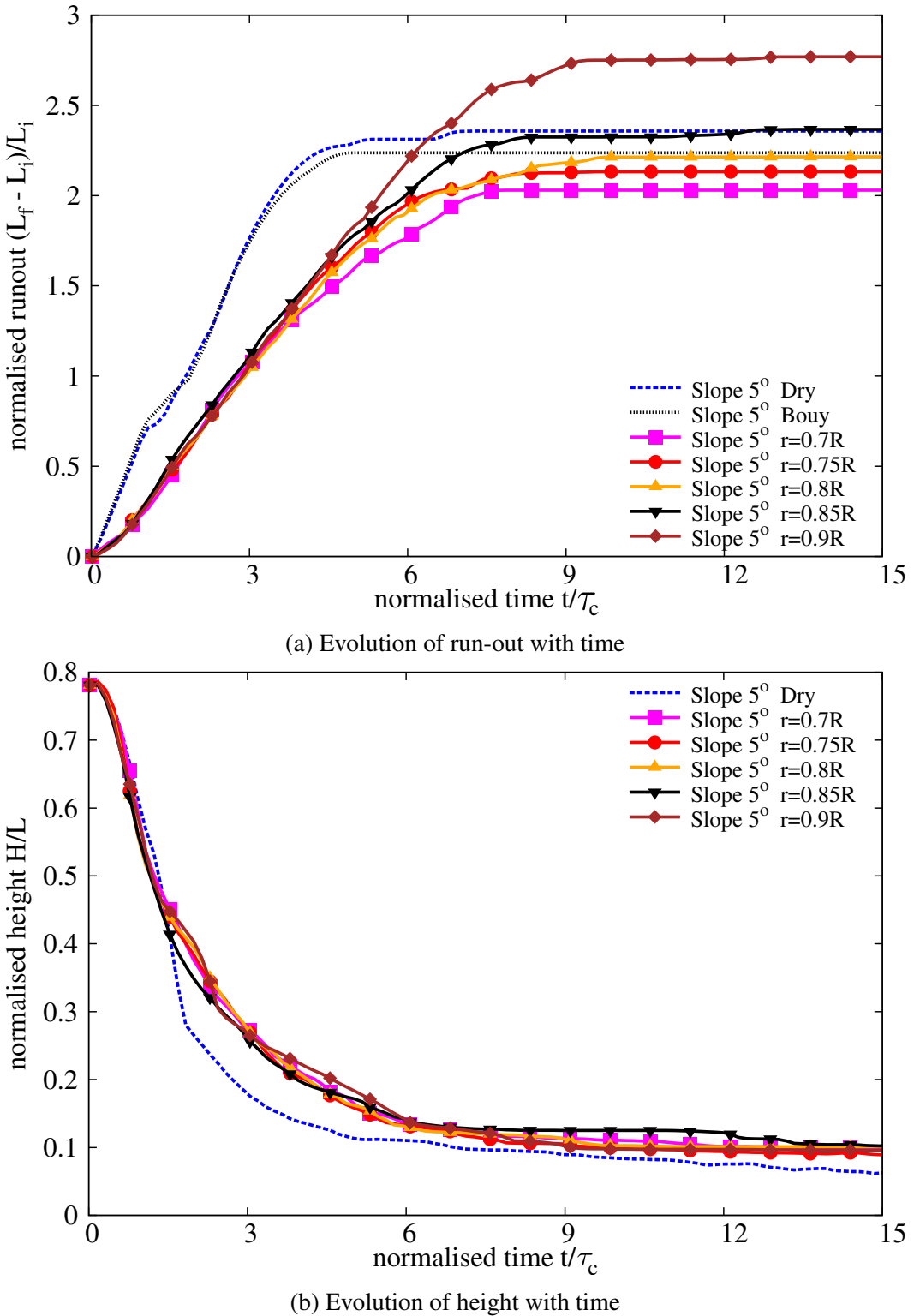


Figure 6.42 Evolution of run-out and height with time for different permeability (loose slope 5°)

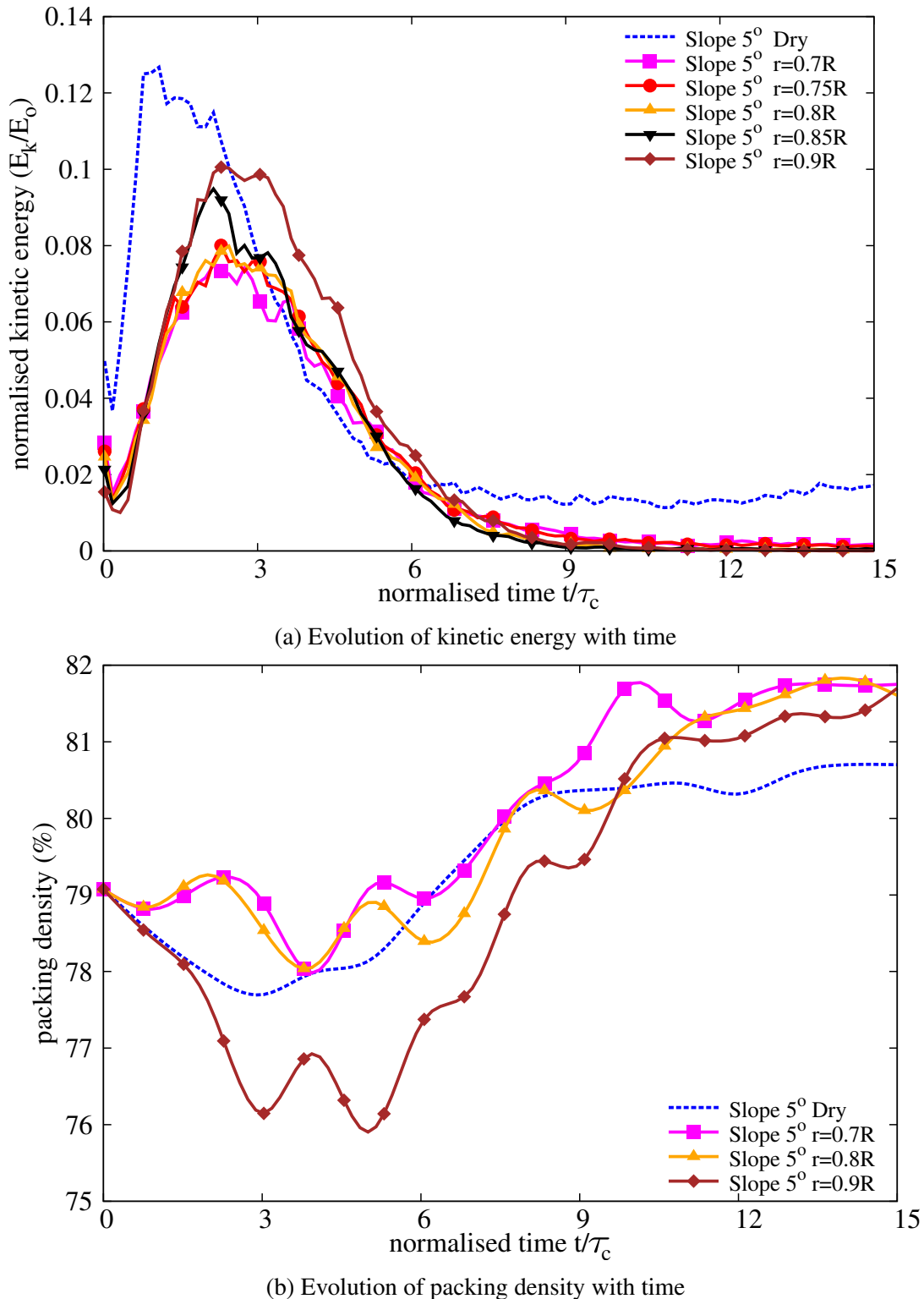


Figure 6.43 Evolution of kinetic energy and packing density with time for different permeability (loose slope 5°)

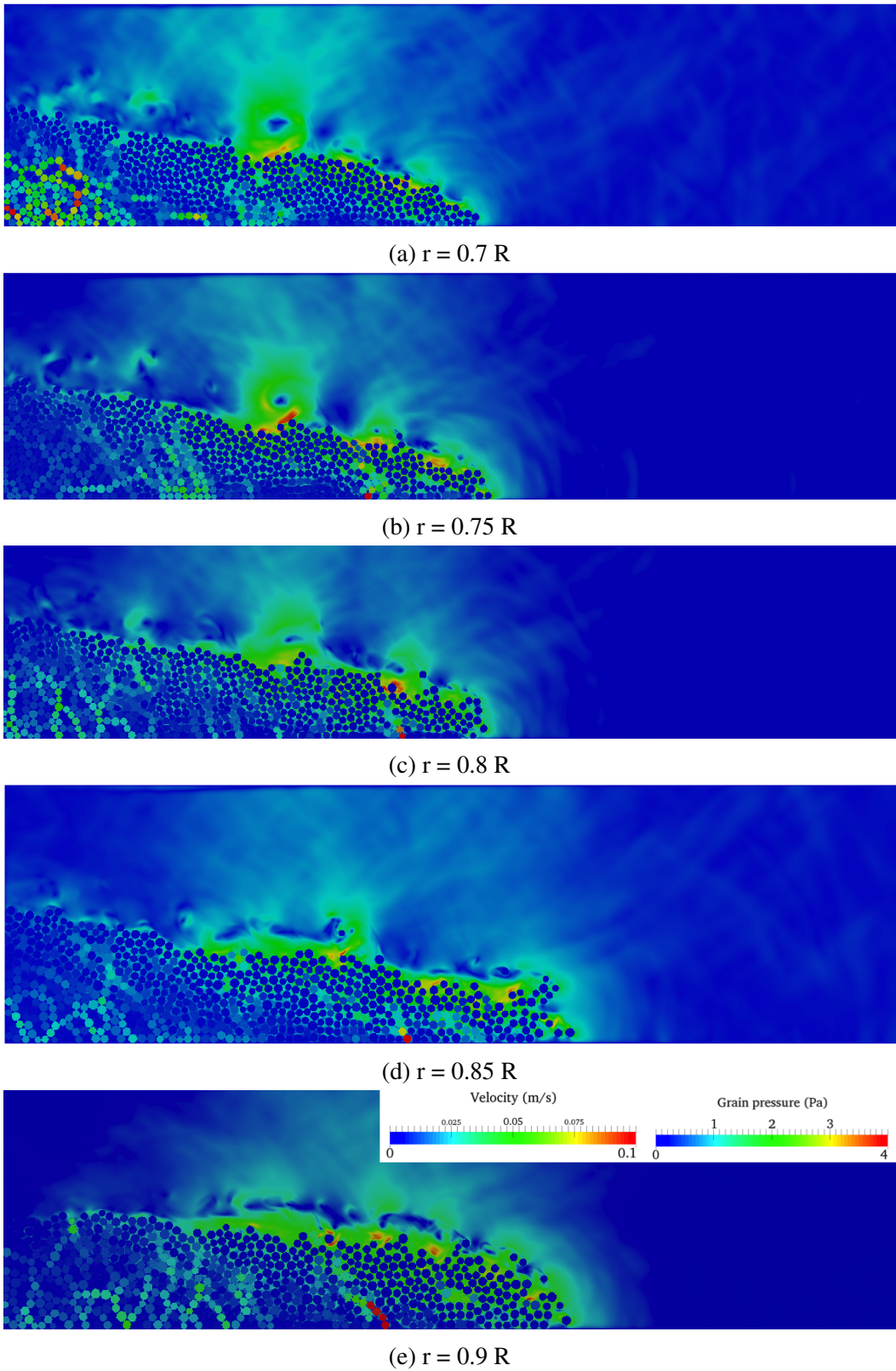


Figure 6.44 Evolution of the flow front at $t = 3\tau_c$ for different permeabilities (loose slope 5°).

distance for both dense and loose conditions. However at a low permeability ($r = 0.9 R$), hydroplaning is observed in the case of loose granular column resulting in a substantially longer run-out distance than the dense granular column in submerged condition.

6.5 Tall columns

In the case of tall columns, the amount of material destabilised above the failure plane is larger than that of short columns. Hence in tall columns, the surface area of the mobilised mass that interacts with the surrounding fluid is significantly higher than the short columns. This increase in the area of soil - fluid interaction results in an increase in the formation of turbulent vortices that alter the deposit morphology during the collapse. It is observed that the vortices result in formation of heaps that significantly affect the distribution of mass in the flow (section 6.3.2) . Staron and Hinch (2007) observed that the distribution of mass in a granular flow plays a crucial role in the flow kinematics. In order to understand the behaviour of tall columns, the run-out behaviour of a dense granular column with an initial aspect ratio of 6 is studied. The collapse of a tall granular column on slopes of 0° , 2.5° , 5° and 7.5° are studied. A hydrodynamic radius of $r = 0.85 R$ is adopted.

Snapshots of the collapse of an aspect ratio 6 column in fluid on a horizontal surface are shown in figure 6.47. The initial stage of collapse is characterised by the free-fall of grains above the failure surface. Unlike the dry condition, as the grains undergo free-fall due to gravity, they interact with the surrounding fluid experiencing drag forces. This results in a significant drop in the kinetic energy available for the flow. As the grains reach the static region, they interact with the neighbouring grains and the kinetic energy gained during the free fall is converted into horizontal acceleration. Uniquely during this stage ($t = 3\tau_c$) the interactions between the soil grains on the surface with the surrounding fluid result in the formation of eddies. The number of eddies formed during the flow is proportional to the surface area of the granular mass interacting with the fluid. Hydroplaning can be observed at the flow front ($t = 3\tau_c$). Two large vortices with almost the same size can be observed at the final stage of collapse. The soil grains on the surface experience suction due to formation of eddies and this results in formation of heaps of granular mass in front of each vortex. The formation of heaps, although in evidence, doesn't significantly affect the distribution of mass in the case of collapse on a horizontal plane.

Snapshots of the collapse of a granular column ($a = 6$) on a inclined plane at angle of 5° are shown in figure 6.48. The collapse on a slope of 5° show flow evolution behaviour similar to the case of collapse on a horizontal plane. The vortices are formed only during the horizontal spreading stage $t = 3\tau_c$, but the number of vortices formed during the collapse

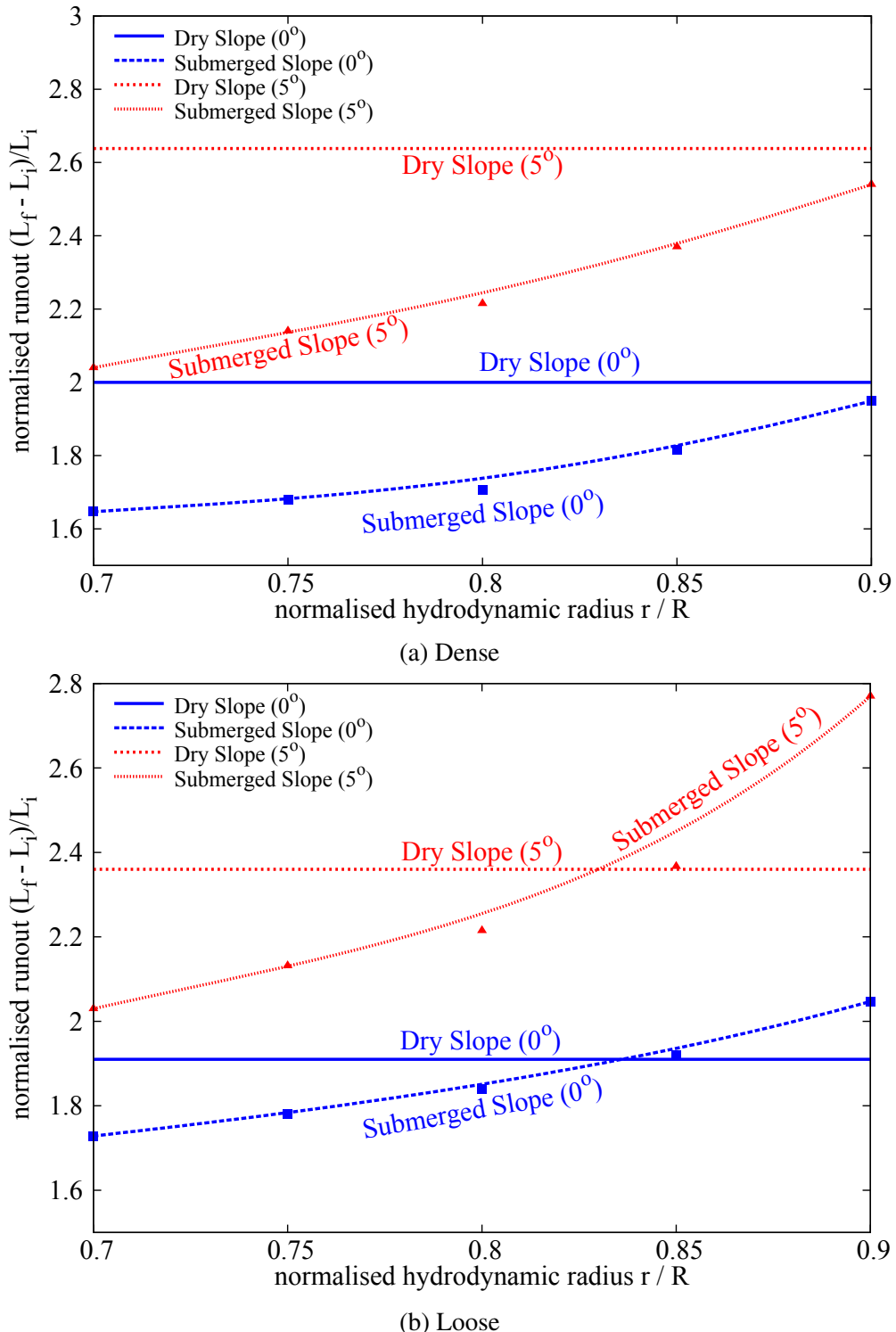


Figure 6.45 Comparison between dry and submerged granular column for a slope angle of 0° and 5° on the effect of permeability on the run-out distance (Dense and Loose).

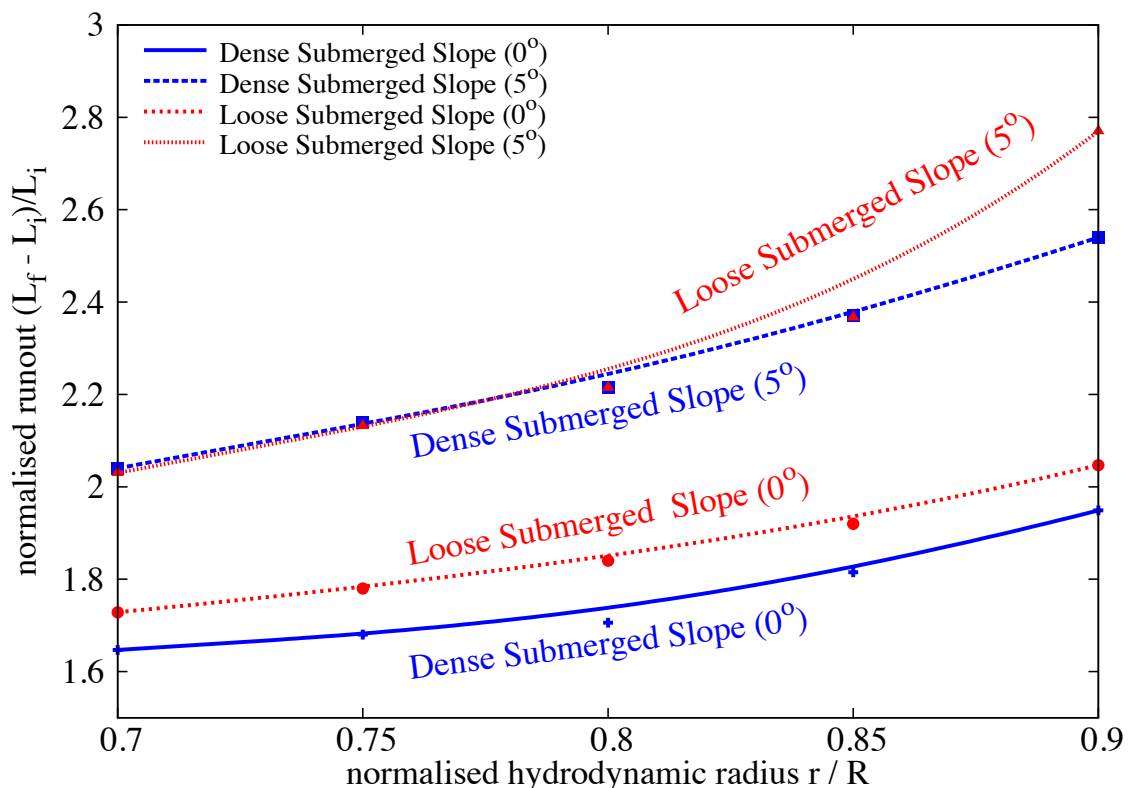


Figure 6.46 Effect of permeability on the run-out behaviour for different slope angle and the initial packing density.

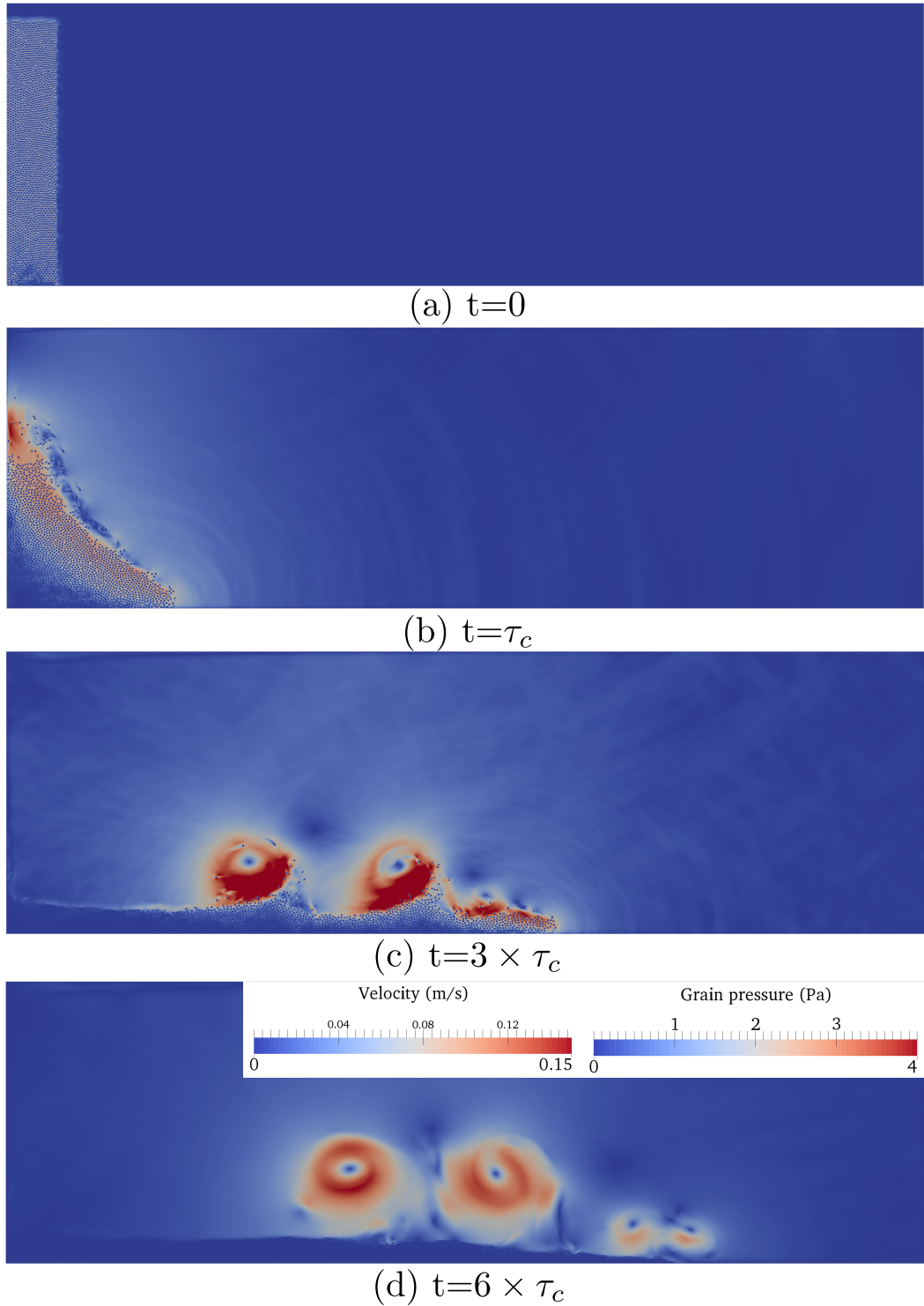


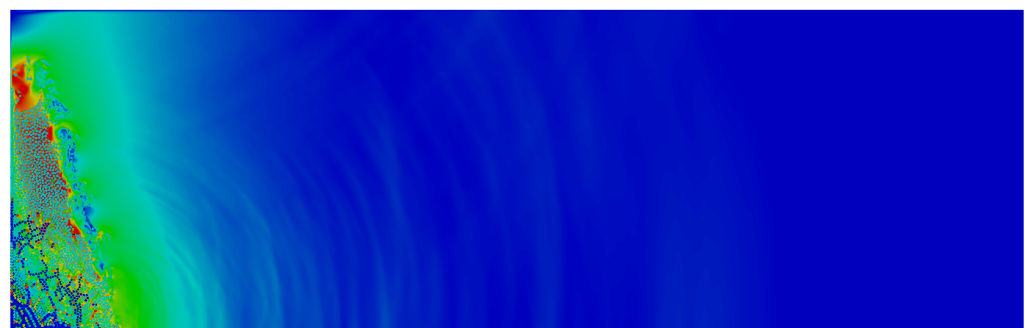
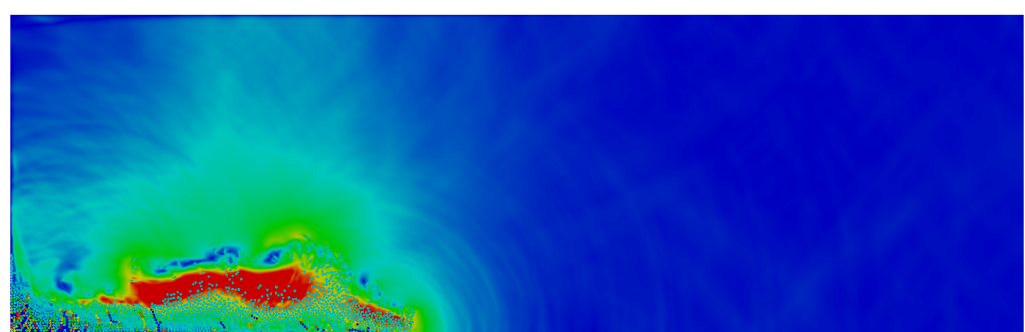
Figure 6.47 Flow evolution of a granular column collapse in fluid ($a = 6$) on a horizontal surface

is higher than the collapse on a horizontal plane. However, as the flow progresses a single large vortex engulfs other smaller vortices, thus having a significant influence on the mass distribution. Figure 6.49 shows the distribution of mass and the packing density at $t = 6\tau_c$ and $t = 8\tau_c$. A heap can be observed in front of the large vortex almost at the middle of the flow. The height of the heap formed in the middle of the granular flow is higher than the collapse height next to the wall. However, when the flow comes to rest and the vortex moves away from the flowing surface, the mass present in the heap gets redistributed (as seen at $t = 8\tau_c$). This behaviour is significantly different from that observed in the case of short columns.

In order to understand the influence of slope angles on the run-out behaviour, the collapse of a granular column with an initial aspect ratio of 6 is performed on slopes of 0° , 2.5° , 5° and 7.5° . The run-out evolution with time for different slope angles are presented in figure 6.50a. The run-out distance increases with increase in the slope angle, however the run-out distance in the fluid is significantly shorter than the dry condition. The slow evolution of run-out in the submerged condition is due to the delay in the dissipation of large negative pore-pressure developed during the initial stage of the collapse. The formation of eddies during the flow indicates that most of the potential energy gained during the free-fall is dissipated through viscous drag and turbulence. This effect predominates over the hydroplaning that is observed during the flow resulting in a shorter run-out distance in the case of fluid. The evolution of the normalised height with time (figure 6.50b) for collapse on different slope angles indicates that the amount of material destabilised in fluid is less than the dry conditions due to the drag forces experienced by the grains, which retards the quantity and the rate of collapse.

Figure 6.51a shows the evolution of the normalised kinetic energy for a granular column ($a = 6$) collapse in fluid on different slope angles. The amount of kinetic energy available for the flow in the submerged condition is almost half that of the dry condition. It can be seen from the figure that the vertical kinetic energy in the fluid condition dissipates a longer duration, in contrast to the free-fall release observed in the dry condition. The slower dissipation is attributed to the viscous drag force experienced by the grains.

The behaviour of tall columns is significantly different from that observed in the case of short columns. The slope angle has a strong influence on the number and size of eddies during the flow. The eddies interact with the surface of the granular flow and forms heaps in front of each vortex. This significantly affects the mass distribution and in turn the run-out evolution. Although tall cliffs are quite rare in submarine condition in comparison to short cliffs or slopes, further research is required to understand the influence of permeability and packing density on the run-out evolution of tall columns.

 $t = 0\tau_c$  $t = 1\tau_c$  $t = 3\tau_c$

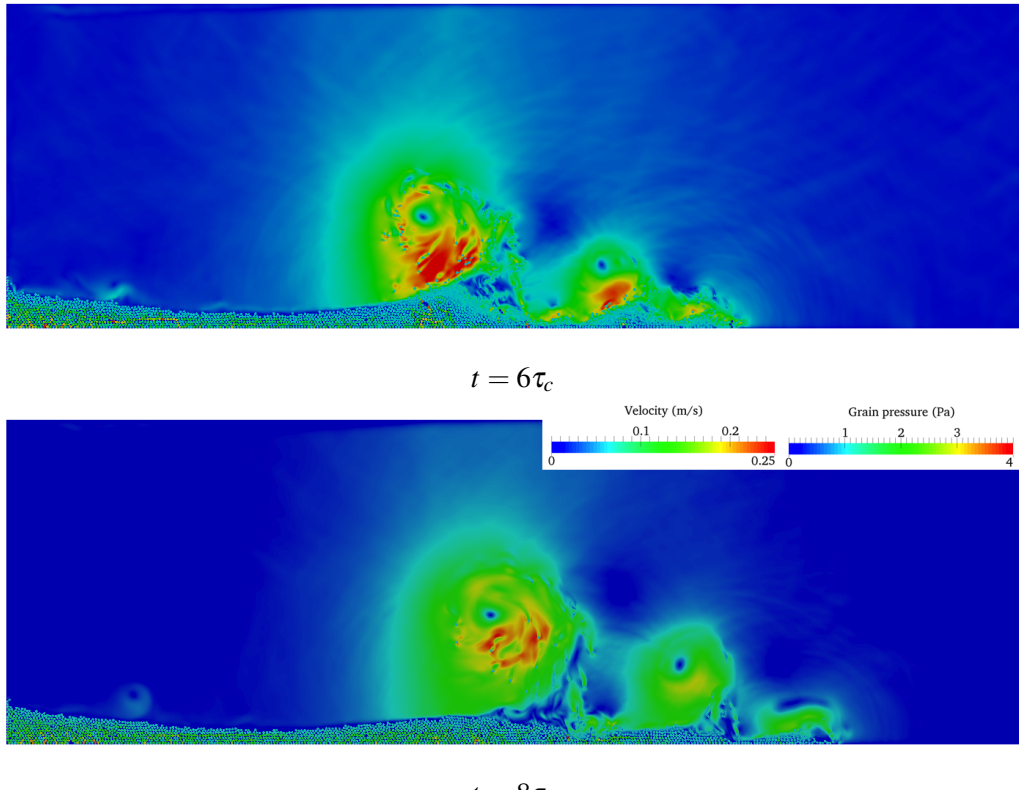


Figure 6.48 Flow evolution of a granular column collapse in fluid ($a = 6$) on a slope of 5° . Shows the velocity profile of fluid due to interaction with the grains (red - higher velocity).

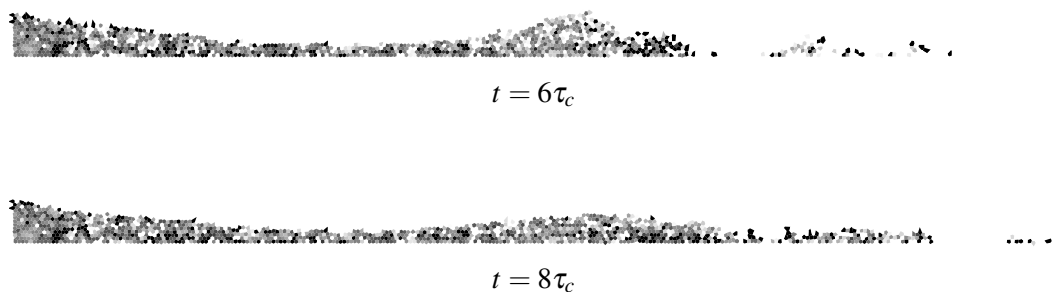
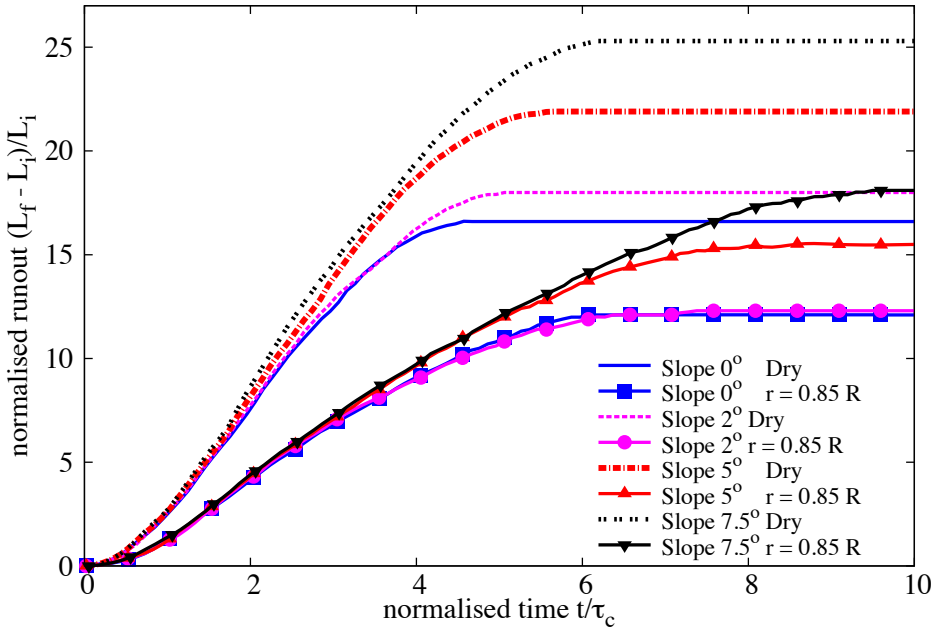
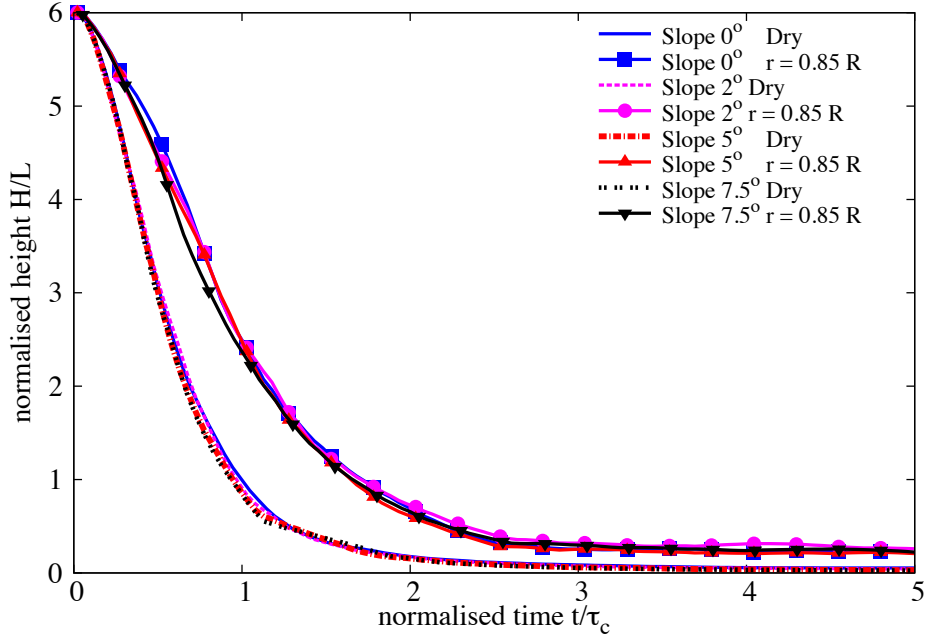
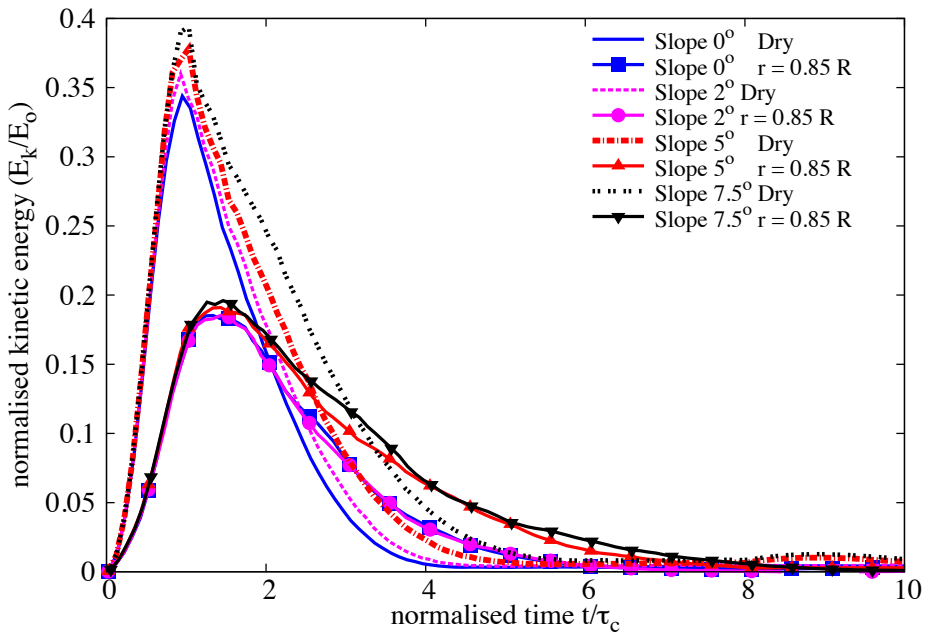
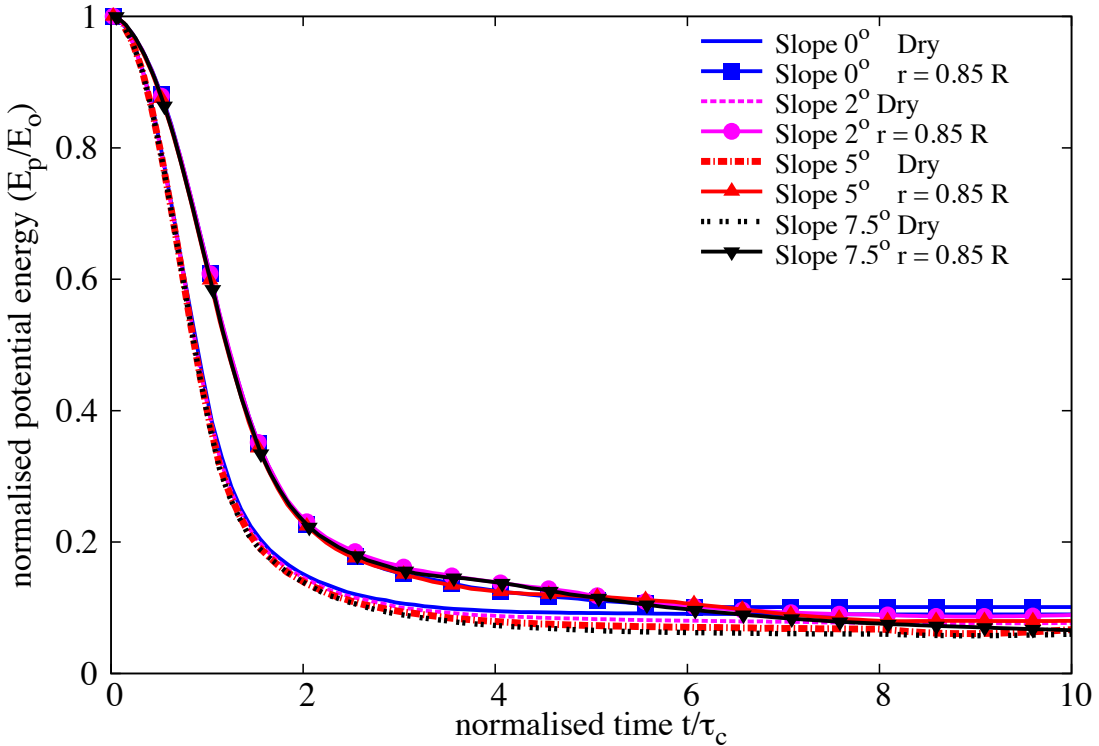


Figure 6.49 Packing density of a granular column collapse in fluid ($a = 6$) on a slope of 5° .

(a) Evolution of run-out for a column collapse in fluid ($a = 6$) on a slope of 5° (b) Evolution of height with time for a column collapse in fluid ($a = 6$) on a slope of 5° Figure 6.50 Evolution of run-out and height for a column collapse in fluid ($a = 6$) on a slope of 5°



(a) Evolution of the total kinetic energy



(b) Evolution of the total potential energy

Figure 6.51 Evolution of the kinetic and the potential energy with time for a granular column collapse in fluid ($a = 6$) on a slope of 5°

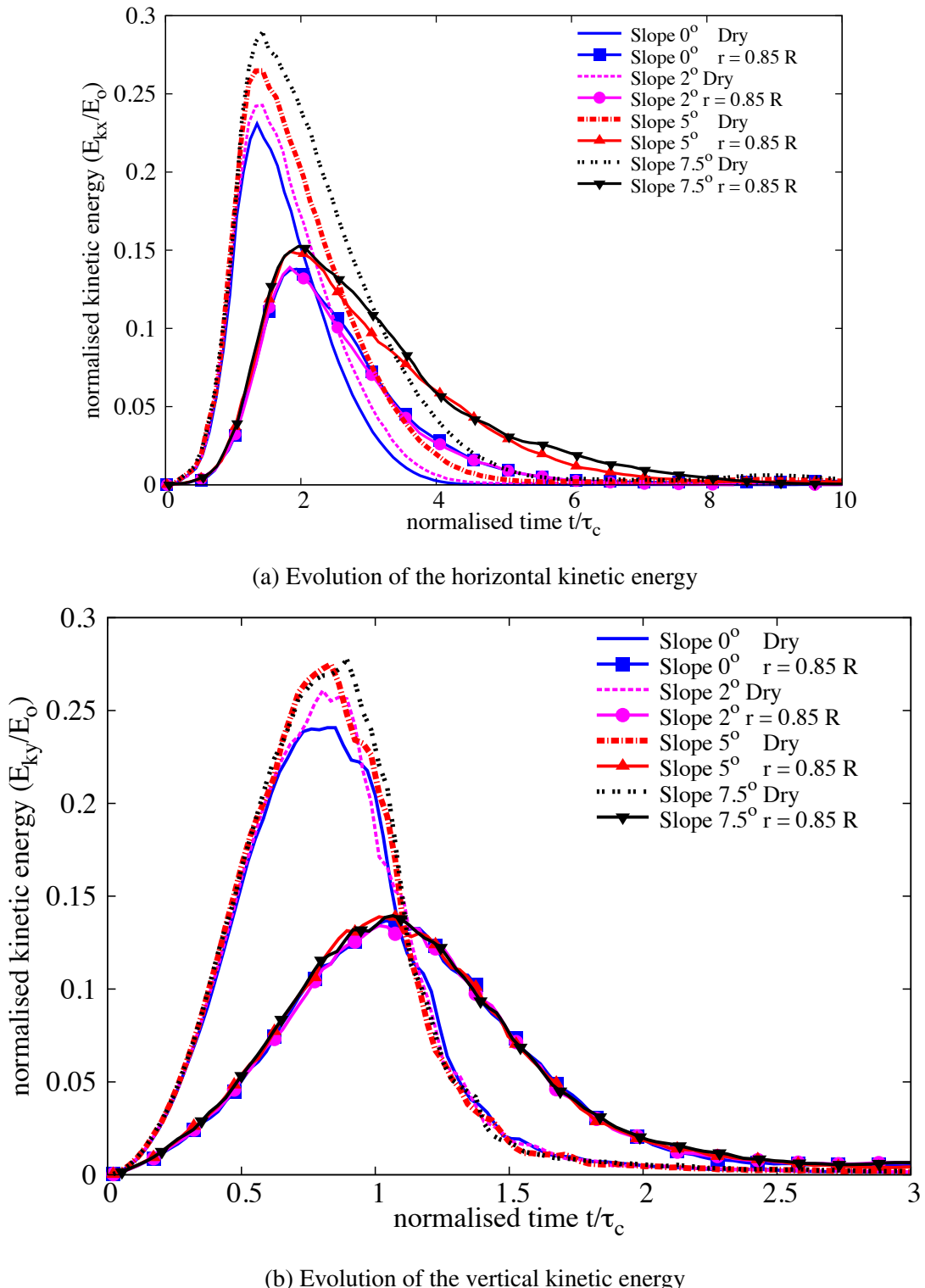


Figure 6.52 Evolution of the kinetic energies with time for a granular column collapse in fluid ($a = 6$) on a slope of 5°

6.6 Summary

Two-dimensional LB-DEM simulations are performed to understand the behaviour of submarine granular flows. Unlike dry granular collapse, the run-out behaviour in fluid is dictated by the initial volume fraction. Although previous studies have shown the influence of initial packing density on the run-out behaviour, a precise understanding of density, permeability and presence of fluid on the run-out behaviour was lacking. The following conclusion are derived based on this study:

- For dense columns, at all aspect ratios, the run-out in the dry case is significantly higher than the submerged condition.
- Granular columns with loose packing and low permeability tend to flow farther in comparison to dense columns and dry conditions, due to entrainment of water at the base of the flow front resulting in lubrication and/or hydroplaning.
- For the same thickness and velocity of the flow, the potential of hydroplaning is influenced by the density of the flowing mass. Loose columns are more likely to hydroplane than the dense granular masses, as they entrain more water at the flow front, leading to partial fluidisation.
- In both dense and loose conditions, the run-out distance increases with decreasing permeability. An increase in the hydrodynamic radius from 0.7 to 0.95 R increases the normalised run-out by 25%.
- For the same value of peak kinetic energy, the run-out distance in fluid is longer than the dry column collapse. Also, with decreasing permeability the run-out distance increases for the same peak kinetic energy.
- The low permeability of the granular mass results in entrainment of water causing hydroplaning. At higher aspect ratios, a decrease in permeability does not have a significant influence on the run-out behaviour, due to the turbulent nature of collapse of tall columns.
- With decreasing permeability, the duration for the flow to initiate increases as the time required to dissipate the large negative pore-pressure increases.
- The number of vortices formed during a collapse in fluid is found to be proportional to the amount of material destabilised. The vortices are formed only during the spreading stage of collapse.

- The formation of eddies during the collapse of tall columns indicates that most of the potential energy gained during the free-fall is dissipated through viscous drag and turbulence.
- For dense granular columns at various slope angles, the run-out in the dry condition is higher than for submerged conditions. Whereas with increasing slope angle, the loose granular column flows farther than the dry conditions.
- The initial packing density plays a significant role in the case of collapse on a horizontal plane, however at slope greater than 5° , the run-out distance is unaffected by the initial packing density at high permeability conditions.
- At high permeabilities, the viscous drag forces predominate for both dense and loose conditions. However at a low permeability ($r = 0.9 R$), hydroplaning is observed in the case of loose condition.
- The behaviour of tall columns is significantly different from that observed in the case of short columns. The slope angle has a strong influence on the number and size of eddies during the flow. The eddies interact with the surface of the granular flow and forms heaps in front of each vortex. This significantly affects the mass distribution and in turn the run-out evolution of tall columns.

References

- Bonnet, F., Richard, T., and Philippe, P. (2010). Sensitivity to solid volume fraction of gravitational instability in a granular medium. *Granular Matter*, 12(3):317–325.
- Denlinger, R. and Iverson, R. (2001). Flow of variably fluidized granular masses across three-dimensional terrain, ii: Numerical predictions and experimental tests. *J. Geophys. Res.*, 106(B1):553–566.
- Harbitz, C. B. (2003). Hydroplaning of subaqueous debris flows and glide blocks: Analytical solutions and discussion. *Journal of Geophysical Research*, 108(B7):2349.
- Iverson, R. M. (2000). Acute Sensitivity of Landslide Rates to Initial Soil Porosity. *Science*, 290(5491):513–516.
- Meruane, C., Tamburrino, A., and Roche, O. (2010). On the role of the ambient fluid on gravitational granular flow dynamics. *Journal of Fluid Mechanics*, 648:381–404.
- Midi, G. D. R. (2004). On dense granular flows. *European Physical Journal E*, 14(4):341–365.
- Pailha, M., Pouliquen, O., and Nicolas, M. (2008). Initiation of Submarine Granular Avalanches: Role of the Initial Volume Fraction. *AIP Conference Proceedings*, 1027(1):935–937.
- Peker, S. and Helvacı, S. (2007). *Solid-liquid two phase flow*. Elsevier.
- Rondon, L., Pouliquen, O., and Aussillous, P. (2011). Granular collapse in a fluid: Role of the initial volume fraction. *Physics of Fluids*, 23(7):073301–073301–7.
- Schaeffer, D. G. and Iverson, R. M. (2008). Steady and Intermittent Slipping in a Model of Landslide Motion Regulated by Pore-Pressure Feedback. *SIAM Journal on Applied Mathematics*, 69(3):769–786.
- Staron, L. and Hinch, E. J. (2007). The spreading of a granular mass: Role of grain properties and initial conditions. *Granular Matter*, 9(3-4):205–217.
- Thompson, E. L. and Hupper, H. E. (2007). Granular column collapses: Further experimental results. *Journal of Fluid Mechanics*, 575:177–186.
- Topin, V., Dubois, F., Monerie, Y., Perales, F., and Wachs, A. (2011). Micro-rheology of dense particulate flows: Application to immersed avalanches. *Journal of Non-Newtonian Fluid Mechanics*, 166(1-2):63–72.

- Topin, V., Monerie, Y., Perales, F., and Radjaï, F. (2012). Collapse Dynamics and Runout of Dense Granular Materials in a Fluid. *Physical Review Letters*, 109(18):188001.
- Yazdchi, K., Srivastava, S., and Luding, S. (2011). Microstructural effects on the permeability of periodic fibrous porous media. *International Journal of Multiphase Flow*.